Biomechanical Investigation of the Human Foot Deformation under Different Landing Conditions Using Finite Element Analysis

Yaodong Gu

Ph.D. Thesis   2010

The following figures have been omitted on request of the university –

ACKNOWLEDGEMENT

Yaodong Gu

ABSTRACT

In this thesis, a subject specific three dimensional (3-D) finite element (FE) foot model has been developed based on computer tomography (CT) images and validated with subject specific biomechanical tests. The model was successfully used to study deformation of the foot during normal/inversion landing and to develop a new concept of using under calcaneus area (UCA) plug in the midsole for heel pressure relief. The FE model incorporated realistic component structures and material properties of the soft tissues, which was validated by subject specific *in vivo* indentation tests. The plantar pressure was assessed in controlled balance standing tests and the data were used to validate the FE model and establish the optimum loading conditions and meshing scheme through mesh sensitivity tests. The validated model, combined with specially designed biomechanical test, was then used to simulate the foot deformation in landing and to predict the effects of UCA plugs of different materials and sizes on the heel pressure distribution.

The forefoot deformation and stresses in metatarsals during normal landing and inversion landing have been comparatively studied with both biomechanical tests and FE modelling. Subject specific biomechanical tests under controlled landing tests were performed and the data were used to validate the FE model. Larger group landing tests with 10 selected subjects tests were also performed. The pressure distribution, maximal force and force time integral of the five metatarsals of the subjects determined and the difference between normal landing and inversion landing was established. The test results showed that the major loading was focused on the medial side of the forefoot during normal landing, while the loading position changed to the lateral side during inversion landing with the fifth metatarsal region experienced the most significant load change. The numerically predicted plantar pressure distribution showed a good agreement with data from controlled biomechanical tests. The stresses in the five metatarsals were predicted and the effects

of the inversion angle were established. The modelling results showed that the stresses in the lateral metatarsals increased while the medial metatarsals stress decreased with increasing inversion angles. The peak stress point was found to be near the proximal part of the fifth metatarsal, which agrees with reported clinical observation on the metatarsal injuries.

Pressure relief is an active research area in biomechanics research with a fundamental importance for footwear development. The subject specific FE model has been used to evaluate a new concept of subject specific midsole design using softer plugs (in comparison to the midsole material) under calcaneus bone for heel plantar pressure management has been proposed and evaluated. Plugs of different materials and relative sizes to the dimension of the calcaneus bone have been incorporated in the heel region of the midsole. FE models were developed to simulate biomechanical tests on midsoles of different UCA plugs; the numerically predicted plantar pressure showed reasonable agreement with the experimental data on the same subject. For each plug dimension, the effect of material properties and thicknesses of the UCA plug on the plantar pressure distribution and peak pressure level during the heel strike phase of normal walking was systematically studied. The results showed that the UCA midsole insert could effectively modify the pressure distribution and its effectiveness was directly associated with ratio between its dimension to the size of the calcaneus bone of the subject. A medium hardness plug with a size of 95% of the calcaneus bone has achieved the best performance in peak pressure relief in comparison to the pressure level for a solid midsole, while a smaller plug with 65% of the calcaneus size and an insert with a very soft material showed minimum beneficial effect. This established approach potentially could open up a new way of heel pressure relief from the traditional approach of using insoles.

Contents

List of Figures

Chapter 2

Chapter 3

Chapter 4

CHAPTER ONE

INTRODUCTION

1.1 Introduction

The human foot is a very important part of the human body, which provides the direct source of contact with the supporting surface, and plays an important role in all weight bearing tasks. During gait, the foot contributes to shock absorption, adapts to irregular surfaces and contributes to generating momentum for forward propulsion (*Scott et al., 2007*). The feet need to be stable and supportive, flexible, and energy efficient to be able to support the body weight, withstand the forces generated by contact with the ground, propel the body forward, and to cope with different types of footwear (*Briggs, 2005*). These functions of the feet are supported by a complex structure and system of biological materials that deform and absorb energy. An in-depth understanding of the deformation of foot structure is important for injury prevention, performance enhancement and technological advancement of the design and manufacturing of sport footwear. Most importantly, information on the internal stress and strain of some key internal components is essential to enhance the knowledge on the biomechanical behaviour of the whole foot complex, however, direct measurement of those parameters is difficult and one effective way is using comprehensive computational foot model to acquire those important biomechanical data.

Landing is an important human locomotion and many foot problems, such as ankle sprain, plantar ulcer and bone fracture, have been associated with the deformation of the foot during this process *(Busch and Chantelau, 2003; Pontaga, 2004; Ekrol and Court-Brown, 2004)*. During the landing process, one of the critical foot region is the forefoot, in particular the metatarsals. The metatarsals act as a unit in the forefoot to provide a broad plantar surface for load bearing and play a major role in the propulsion and support function of the foot. The metatarsals are made up of thin long bone and are susceptible to injury caused by direct trauma, overuse and excessive rotation (*LaBella, 2007*). This is particularly profound with abnormal landing such as inversion landing when the subject lands on the lateral side of the foot. However,

there appears to be little or no research that has been conducted to study this challenging problem. It is difficult to investigate controlled foot posture such as inversion landing solely through extensive large panel biomechanics test of the human movement for safety reasons. In addition, the current biomechanical testing methods are not able to provide the internal stress values within the metatarsals due to the complex structure and boundary conditions of the system. A combined experimental and numerical approach represents an effective way for studying the deformation of foot through subject specific finite element (FE) modelling.

Another issue of interest is the use of FE modelling in subject specific footwear development for heel pressure relief. Heel pad of the foot plays an important role for load bearing and protection to the underlying tissue and bones (*De Clercq et al., 1994*). It normally experiences significant force during daily human movements/activities, which could cause heel pain as one of the most common foot complaints (*Reiber et al., 1992*). The high pressure of the heel region was also related to many foot problems such as heel spurs (*Aldridge, 2004*), plantar warts (*Schon et al., 1993*) and plantar ulcers (*Busch and Chantelau, 2003*). Recent developments of experimental and numerical biomechanics have greatly improved the understanding of the relationship between load and tissue damage, this has opened up the possibilities of design for optimal pressure relief that may lead to measure for the enhancement of both tissue resistance and repair (*Zheng et al., 2000; Erdemir et al., 2005*). Recent biomechanical studies showed that footwear design with special structures and/or materials had become the most effective way to relieve high plantar pressure (*Hennig and Milani, 1995; Li et al., 2000; Hennessy et al., 2007*). However, most of these works were based on generic design optimisation without considering the bone (e.g. calcaneus) structure. A subject specific design approach of the midsole structure under the calcaneus could potentially further improve the pressure distribution by combining imaging data with computational modelling.

1.2 Aims and objectives

This work aims to develop a detailed subject specific FE human foot model to study the deformation of the forefoot/metatarsals during normal and inversion landing and develop a new concept of using under calcaneus area (UCA) plug in the midsole for heel pressure relief.

Main objectives are:

• To develop a three dimensional (3-D) FE model of the human foot based on CT images incorporating detailed subject specific material property and establish the optimum meshing and loading conditions;

• To design and perform biomechanical tests for different landing conditions and compare the data with the FE foot model;

• To simulate the deformation of the forefoot in normal landing and inversion landing and establish the effect of inversion angle on the stress in the forefoot and the five metatarsals;

• To develop a new subject specific midsole design approach using UCA plug for heel pressure relief and establish the optimum materials and dimensional parameter.

The development of geometrically detailed FE foot model would provide new insights into the internal load distribution of the foot, which took into account realistic material and contact properties. Simulation of normal gait with idealized position of the foot can not truly represent the complex loading situation the foot experience in real landing conditions (*Chen et al., 2001; Gefen, 2003*). It is essential to establish the mechanical response of the metatarsals at an inversion position that is a common factor associated with foot injuries. Heel pad of the foot, plays an important role for load bearing and providing protection to the underlying tissue and bones (*De Clercq et al., 1994*). The high pressure of the heel region was also related to many foot problems. Footwear design with special structures and/or materials has become the

most effective way to relieve high plantar pressure. However, most of these works were based on generic design optimization without considering the structural difference of the subject. A subject based design approach of the sole structure could potentially further improve the pressure distribution by combining the imaging data with computational modelling.

1.3 Outline of the thesis

In Chapter 2, background information and current research on functional anatomy of the human foot, human biomechanical testing, FE human body modelling and their application in biomechanical study are reviewed. It also covers different types of foot biomechanical testing on human movements. A summary of the mechanical behaviour of biological material and testing methods characterising of foot soft tissue and the use of inverse FE modelling to identify materials parameters was presented. Current works of FE modelling in lower limb movement, foot mechanics and footwear development have been critically reviewed with the limitation and potential area to improve discussed. The significance of an improved understanding of the foot biomechanics of inversion landing for injury prevention and footwear development was also discussed.

In Chapter 3, the main procedures and parameters used in developing a FE model based on CT foot scans was presented in details. The FE model incorporated realistic structures and material properties of the soft tissues, which was validated by subject specific *in vivo* indentation tests. The experimental procedures and testing schemes for balance standing tests conducted were described and the data was used to validate the FE foot model. Detailed the testing procedure and data analysis process designed for studying inversion landing were presented and the difference in some key biomechanical characteristics, including the pressure distribution, maximal force and force time integral of the five metatarsals, between normal and inversion landing were analysed. The loading and boundary conditions used for simulating the physiological loading conditions of the human foot in a landing test were explained in details. The FE modelling results on the stresses in the metatarsals were presented and the effects of the inversion angle were established. Finally, the significance of the work was discussed with reference to some published clinical observation on metatarsal failures is discussed.

In Chapter 4, a new concept of subject specific midsole design using UCA plug for heel plantar pressure relief was presented, together with details of the manufacturing, X-ray imaging based positioning and biomechanical testing procedures. The subject specific biomechanical tests and FE modelling results were compared for validation purpose. The numerical results of midsole with three different plug materials of different hardness (in comparison to the midsole EVA foam) were compared to establish the effect of material properties and thicknesses of the UCA plug on the plantar pressure distribution and peak pressure level during the heel strike phase of normal walking. Limitation of the work and potential future development based on the concept developed was discussed in the final part of the chapter.

Chapter 5 summaries the findings in this study and its clinical implications regarding different simulated conditions of the foot and future footwear development. Suggestions on the further improvements of the FE model and other future research directions of this study were highlighted.

CHAPTER TWO

BACKGROUND AND LITERATURE REVIEW

2.1 The functions and structure of the human foot

The human foot (Figure 2.1) is a very important part of the human body. It provides the direct source of contact with the supporting surface in different maneuvers, and plays an important role in all weight bearing tasks. During gait, the foot contributes to shock absorption, adapts to irregular surfaces and contributes to generating momentum for forward propulsion (*Scott et al., 2007*). Feet need to be stable and supportive, flexible, and energy efficient to be able to support body weight, withstand the forces generated by contact with the ground, propel the body forward and cope with uneven surfaces and various types of footwear (*Briggs, 2005*). These functions are supported by a complex structure and materials system.

The whole foot is made up of bones, cartilages, muscles, tendons and ligaments. There are thirty three joints in the foot and more than one hundred muscles, tendons and ligaments. In addition, there is a network of blood vessels, nerves, skin, and soft tissue (*Rohen and Yokochi, 1988*). Normally, the foot is considered as having three main parts: the forefoot, midfoot and rearfoot (Figure 2.1). The rearfoot (hindfoot) articulates with the midfoot through the talonavicular and calcaneocuboid (midtarsal) joints, and the forefoot is connected with the midfoot through the tarsometatarsal joints. These parts work together to provide the body with support, balance, and mobility. The supportive function of the foot is mainly provided by the bones, joints and ligaments of the midfoot, the central tarsometatarsal joints, and the midtarsal joint. Subtalar, talonavicular, medial and lateral tarsometatarsal flexibility allows the foot to adjust to uneven ground and for the changing shape of the foot during heel elevation and propulsion. The plantar aponeurosis and deep transverse intermetatarsal ligaments support the foot and also have dynamic functions in stabilisation and movements (*Kitaoka et al., 1997*).

The underlying structure of the foot allows it to undergo complex deformation and movement for different functions. In order for the foot to propel the human body

forward efficiently, it must be able to change between being a strong rigid structure and a softer more flexible one. The combination of the stable and sturdy 2-arched bone structure and the more mobile and elastic soft tissues means that the function of the foot can alternate between the following states: (i) Foot is a mobile adapter - the soft tissues expand which allows the arches to lower. This action is the body's defense mechanism, designed to prevent damage and jarring to the weight-bearing joints throughout the body; (ii) Foot is also a rigid lever - the soft tissues contract which causes the arch to heighten. This rigidity provides strength and power that propels the body forward. The sequence and timing of the foot motion as it switches between a mobile adapter and a rigid lever is termed the gait cycle (*Winter, 1979*). Detailed structures of the bone and tendon system are described in the next two sections.

2.1.1 Bones of the foot

Figure 2.2 illustrates the main bone structures of the foot (*Schuenke et al., 2006*). The skeleton of the foot begins with the talus, or ankle bone, that forms part of the ankle joint. The two bones of the lower leg, the large tibia and the smaller fibula, come together at the ankle to form a very stable structure known as a mortise and tendon joint. The two bones that make up the back part of the foot are the talus and the calcaneus. The talus bone is connected to the calcaneus at the subtalar joint, which allows the foot to rock from side to side. Just down from the talus is a set of tarsal navicular bones that work together as a group. These bones are unique in the way they fit together with multiple joints between them. These tarsal bones and the cuneiforms are part of the midfoot. When the foot is twisted in one direction by the muscles of the foot and leg, these bones lock together and form a very rigid structure. When they are twisted in the opposite direction, they become unlocked, and the foot conforms to whatever surface it is contacting. The tarsal bones are connected to the five long bones of the forefoot called the metatarsals. These two groups of bones are fairly rigidly connected, without much movement at the joints. As shown in Figure 2.2, the five metatarsal bones are connected to a group of smaller bones called phalanges,

which are the bones of the toes (*Rohen and Yokochi, 1988*). These bones are much thinner that than the bones in the hindfoot and midfoot, and are known to be vulnerable to injuries in sport or normal gait (*Matheson et al., 1987*).

2.1.2 Tendons and ligaments of the foot

Tendons and ligaments are very important structure for the human foot. A tendon is a band of fibrous tissue that connects a muscle to a bone. When a muscle contracts, it pulls on the tendon, which moves the bone. As shown in Figure 2.3, there are various tendons attaching muscles to the bones in the foot. One of the most prominent tendons is the Achilles tendon, which can be felt at the back of the foot just above the heel. The Achilles tendon is the most important tendon during walking, running, and jumping (*Hof et al., 2002*). It attaches the calf muscles of the lower leg to the heel bone and allows the subject to rise up on our toes. The posterior tibial tendon (Tibialis posterior) attaches one of the smaller muscles of the calf to the underside of the foot. This tendon supports the arch and helps to turn the foot inward. The anterior tibial tendon (Tibialis anterior) allows us to raise the foot. The two peroneal tendons that run behind the outer bump of the ankle (Peroneus longus and Peroneus brevis) help to turn the foot outward. The phalanges of the foot have tendons attached that can bend the toes down and straighten the toes. These smaller tendons are located on the bottom and top of the foot near the toes that they control. Tendons are sometimes torn or ruptured, but a tendon rupture in the foot is not very common, while inflammation of the foot tendons is more prevalent due to cyclic loading.

Ligaments are very similar to tendons. The difference is that tendons attach muscles to bones, while ligaments attach bones to bones. As shown in Figure 2.4, there are many ligaments in a human foot to help hold the bones together. Ligaments are made up of small fibers called collagen, which are bundled together to form a rope-like structure (*Altman et al., 2002*). The thickness of the collagen bundle determines the strength of the ligament. One major function of the ligaments is stabilizing and guiding the

subtalar joint during movement. These ligaments are classified by their location as belonging to the talocrual or subtalar joint, the metatarsus, the forefoot, or the sole of the foot (Figure 2.4). The longest ligament is plantar fascia (Figure 2.5), that is an important part of the arch extending from the toes to the heel. Its expansion and contraction allows the curving and flattening of the arch to provide balance and strength to the foot so that it bears the entire body's weight (*Cheung et al., 2004*).

2.1.3 Arches of the foot

The arches of the foot are formed by the tarsal and metatarsal bones and, strengthened by ligaments and tendons. This unique structure allows the foot to support the weight of the body in the erect posture with the least weight. The main arches are the antero-posterior arches, which may, for descriptive purposes, be regarded as divisible into two types—a medial and a lateral (*Abboud, 2002*).

The medial arch is made up by the calcaneus, the talus, the navicular, the three cuneiforms, and the first, second, and third metatarsals. Its summit is at the superior articular surface of the talus, and its two extremities or piers, on which it rests in standing, are the tuberosity on the plantar surface of the calcaneus posteriorly and the heads of the first, second, and third metatarsal bones anteriorly. The main characteristic of this arch is its elasticity, which is determined by its height and the number of small joints between its component parts. The arch is further supported by the plantar aponeurosis, by the small muscles in the sole of the foot, by the tendons of the Tibialis anterior and posterior and Peronæus longus, and the ligaments of all the articulations involved.

The lateral arch is composed of the calcaneus, the cuboid, and the fourth and fifth metatarsals. Its summit is at the talocalcaneal articulation, and its main joint is the calcaneocuboid, which possesses a special mechanism for locking, and allows only a limited movement. The most marked features of this arch are its solidity and its slight elevation; two strong ligaments, the long plantar and the plantar calcaneocuboid,

23

together with the Extensor tendons and the short muscles of the little toe, preserve its integrity.

2.2 Typical movements of the foot in different planes and axes

The joints of the foot are controlled by extrinsic and intrinsic muscles of the lower limb and provide for major motion function, angulation and support of the foot (*Kura et al., 1998*). Motion occurs by rotation about an axes in a plane of motion for all the joints. The foot may undergo different types of movement in locomotion. In general it can be classified into three main types in accordance of different planes and axes (Figure 2.6). The three planes of motion in the foot are defined as: sagittal plane (SP), frontal plane (FP) and transverse plane (TP). The foot, or any part of the foot, is defined as being adducted when its distal aspect is angulated towards the midline of the body in the transverse plane and deviated from the sagittal plane passing through the proximal aspect of the foot, or other specified anatomical reference point. Abduction occurs when the distal aspect is angulated away from the midline. The foot is defined as being plantar flexed when the distal aspect is angulated downwards in the sagittal plane away from the tibia, and dorsiflexed when the distal aspect is angulated towards the tibia in the sagittal plane. The foot is described as being inverted when it is tilted in the frontal plane, such that its plantar surface faces toward the midline of the body and away from the transverse plane, and everted when its plantar surface faces away from the midline of the body and away from the transverse plane. The foot is considered to be supinated when it is simultaneously adducted, inverted and plantar flexed, and pronated when it is abducted, everted and dorsiflexed (*Wright et al., 2000*).

The minimum range of ankle joint motions as necessary for normal locomotion is 10^0 of dorsiflexion and 20^0 of plantar flexion. The ankle joint also has slight movement in the transverse plane during plantar flexion, which cause the instability of this joint (*Robbins et al., 1995*). One of the most important joints in the hindfoot is the joint between the talus and calcaneus, which is termed the subtalar joint. It could perform complex motions in three planes. It produces the motions of supination and pronation, clinically referred to as subtalar inversion and eversion. Average subtalar motion is

20° to 30° inversion and 5° to 10° eversion. During the gait cycle, the heel strikes the ground in slight inversion, followed by rapid eversion to a maximum of 5° to 10° of the gait cycle (*Sarrafian, 1993*).

In the midfoot region, talonavicular and the calcaneocuboid joints together form the midtarsal joint. This joint has two axes of motion, an oblique axis and a longitudinal axis (Figure 2.7) which are confined as the talonavicular joint and the calcaneo-cuboid joint, respectively. *Ouzonian and Shereff* (*1989*) determined *in vitro* talonavicular motion to be 7° in flexion- extension and 17° in pronation- supination. In the same work, the calcaeocuboid motion was found to 2° in flexion-extension and 7° in pronation- supination. The interfaces between the posterior aspect of the metatarsal bones and the lesser tarsus produce the tarsometatarsal joints which have a very limited range of gliding action. The motion of the first three metatarsocuneiform joints is minimal compared with the fourth and fifth metatarsocuboid joints. Based on *in vitro* studies by *Ouzonian and shereff (1989)*, the first metatarsal-medial cuneiform motion was about 3.5° flexion-extension and 1.5° pronation–supination, while the fourth and fifth metatarsocuboid joints were 9° to 100° flexion-extension and 9° to 110° pronation-supination. In an *in vivo* study of first metatarsocuneiform motion, a mean sagittal motion of 4.4° has been identified *(Fritz and Prieskorn, 1995)*. There has been concern that hyper-mobility of the first metatarsocuneiform joint may lead to offloading of the first ray and subsequent hallux valgus deformity *(Klaue et al., 1994)*. *Mizel (1993)* described the plantar first metatarsocuneiform ligament as the major restraint to displacement of the distal first metatarsal head.

2.3 Foot injury and metatarsal injuries

2.3.1 Types of foot injury

Foot injury is one of the most common problems in daily activities and sport. There are many types of the injuries associated with the bone or soft tissues of the foot. Typical soft tissue injuries or problems include heel pad pain, diabetes ulcer, rupturing of the tendon or ligaments *(Rome et al., 2001; Ribu et al., 2007; Al-Qattan, 2007; Tryfonidis et al., 2008)*. One most common of foot injury associated with sport is over stress or over use. Experimental studies demonstrating the specific mechanism for overuse injuries in distance runners have not been reported, but high stresses related to both impact *(Vitasalo and Kvist, 1983; Denoth, 1986; Nigg et al., 1987;)* have been implicated. Overuse injuries result from stresses applied to tissues at intensities that cause a gradual breakdown and eventual failure of the tissues *(Sijbrandij et al., 2002)*. Critical factors determining injury susceptibility are stress to the tissues and the bodies' response to the stress *(Malanga and Ramirez, 2008)*. The increase in stress leads to microscopic damage at the cellular level that stimulates remodelling of affected tissues *(Murley et al., 2009)*.The athlete is forced to reduce the intensity of training until the body is able to remodel the tissues sufficiently to be able to handle the applied stresses *(Sijbrandij et al., 2002)*.

2.3.2 Metatarsals injuries

Fracture of the metatarsal is one of the most common foot injuries *(Ekrol and Court-Brown, 2004; Popovic et al., 2005, Dixon et al., 2006; Logan et al., 2007)*, in particularly in athletes and soldiers. Several high-profiled athletes suffered from the same injury- David Beckham, Steve Gerrard, Michael Owen, and Wayne Rooney. A prospective study of 205 soldiers by *Milgrom et al (1985)* showed 184 stress fractures of the lower extremity, 7.6% of which were with the metatarsals. In another study, up to 20% of stress fractures in athletes and 23% in military recruits were found to be

located in the metatarsals *(McBryde, 1985; Matheson et al., 1987)*. Information on the internal stress and strain of the five metatarsal bones during sports is valuable for improving the knowledge on metatarsal bones fracture principle.

The metatarsals act as a unit in the forefoot to provide a broad plantar surface for load bearing and play a major role as propulsion and support in foot's function. As shown in Figure 2.2, metatarsal bones are long and slender bones found in between the tarsal bone and the phalanges. These bones act like a rigid lever in the propulsion of the ankle and the foot. They also act like a flexible structure that will help with balancing and holding up of the entire body. Metatarsal fractures could be caused by direct trauma, overuse and excessive rotation *(LaBella, 2007)*. Bone injuries in these structures are very common since there is very little soft tissue that protects the top of the foot *(Donahue et al., 1999)*. Stress fractures of the metatarsals in normal gaiting most frequently occur in the second and third metatarsal bones. As they are the longest and the narrowest while the fracture of the first metatarsal accounts for 7-8%, and the fourth and fifth 3% *(Levy, 1978)*. Fracture of the proximal portion of the fifth metatarsal bone (Figure 2.8) is also a common foot injury that causing dorsolateral proximal forefoot pain *(Dameron, 1975)*. As shown in Figure 2.8, three fracture types in the proximal portion of the fifth metatarsal bone have been described: Jones fracture (1), tuberosity avulsion fracture (2), and diaphyseal stress fracture (3). Mechanisms of these fractures may involve repetitive stress, usually as a result of frequent impact weight-bearing exercise, which eventually yield to a fracture due to continued loading. Biomechanical abnormalities, such as excessive pronation, hypersupination, lower extremity malalignment, external or internal femoral rotation and limb- length discrepancy can all lead to an alteration in normal gait and then lead to stress fractures. The fifth metatarsal is also commonly injured as acute sports-related trauma, which always happens in a situation involving sudden inversion of the hind-foot with weight on the lateral metatarsals *(Logan et al., 2007)*. For an understanding of this injury, it is essential to study the internal stresses of the foot under normal and abnormal conditions by combining numerical modelling and

experimental tests.

2.4 The functions and structure of sports shoes

Reducing injury and improving performance are the main attributes of a sports shoe *(Lake, 2000)*. An appropriately designed sports shoe can reduce the risk of injury by improving the effects of repeated impacts and pronation of the foot, as stated by *Shorten (2000)*. In addition, shoe design should also reduce the energy being lost by an athlete and to increase the energy returned to the athlete. Sports shoes can be broken down into 4 main areas; upper shoe, inserts, mid-soles and the outsole (Figure 2.9). While the upper shoe functions are mainly to hold the sports shoe together, it also helps to stabilize the foot during running.

The functions of the inserts are to help arch support and to dissipate heat and moisture away from the foot. Traction, wear resistance and shock absorption are the main functions of the outsole. The mid-soles function is the most important part of a sports shoe. It is used to control excessive foot motion (mainly pronation), provide cushioning and shock absorption, help prevent injury and fatigue and help limit the peak impact forces in heel strike whilst running. The function of the outsole is to provide the foot support, wear resistance and the traction. It is normally made of rubber or plastic.

The midsole of a sports shoe aims to help spread the impact forces so the peak ground reaction force is not placed directly to the foot, leg and knee, which is how most injuries have occurred. A good mid-sole design is one that will provide some type of energy back to the body when compressed *(Shorten, 2000)*. This is because the energy returned to the athlete would normally require muscular contraction to perform and would therefore make the athlete use energy that could be prevented. Durability is another important property in sports shoe design. *Verdejo and Mills (2004)* have stated that mid-sole durability is related directly to the cushioning and the fatigue form impact attenuation. Ethylene Vinyl Acetate (EVA) foam is usually used for the mid-sole cushioning properties. EVA foam is made up of tiny gas bubbles; the

molecular structure and number of bubbles can affect the materials strength and hardness. During a long distance run, for example a marathon, *Verdejo and Mills (2004)* found that EVA foam doesn't fully recover, decreasing the cushioning and the energy returned to the athlete and therefore increasing the probability of injury.

Schwellnus et al. (1990) reported that neoprene insoles can significantly reduce the incidence of tibia stress syndrome through better shock absorption. Some studies have found that neoprene insoles reduce transmitted forces better than viscoelastic insoles (*Brodsky et al., 1988*). *Bus et al. (2004)* found that the use of custom-molded insoles was significantly better than that of flat insoles in terms of peak pressure reduction (Figure 2.10). It should be noted, however, that the use of the same custom design may result in significant differences in performance for individual foot structure. *Cook et al. (1985)* attributed the increase in risk of stress fractures to a loss of mechanical support or the shock-absorbing properties of the midsole of footwear. *Verdejo and Mills (2004)* also proposed an impact machine to analyse the changes in the mechanical response of shoe midsole foams. In the work they analysed the changes in stress–strain responses of foams under repeated impacts that simulate heel strikes. The key design parameters of the impact machine identified are the impact frequency and the peak pressure. A different approach was made by *Goonetilleke (1999)*, a 20 participant panel was used to evaluate the perceived levels of cushioning which in turn was correlated with the footwear impact test results. It was reported that, during walking, the magnitude of the peak deceleration on the impact tester appears to be a good prediction of perceived levels of cushioning. Moreover, it was concluded that impact characterisations can reveal important differences between materials and how the feel of the subjects.

2.5 Typical biomechanical testing systems and applications

Biomechanics is the study of the mechanics (kinetics and kinematics) in the musculoskeletal system by analyzing forces and their effects on anatomical structures. In order to electively treat any part of the human musculoskeletal system, it is important to fully understand its biomechanics. The understanding of the biomechanics of the foot has been improved due to the recent scientific advances in both measurement instrumentation and theoretical methodology. A variety of experimental methods have been developed and used to assess human locomotion under different conditions, including high speed camera and image analysis *(Williams, et al., 2001)*; pedometer *(Gayle et al., 1977; Washburn et al., 1980)*, accelerometer *(Hayes et al., 1983; Meijer et al., 1991; Bouten et al., 1994)*, doubly labeled water *(Bratteby et al., 1998)*, force transducer *(Dion et al., 1982)*, foot contact monitor *(Hoyt et al., 1994)*, heart rate monitors *(Leonard et al., 1995)* and muscle electricity signals *(Arampatzis et al., 2003)*.

Figure 2.11 shows some typical biomechanical tests of body movements, force reaction and pressure distribution. The body movements are commonly studied using high speed cameras. In these tests, the camera will continuously monitor the movement of reflective markers on the surface of the components (e.g. a shoe or bare foot), then the data is collected and analyzed to reveal the path of each part. The system is normally calibrated using a rigid structure (e.g. T-shaped frame) (Figure 2.11 (a)) before being used for real biomechanics tests. Figure 2.11(b) shows the movement of the shoe during a running process, with different markers to represent the path (with different colors) of the heel and mid section of the shoe.

Force platforms are commonly used in biomechanics laboratories, and ground reaction forces (GRFs) are one of the most commonly measured biomechanical variables (Figure 2. 11(c)). The GRFs show the magnitude and direction of loading directly applied to the foot structures during locomotion. Because the foot is the first

part of the body involved in contact with the ground during walking/running or jumping, they must be able to withstand and transmit these GRFs. A typical example of force change in running is shown in Figure 2.11 (d). The GRF shows the reaction force in the different phases of running form. They are heel contact, heel strike, mid-stance, forefoot contact, push off and toe off. These could provide important information necessary for the calculation of ankle-joint reaction moment *(Lichtwark and Wilson, 2005)*.

The information provided by the force plate systems is limited since the force information is not specific to foot anatomical locations. For example, the forces recorded may occur underneath both the fore and rear parts of the foot simultaneously so that the centre of pressure (COP) may fall at some intermediate point. Pressure distribution devices provide more specific location of pressures as they occur beneath the moving foot. In-shoe pressure measurement systems (Figure 2.11 (e)) are useful tools to obtain plantar pressure during dynamic movements. A typical pressure distribution in walking is shown in Figure 2.11 (f). Such systems are widely used in locomotion *(Mueller and Strube, 1996)*, sports *(Higbie et al., 1999)* and footwear research *(Henning and Milani, 1995)*. The results from research on pressure distribution have led to many successes in clinical applications *(Abboud and Rowley, 1996)*. The repeatability and accuracy of data measured using various commercial in-shoe pressure measurement systems could be found in some published literatures *(Ahroni et al., 1998; Kernozek and Zimmer, 2000; Putti et al., 2007)*. These measurements techniques could provide important information on the movement of the feet and the reaction forces; it could also provide the loading/boundary conditions for detailed studies of the internal foot deformation through computational modelling.

2.6 Dynamic foot movement and internal deformation in different locomotion

2.6.1 Dynamic modelling of the foot deformation

The deformation of the foot during different movement and contact with external objects is a complex problem and excessive deformation may cause injury to the bone or the soft tissues *(Burns et al., 2005)*. Many efforts have been made to monitor the foot deformation in locomotion with test such as skeletal tracking *in vivo*, cadaveric test, stereo camera matching as shown in Figure 2.12.

Dynamic modelling of the foot requires multi-segment motion analysis, which takes into account deformity *(Davis, 2004)*. Initially, only a limited number of segments could be analysed *(Scott and Winter, 1991; Moseley et al., 1996)*. Subsequently mid-foot and fore-foot segments were only included in the models with the increased availability of more reliable instrumentation *(Stebbins et al., 2006; Simon et al., 2006)*. These works have improved the understanding of internal bone deformation, however, the accuracy of the information and application is still rather limited. Skeletal tracking *in vivo* was regarded to be inappropriate in routine clinical assessment due to the complexity of the setup *(Arndt et al., 2007)*. Cadaveric studies allows the measurement of movement of the individual bones of the foot through the use of bone markers, however, these data cannot be directly extrapolated to *in vivo* mechanics due to lack of representation of the real boundary condition *(Nester et al., 2007)*. The camera matching system has improved the capacity of measuring the shape of the dynamic foot. It relies on the triangulation between the projection pattern and the camera image (basic concept is just like stereo matching between multiple cameras), but the accuracy still needs improving *(Kimura et al., 2009)*.

2.6.2 Internal foot deformation

The internal foot deformation is directly linked with the deformation of the soft tissue and bone in the foot, which has great significance to understand injury mechanisms and technological development in injury prevention. A range of techniques has been

used to study the internal foot deformation by combining biomechanical tests and imaging techniques such as fluoroscopy, ultrasound, computed tomography (CT), and magnetic resonance imaging (MRI). All of these have the potential to provide information about the internal deformation of the foot (Figure 2.13).

Fluoroscopy is a transmission technique that creates two-dimensional projections of three-dimensional structures. Fluoroscopy has been used with a plantar-pressure monitoring device to provide real-time imaging of dynamic foot deformation *(Gefen et al., 2000)*. The work provided evidence that the technique could monitor the motion of bones within the soft tissue envelope, unfortunately, it had difficulty to distinguish different types of soft tissues due to poor contrast and resolution. This made it difficult to reconstruct deformations in closely spaced discrete structures, such as the tissue underneath the metatarsal heads.

Ultrasound is relatively inexpensive and the machine is portable. The technique has been used to determine the thickness of structures, such as the forefoot fat pad, during standing *(Gooding et al., 1985; Gooding et al., 1986)* and walking *(Cavanagh, 1999)*. It has also been used in combination with a force measurement device to characterise the mechanical properties of the human heel pad *(Erdemir et al., 2006)*. The limitations of the ultrasound method are that the utility is restricted by depth limitations, adversely influence of shadowing by bones, and relatively poor soft-tissue contrast.

CT and MRI methods have much better resolution for studying the internal structure and are increasingly used in studying foot deformation. A CT-compatible loading device has been developed to investigate deformations within prosthetic limbs *(Madsen et al., 2000)* and in the diabetic feet *(Smith et al., 2000)*. In the work by *Smith et al. (2000)* a total vertical load of 50% of body weight was applied with the foot fixed in 15° of plantar flexion was used to simulate the late stance phase of walking. The work was able to capture the overall internal deformation but the CT

could only provide poor contrast between individual soft tissue layers. MRI is better suited for imaging internal strains since it can provide high-level soft-tissue contrast without exposing the subject to ionizing radiation. MRI has been successfully used to visualize the *in vivo* deformation of soft tissue in the buttocks where decubitus ulcers often form *(Reger et al., 1990)*. Elastography *(Weaver et al., 2005)* and other MRI deformation monitoring techniques *(Gefen et al., 2001)* have been used to estimate the elastic response of foot tissue. However, due to the longer scanning time required in MRI, none of the MRI techniques have been applied to explore the dynamic 3-D nonlinear relationship between external force and internal stress or strain.

One major limitation for experimental biomechanical measurements lies in the fact that it can not directly assess the internal stress state of the foot, which is very important to improve the understanding of sport injuries. In addition, it is difficult to investigate controlled foot posture such as inversion landing directly through biomechanics test of the human movement for safety reasons. One effective approach is combining experimental a computational methods in order to improve structure/parts specific understanding which can be directly linked to clinical diagnosis and treatments.

2.7 Finite element (FE) modelling and its applications in biomechanics

2.7.1 Principle of FE modelling

Modelling refers to the development of a system or thing used as an example to follow or imitate - a simplified description, especially a mathematical one, of a system or process, to assist calculations and predictions. A numerical model works by series of estimated the solution to a "hard" problem through numerical approximations. Consider, for example, a body in which the distribution of an unknown variable (such as temperature or displacement) is required. Firstly, the region is divided into an assembly of subdivisions called elements, which are considered to be interconnected at joints, known as nodes. The variable is assumed to act over each element in a predefined manner, with the number and type of elements chosen so that the variable distribution through the whole body is adequately approximated by the combined elemental representations. The distribution across each element may be defined by a polynomial (for example, linear or quadratic) or a trigonometric function. After the problem has been discretized, the governing equations for each element are calculated and then assembled to give the system equations. The element equations may be found in a variety of ways, the equations of a particular type of element for a specific problem area (stress or thermal, for example) have a constant format. Thus, once the general format of the equations of an element type is derived, the calculation of the equations for each occurrence of that element in the body is straightforward; it is simply a question of substituting the nodal coordinates, material properties and loading conditions of the element into the general format.

The individual element equations are assembled to obtain the system equations, which describe the behaviour of the body as a whole. These generally take the form

$$[k]\{U\} = \{F\} \qquad (2.7.1)$$

Where [k] is a square matrix, known as the stiffness matrix; {U} is the vector of

(unknown) nodal displacements or temperatures; and {F} is the vector of applied nodal forces.

Equation 2.7.1 is directly comparable to the equilibrium or load-displacement relationship for a simple one-dimensional spring, where a force F produces a deflection U in a spring of stiffness k. To find the displacement developed by a given force, the relationship is inverted. The same approach applies to the FE method; however, before Eq. 2.7.1 can be inverted and solved for {U}, some form of boundary condition must be applied. In stress problems, this means that the body must be constrained to prevent it from performing unlimited rigid body motion. For thermal problems, the temperature must be defined at one or more of the nodes.

The solution of Eq. 2.7.1 is not trivial in practice because the number of equations involved tends to be very large. However, [k] is banded, and computational techniques have been developed to store and solve the equations efficiently. After solving for the unknown nodal values, it is then simple to use the temperatures to calculate the element heat flows, or the displacements to find the strains and then the elemental stresses.

2.7.2 Application of FE modelling in human biomechanics

The FE method has been used increasingly in many biomechanical investigations with great success due to its capability of modelling structures with irregular geometry and complex material properties under complicated boundary and loading conditions in both static and dynamic analyses (*Lotz et al., 1991; Akay and Aslan, 1996*). FE methods combined with experimental approach could predict the load distribution between the foot and different supports and offer additional information such as the internal stress and strain of the whole foot. In addition, the FE analyses could allow efficient parametric evaluations for the outcomes of the shape modifications and other design parameters of footwear without the prerequisite of fabricated footwear and

replicating patient trials. Two major application fields are relevant to human biomechanics. One of the main application areas of FE modelling in human biomechanics is to obtain fundamental anatomical knowledge about the skeleton. The analysis of bones, cartilage, ligaments and tendons comes under this heading. The second field is the use of FE modelling for orthopaedic implant design. Many designs of joint replacement prostheses have been studied using FE modelling, either by the manufacturer or by university laboratories. Although quantitative accuracy can never be assured because of anthropometric differences between patients, FE analysis can be used to conduct parametric studies of implant material stiffness and geometric change. Some typical examples are shown in Figure 2.14, and explained in sections 2.7.3-2.7.6.

2.7.3 FE modelling of skeletal parts/systems

The stress distribution in bones during testing has been studied by several authors, including the effect of elasticity or plasticity. One of the early FE models of trabecular bone architecture *(Beaupre et al., 1985)* used a 3-D model of a repeating bone unit (Figure 2.14a). Using isotropic material constants for the bone tissue, the apparent-level anisotropic material constants of trabecular bone and stress distributions within individual trabeculae were calculated. Another area of research involves applying homogenization theory to compute elasticity for different fibre architectures within the Haversian lamellae or calculate trabecular level stresses for different kinds of trabecular microstructure *(Hollister et al., 1991; Crolet et al., 1993)*. In the work by *Hollister et al. (1994)*, a micro structural finite element model of a 1 mm^3 trabecular bone element was generated to calculate the ratio of 'tissue strain-energy' to 'continuum strain energy'. A different approach of using serial reconstruction techniques to construct large-scale finite element models of 10 mm^3 samples has been pursued by *Van Rietbergen et al.(1995)*. They have been able to compute histograms of the true stress in the trabecular tissue and have found that trabeculae can be under tensile loading even when the global loading is completely

compressive due to the microstructure effect. In some of these works, finite element models have established the best-fit orthotropic representation of trabecular bone elastic properties *(Van Rietbergen et al., 1996)*. By a comparison, experimental results and numerical prediction for the stiffness measurements of trabecular bone samples. *Muller and Ruegsegger (1995)* used CT scans with a resolution of 250 μm to generate finite element models with tetrahedral elements (Figure 2.14b) to guarantee smooth surface representations. The model was then used to calculate the apparent Young's modulus of 0.564 GPa and, in a later study, they quantified the decrease in Young's modulus and quantified the decrease in Young's modulus due to bone atrophy *(Muller and Ruegsegger, 1996)*.

2.7.4 FE modelling of the human body joints

Although the general kinematic function of joints can be described without the use of FE modelling, there is considerable interest in knowing the stress and strain fields and other biophysical quantities within joint tissues to establish the complex response of tissues during load transfer, and the potential role of biophysical stimuli in the pathogenesis of degenerative diseases.

The deformation and the fracture of the femoral head has been studied by several FE analysis studies. *Yosibash et al., (2007)* constructed patient-specific FE models (from CT scans) of proximal femur with distinct trabecular and cortical sub-domains (Figure 2.14c). Both displacements and strains are predicted in the same range of accuracy as the experimental results, making it suitable for routinely clinical application. In an earlier study, an FE model has been used to predict femoral head fracture using 3-D finite element models using both linear and non-linear stress strain relationships for the bone *(Lotz et al., 1991)*. The results showed good agreement with strain gauge data, and could use von Mises stresses as the indicator predicated that the fracture site was shown to be the intertrochanteric region for falling, and the subcapital region for a one-legged stance. *Li et al. (2007)* used CT scan to determine pelvis geometry, for validation purpose, measurements of the force–time response observed at the impact site during previous drop tower experiments. In the work, the biomechanical response

of the pubic symphysis under conditions where an impact force was applied to the greater trochanter of the pelvis structure in a seated posture (Figure 2.14d).

The biomechanical challenge of hip replacement is enormous because a dynamic load of several times the body weight must be sustained over several decades. Several researches had described the effect of materials selection on stresses in the various components. It has been shown, for example, that stiffer prostheses generate higher prostheses stresses, lower bulk cement and cement interface stresses *(Akay and Aslan, 1996)*. Interfacial micromotion has been studied using concentric cylinder geometrical models of intramedullary fixation. The prediction is that reduced prosthesis stiffness causes increased micromotion, depending on the amount of interfacial friction and in growth *(Harrigan and Harris, 1991)*. Some FE models have also been developed to study specifically the degeneration of the cement layer in cemented hip prosthesis - cementation being the most common form of fixation *(Harrigan et al., 1992)*.

2.7.5 FE modelling of the lower limb system

The FE work on the knee has been focused on implant evaluation, ligaments forces, contact force/areas and cartilage stress. In a recent work, *Papaioannou et al. (2010)* evaluated the patient-specific FE knee model to study the effect of defect size on defect rim stress concentration, peak rim stress, and load redistribution across adjacent cartilage over the weight bearing area of the medial and lateral femoral condyles in the human knee. The natural knee FE modelling results can be used as a guideline to determine whether the kinetic or kinematic responses from implant FE modellings are reasonable. *Beillas et al. (2004)* developed a generic FE modelling of the entire lower limb using data from two patients to validate a one-legged forward hopping test. They also felt that a one-legged hopping test on a healthy leg would provide a better assessment of *in vivo* knee joint behavior than other techniques such as gait analysis, since the healthy leg does not have to offset the response of the injured limb. *Miyoshi et al. (2002)* developed a three-dimensional FE model of a total knee replacement's articulating surface to examine the component with and without a posterior cut-out

slot (Figure 2.14e). The cut-out slot design can be used when the posterior cruciate ligament (PCL) will be retained after total knee arthroplasty. However, if tension of the PCL was not applied, as both models are assumed to be PCL sacrificing. Although very few researchers have used a probabilistic approach to knee implant analysis, several studies have used knee wear simulators for wear, stress and kinematic analyses. *Werner et al. (2005)* subjected seven cadaveric limbs to a certain extension load to simulate the typical trial reduction performed during a total knee replacement surgery. *Fregly et al. (2005)* developed a computational model for tibial component wear prediction that included fluoroscopic motion analysis data and a dynamic contact model.

The Achilles tendon (AT) has been an important link between the lower limb and the foot. Human AT is subjected to substantial force during human locomotion, and it is frequently associated with acute and overuse injuries related to habitual loading, including complete tendon ruptures *(Maffulli, et al., 2003)*. The high incidence of AT injuries during physical training is also related to the high forces involved. It has been reported that injuries caused by overuse (referred to as tendinous pain) affects millions of people in occupational and athletic environments *(Almekinders and Temple, 1998, Khan et al., 2002)*. Many injuries were attributed to changes in activity, such as abrupt increase in the duration or intensity of athletic training *(Jozsa et al., 1997; Wren et al., 2001)*. It has been estimated that the human AT load may reach tensile forces of 1400-2600 N during walking *(Finni et al., 1998)* and 3100-5330 N during running *(Giddings et al., 2000)*. Several studies have suggested that the AT experiences greater levels of stress than other human tendon. Based on *in vitro* measurement. *Komi et al. (1992)* provided evidence that the human AT may receive peak stresses in excess of 70MPa during maximal eccentric plantar flexions, while most tendons in other body regions experience peak stresses below 30MPa. In a related article, *Ker et al. (1988)* suggested that *in vivo* stresses are higher in the human AT based on transducer data. Recently, *Kongsgaard et al. (2005)* reported peak stresses of 57.4MPa for running and 70.3MPa for playing volleyball. This

biomechanical data has improved the understanding of tendon loading, however, the load transfer mechanism and internal stress/strain states within the tendon and bony structures were not well addressed, which is crucial to the understanding of soft tissue injuries.

Recently, *Gu et al. (2008)* has presented a study investigating the mechanical properties of human AT during different human locomotion, by combining biomechanical tests and numerical modelling. The human AT force was determined through inverse muscle force calculation. A 3-D FE model was developed using CT scan images to simulate the deformation of Achilles tendon during hopping and walking. The stress/strain within the AT during different sub- phases (e.g. heel strike, midstance, forefoot contact, push off and toe off) was successfully predicted. As shown in Figure 2.15, the AT stresses in heel strike and the push-off phase has been successfully predicted. Results identified that the muscle forces in hopping were much higher than in normal gait. The maximum stress value in hopping is three times of the stress in walking. The tendon stress increased with external load over different subphases and the maximum ATF was found to be in the push-off phase.

2.7.6 FE modelling of the human foot

A common approach to develop a FE foot model is to use 3-D CT data by converting voxel data (CT or MRT images) to 2-D or 3-D FE elements *(Gefen et al., 2000; Goske et al., 2006)* as shown in Figure 2.16. The 2-D model in Figure 2.16(a) was developed to study insole design to reduce peak plantar pressure; while the 3-D model shown in Figure 2.16 (b) was used to study the stress in the foot during the normal gait. *Cheung et al. (2005)* employed a 3-D model to investigate the foot plantar pressure distribution under different custom orthotic design. *Gu et al. (2008)* investigated the hind-foot bone impact during a one-leg hoping motion using FE modelling. Most published works have been focusing on normal foot movement; however, many injuries were known to be related to abnormal loading conditions. For example,

metatarsal injuries are known to be directly associated with the inversion angle. It is essential to extend the application of numerical modelling to these abnormal positions such as inversion, which requires much more complex FE models regarding the details of the structure, materials properties, loading and boundary conditions.

The human foot is a complex structure and the contribution of each part (i.e. bone or tissue) may alter for different movement. A detailed foot model could potential provide a better understanding of the internal deformation therefore a more realistic representation of the foot movement/deformation. However, most published works have used simplified geometry with relatively restricted joint movement, and simplified material properties *(Jacob and Patil, 1999; Kitagawa et al., 2000; Chen et al., 2001; Gu et al., 2005; Goske et al., 2006)*. These approaches could adequately simulate a normal foot movement but a more detailed model is required for conditions such as inversion landing. The model has to be able to simulate the bone structure, which has not been sufficiently represented in the current FE models available.

2.8 The mechanical behaviours of plantar soft tissue

2.8.1 Material properties of biological materials

The behaviour of materials subject to tensile/compression forces can be described by a stress-strain graph. Figure 2.17 shows schematically the three main type of stress strain relationships in soft materials (such as rubber, foams and biological tissues), namely linear elastic (a), elastically non-linear (b) and viscoelastic (c). For an elastic material, the stress is proportional to strain, the strain is recoverable if the stress is removed, i.e. the specimen returns to its original dimensions. This occurs in the initial linear region of the stress-strain curve of flexible foams and some rigid foams. A linear elastic relationship between compressive or tensile stress and strain can be described by:

$$\sigma_x = E\varepsilon_x \qquad (2.8.1)$$

where the constant E is the Young's modulus.

The absolute value of the ratio of the lateral strain to the longitudinal strain is the Poisson's ratio:

$$v = -\frac{\varepsilon_y}{\varepsilon_x} \qquad (2.8.2)$$

At small strain, for both compression and tension, the average experimentally observed Poisson's ratio, v, of foams is about 0.33. At larger strains it is commonly observed that Poisson's ratio is effectively zero during compression — the buckling of the cell walls does not result in any significant lateral deformation. However, during tension, the Poisson's ratio is non-zero, which is a result of the alignment and stretching of the cell walls. For an isotropic material, the shear modulus G can be calculated using:

$$G = \frac{E}{2(1+v)} \qquad (2.8.3)$$

As shown in Figure 2.17 (b), non-linear relationships between stress and strain are usually convex upwards in compression (compressive stresses and strains are taken to be positive). For foam or biological tissues, the non-linearity occurs due to changes in

its geometry at high strains *(Ren and Silberschmidt, 2008)*. At small strains the material deforms in a linear, elastic manner as a result of cell wall bending. At large strain, the cell walls rotate and align, resulting in an increased stiffness. The walls are substantially aligned at a tensile strain of about 0.33. When the material is under cyclic loading, it will exhibit a typical viscoelastic material behaviour illustrated in Figure 2.17 (c). This is a type of deformation exhibiting the mechanical characteristics of viscous flow and elastic deformation. Most foam materials and biological material exhibited highly nonlinear and viscoelastic behaviors *(Mills et al., 2003)*. Nonlinear material behaviour is significantly different from linear deformation and it has to be understood based on the nonlinear mechanics.

2.8.2 The basics of non-linear continuum mechanics for FE analysis

Deformation gradient

In continuum mechanics, an initial configuration k^0, and a deformed configuration k^t of the considered continuum has to be considered.

$x \in k^t$, is the corresponding configuration mapping of the initial configuration $X \in k^0$ transformed through a displacement vector $u(X)$.

$$x = u(X) + X \qquad (2.8.4)$$

$$x = \varphi(X,t) \qquad (2.8.5)$$

The components of the total differential dx is given in terms of the components of dX and the partial derivatives of φ by Atkin and Fox *(1980)*.

$$dx_i = \frac{\partial \varphi_i(X,t)}{\partial X_A} dX_A = \varphi_{i,A} dX_A \qquad (2.8.6)$$

The quantities $\varphi_{i,A}$ are known as the deformation gradients. They are the components of a second-order tensor known as the deformation gradient tensor denoted by F.

$$F_{iA} = \varphi_{i,A} = \frac{\partial x_i}{\partial X_A} (i, A = 1,2,3) \qquad \text{or} \qquad F = \frac{\partial \varphi}{\partial X} = \frac{\partial x}{\partial X} \qquad (2.8.7)$$

Where F is the deformation gradient tensor with component $F_{i,4}$. By the rules of index notation that F is a second order tensor, since it has two independent indices. It is also important to note that F is not symmetric. The deformation gradient tensor can also be written in matrix format as:

$$F = \begin{pmatrix} F_{11} & F_{12} & F_{13} \\ F_{21} & F_{22} & F_{23} \\ F_{31} & F_{32} & F_{33} \end{pmatrix} = \begin{pmatrix} \dfrac{\partial \varphi_1}{\partial X_1} & \dfrac{\partial \varphi_1}{\partial X_2} & \dfrac{\partial \varphi_1}{\partial X_3} \\[2mm] \dfrac{\partial \varphi_2}{\partial X_1} & \dfrac{\partial \varphi_2}{\partial X_2} & \dfrac{\partial \varphi_2}{\partial X_3} \\[2mm] \dfrac{\partial \varphi_3}{\partial X_1} & \dfrac{\partial \varphi_3}{\partial X_2} & \dfrac{\partial \varphi_3}{\partial X_3} \end{pmatrix} \qquad (2.8.8)$$

The deformation gradient is the most basic object used to quantify the local deformation at a point in a solid.

Assuming the Jacobian exists at each point of deformed configuration, which physically can be interpreted as the ratio of the undeformed volume over the deformed volume for a homogeneous deformation at a material point.

$$J = \det(F) > 0 \qquad (2.8.9)$$

Then the material of the body cannot penetrate itself, and that material occupying a finite non-zero volume in initial configuration cannot be compressed to a point or expanded to infinite volume during the motion *(Atkin and Fox, 1980)*. Assuming that a volume element dV_0 in initial configuration deforms into a volume element dV in deformed configuration where

$$dV = JdV_0 \qquad (2.8.10)$$

Let ρ denote the density of the body in the deformed configuration and ρ_0 the density in initial configuration. Then the next equation should exist

$$J = \frac{\rho_0}{\rho} \int_v \rho dV = \int_{v_0} \rho_0 dV_0 \qquad (2.8.11)$$

So

$$J = \frac{\rho_0}{\rho} \qquad (2.8.12)$$

Where ρ_0 and ρ are the initial and deformed material densities, respectively. For an incompressible material, J=1 for all admissible deformations *(Weiss and Gardiner, 2001)*.

Strain energy functions

Strain energy refers to the Potential energy stored in a body by virtue of deformation. If the material is perfectly elastic the strain energy is equal to the work that must be done to produce both normal and shear strains. Once the stress causing the strain is removed, the strain energy is recovered. The recovery is total for perfectly elastic material and partial for plastic material due to energy dissipation. The strain energy function, *W*, is a function which relates the strain of a material to the energy developed by this deformation. Such a function is only properly defined for elastic material. Strain energy density (*U*): Strain Energy Density (SED) is strain energy measured per unit volume of the body. SED represents a better indication of the material since it is normalized to the size of the body. The strain energy function can be viewed as a generalization of Hooke's law that allows us to describe complex elastic components (linear and nonlinear as shown in Figure 2.17) in a systematic way.

Nonlinear elastic materials can undergo a very large deformation generally known as hyperelastic behaviour. For an elastic material, the stress at any point can be defined solely as a function of the deformation gradient F at that point. A change in stress arises only in response to a change in configuration, and the material is indifferent to the manner in which the change in configuration arises in space and time. For a hyperelastic material, the above definition applies, and there is an additional scalar function from which the stress can be derived at each point. The scalar function is the stored energy or strain energy function, *W*, which can also be defined solely in terms of the deformation gradient *(Weiss and Gardiner, 2001)*.

$$W = \tilde{W}(F) \qquad (2.8.13)$$

The strain energy, W, must obey the Principle of Material Frame Indifference. This principle ensures that rigid body motions will not change the value of the strain energy function. Consequently, W may be expressed in the form

$$W = \tilde{W}(C) \qquad (2.8.14)$$

where C is the right Cauchy-Green strain tensor. Then, the second Piola-Kirchhoff stress is derived directly from the strain energy as

$$S = 2\frac{\partial W}{\partial C} \qquad (2.8.15)$$

Hyperelasticity provides a convenient framework for the formulation of constitutive equations for materials such as foams or biological soft tissues because it allows for large deformations and anisotropy *(Weiss and Gardiner, 2001)*.

Any hyperelastic material maybe represented by a strain energy function. For Hookean (linear) elastic materials, this takes the following form:

$$W = W(I_1, I_2, I_3) \qquad (2.8.16)$$

Where

$$I_1 = trC; \qquad I_2 = \frac{1}{2}[(trC)^2 - trC^2]; \qquad I_3 = \det C \qquad (2.8.17)$$

The isotropic hyperelastic material reduces to linearised elasticity when appropriate assumptions regarding the magnitude of strains and rotations are made *(Weiss and Gardiner, 2001)*.

For nonlinear Finite Element analysis, the solution process often proceeds by searching for a configuration that is close to a known equilibrium state that provides a balance between incrementally applied loads and the current stress field in the material. In this case, the elasticity tensor plays an important role in the iterative solution process *(Weiss and Gardiner, 2001)*.

2.8.3 Typical testing methods for characterization of mechanical behavior of the plantar soft tissues

Foot soft tissue testing and its interaction with the supporting structure (shoe) is an important research field for sport or medical engineering. The human heel pad is uniquely designed to enable pain-free weight bearing and locomotion *(Rome, 1998)*. It also has the ability to attenuate impact forces at heel strike of the gait cycle so as to protect the underlying calcaneus bone *(Noe et al., 1993; Narvaez et al., 2000)*. All these functions are directly linked to the mechanical behavior of the foot. A detailed understanding of the heel pad mechanics is indispensable, in order to understand its roles as well as injury and medical conditions. In addition, the properties of the heel pad also have great importance in product design in terms of providing stability and comfort for sport shoes and protection equipments. All these require detailed investigation with a proper testing and analysis method.

Examinations of the mechanical properties of the foot soft tissue have been taken two routes: *in vitro* testing and *in vivo* testing. An *in vitro* biological study is carried out on tissues in isolation from a living organism. An *in vivo* biological study is the one taking place within a living biological organism. Both methods have been widely used in many biological systems such as skin and internal organs. The testing method mode can be indentation, compression, tension or torsion depends on the condition of the biological system and the physiological condition of the organ *(Serup and Jemec, 1999; Ren et al, 2005, 2006)*.

In vitro tests of the foot soft tissue

Figure 2.18 (a) shows the setup of an *in vitro* compression test on the foot soft tissue *(Ker, 1996)*. The heel specimen with skin, fatty tissue and calcareous were separated from the subject and loaded with a metal plate attached to an actuator. The pad is covered by plastic cling film to avoid risk of drying. This approach was also used by

other researchers *(Aerts et al., 1995)*. As shown in the Figure 2.18 (a), the skin of the heel impacts against a horizontal circular plate of 64 mm diameter. The load and displacement are monitored representing the resistance of the heel to the compression loading. Typical force displacement data is shown in Figure 2.18 (b). Both the loading and unloading curves are highly nonlinear with significant stiffening at high strain level and hysteresis loop. The *in vitro* tests are similar to conventional material tests once the sample is ready, however, one major problem with *in vitro* studies lies with the fact that the tissue no longer has the same physiological properties as *in vivo* situation due to the loss of water etc.

In vivo tests of the foot soft tissue

In vivo tests are performed on biological tissue in its natural state with the material behavior close to the real physiological condition. It has been increasingly used to study the deformation of biological tissue such as human skin, biological organs, heel pad as well some internal organs. The most frequently encountered techniques included tension tests, compression tests, torsion tests, suction tests or indentation tests *(Gunner et al., 1979; Sugihara et al., 1991; Tong et al., 2003; Pailler-Mattei and Zahouani, 2006)*. Two most suitable methods for heel tests are the compression and indentation tests.

Figure 2.19 shows a typical set-up of *in vivo* compression testing of the human heel pad *(Tong et al., 2003)*. The test rig used includes a base plate, a support frame with a see-through Perspex foot mount plate attached to it, a foot rest jig incorporating a linear lead screw slide unit with a rotating handle at the end of it and a L-shaped plate which supports the probe holder with the ultrasound transducer probe. A force transducer and linear variable displacement transducer (LVDT) measured the compression force and displacement. Velcro straps are used to restrain patient foot movement relative to the test rig. The heel pad thickness at unloaded condition (TU) and loaded condition (TL) was measured using Ultrasound.

Klaesner et al. (2001) used a portable indentation device to determine the force displacement data on soft tissue in a clinical setting. In the test, the foot is stabilized using clay to minimise movement of the metatarsals and the stiffness can be measured using the indentation test (r=4mm indenter was used). The data is then used to calculate the effective Young's modulus for the tissue using equations derived by *Zheng et al. (1999)*. The test is convenient to perform, however, the results of the approach were in a wide range of values, dependent upon the portion of the curve used as shown in Figure 2.20. This clearly shows that the stiffness is strongly strain level dependent, which made the interpretation of indentation data more difficult. It also made it difficult to directly compare results from different sources.

2.8.4 Combined numerical and experimental method and inverse FE mdeolling

Recently, some effort has been made to use non-standard tests under more complex conditions to determine the material parameters. The uses of a range of tests have been explored including suction, tension, torsion, bending test or indentation *(Vannah and Childress, 1996; Vescovo et al., 2002; Mattei and Zahouani, 2004)*. Generally, these tests involve applying a predefined stress /deformation on the sample surface and monitor the displacement/load. In the case of indentation test, an indenter is pressed onto the sample surface and the force-indentation depth data is used to represent the resistance of the material. This method is convenient to use and requires smaller testing areas than other testing methods. In addition, the loading mode is directly relevant to the human perception of materials softness. These made it attractive method for application in biomedical or sport engineering *(Bader and Boeker, 1983; Erdermir et al., 2006)*. Conventional hardness test, such as the Shore method, requires special samples (at least 6 mm thick) and the method only provides information about the hardness of a sample, which could not be directly used to model the detailed material behaviours in service. Recent development of continuous indentation method has greatly improved the information can be determined from indentation tests for different type of materials *(Giannakopoulos, 2006; Vandamme*

and Ulm, 2006). In an indentation test, the stress and strain is not well defined, so it could not be used to directly determine the material parameters. Recent development of inverse modelling techniques opened up the possibility to combine indentation test and FE modelling (simulating the test itself) to derive the material parameters *(Delalleau et al., 2006; Erdemir et al., 2006)* through inverse FE modelling. In this process, the material properties are determined by using FE modelling to find out an optimum material sets which match the experimental test data. The searching and optimisation process is associated with setup of the experimental works and the inverse program.

Kauer (2001) applied an interactive inverse modelling method with suction tests to determine the linear material parameter of the human skin. In this work, the experimental data is the pressure displacement data. The parameters in FE models of the suction test were varied until a close match between the experimental results and numerical was reached. Gerard *et al. (2005)* employed similar iterative optimal method with indentation experiments characterizing the mechanical behavior of the human tongue. To determine the constitutive law from this indentation experiment, i.e. the global relationship that can be assumed between strain and stress inside the body, an optimization algorithm based on an *"analysis by synthesis"* strategy was elaborated. It consisted of (1) assuming a given constitutive law, (2) building a FE analysis of the indentation experiment, (3) comparing the simulations provided by this FEA with the indentation measurements, (4) using this comparison to propose a change of the constitutive law that should bring the FE analysis simulations and the measurements closer, and (5) starting again with (2) up to the point where the comparison carried out in (3) gives satisfactory results *(Gerard et al., 2005)*. Recently, *Ren et al. (2006)* developed parametric approach for determine the results from *in vivo* surface testing. The approach is shown in Figure 2.21. The involved a two-staged approach using a rough range data first then refines the material. This method could effectively reduce the amount of computational works required but the approach has to be based on a good pre-knowledge of the materials. Recently this has been successfully used in

prediction the elastic and plastic properties of welded structures *(Kong et al., 2008)*. For soft tissue such as the heel tissue, this approach represents a simple approach for subject specific biomechanics works.

2.9 Foot deformation and injuries in normal and abnormal landings and footwear development

As shown in the previous three sections, recent research works in biomechanical tests; numerical modelling and material testing method have greatly enhanced the understanding of human movements (such as walking, running, jumping, dancing, etc.) and the technological development in sport engineering *(Tong et al., 2003; Burns et al., 2005; Gu et al., 2008)*. Many of these research work involved investigation of the mechanical deformation of the materials and stress/strain distributions within the structures through FE analysis. The information obtained from numerical modelling could provide important information/data for injury diagnosis, prevention or footwear development *(Gefen, 2000; Goske et al., 2006)*. Due to the fact that the foot structure and properties may vary between subjects, which could directly influence the modelling results for certain conditions, it is essential to develop subject specific model with realistic structure and material properties to be able directly correlate the modelling to subject specific biomechanical tests. This will enable the investigation of more complex loading condition such as inversion lading and development of subject specific footwear.

Landing is an important human movement, which involved the interaction of the forefoot with the ground. One critical part of the foot prone to injuries is the metatarsal regions in the forefoot. Many research works have experimental studied the functions of the system and structural factors causing metatarsal fractures *(Ekrol and Court-Brown, 2004; Popovic et al., 2005; Raikin et al., 2008; Madarevic et al., 2009)*. Landing at an inversion angle is an important factor which potentially could affect the metatarsals deformation and injuries *(Raikin et al., 2008)*, however, most published studies on landing at an inversion angle have been focused on ankle ligament and ankle sprain during this abnormal movement *(Watson, 1999; Pontaga, 2004)*. The effect of inversion angles on the deformation of the metatarsals is still not well understood. Most of published research works on biomechanical landing tests and

numerical simulation have been focused on the foot deformation in normal gait, which may not truly represent the complex loading situation the foot experiences in real landing conditions. It is essential to establish the mechanical response of the forefoot and the metatarsals at different inversion positions through a research program combining subject specific modelling and controlled biomechanical tests.

As detailed in section 2.4, custom made footwear development is currently an active research field, in which subject specific modelling could used as a effective tool for different purposes (such as comfort, safety, performance, pressure management, etc.). One important area is the pressure relief of the heel region during heel strike. Heel pad of the foot plays an important role for load bearing and protection to the underlying tissue and bones (*De Clercq et al., 1994*). The high pressure of the heel region was also related to many foot problems such as heel spurs (*Aldridge, 2004*), plantar warts (*Schon et al., 1993*) and plantar ulcers (*Busch and Chantelau, 2003*). Most of research works have been based on generic shape design optimisation of the insole without considering structural difference of the subject in some key bone structures (*Goske et al., 2006*). A subject based design approach of the midsole structure could potentially further improving the pressure distribution by combing subject specific imaging data with computational modelling. One potential concept is to use soft materials in the under the calcaneus area (UCA) of the midsole. The calcaneus is the main bone in the hind foot and its size is known to directly influence the loading bearing functions of the lower limb (*Gefen and Seliktar, 2004*). This requires an integrated research approach with materials testing, biomechanical tests and FE modelling to establish the effect of UCA plugs and main factors (such as sizes and materials) affecting the performance in pressure relief.

Figure 2.1 Structure of the human foot showing the three main regions: Hind foot, Midfoot and Forefoot (Vonhof, 2006).

Figure 2.2 Main bones of the foot (Schuenke et al., 2006).

Figure 2.3 Tendons of the Foot (Schuenke et al., 2006).

Figure 2.4 Lateral view to show the main lligaments of the Foot (Platzer and Kahle, 2004).

Figure 2.5 Plantar fascia (Platzer and Kahle, 2004).
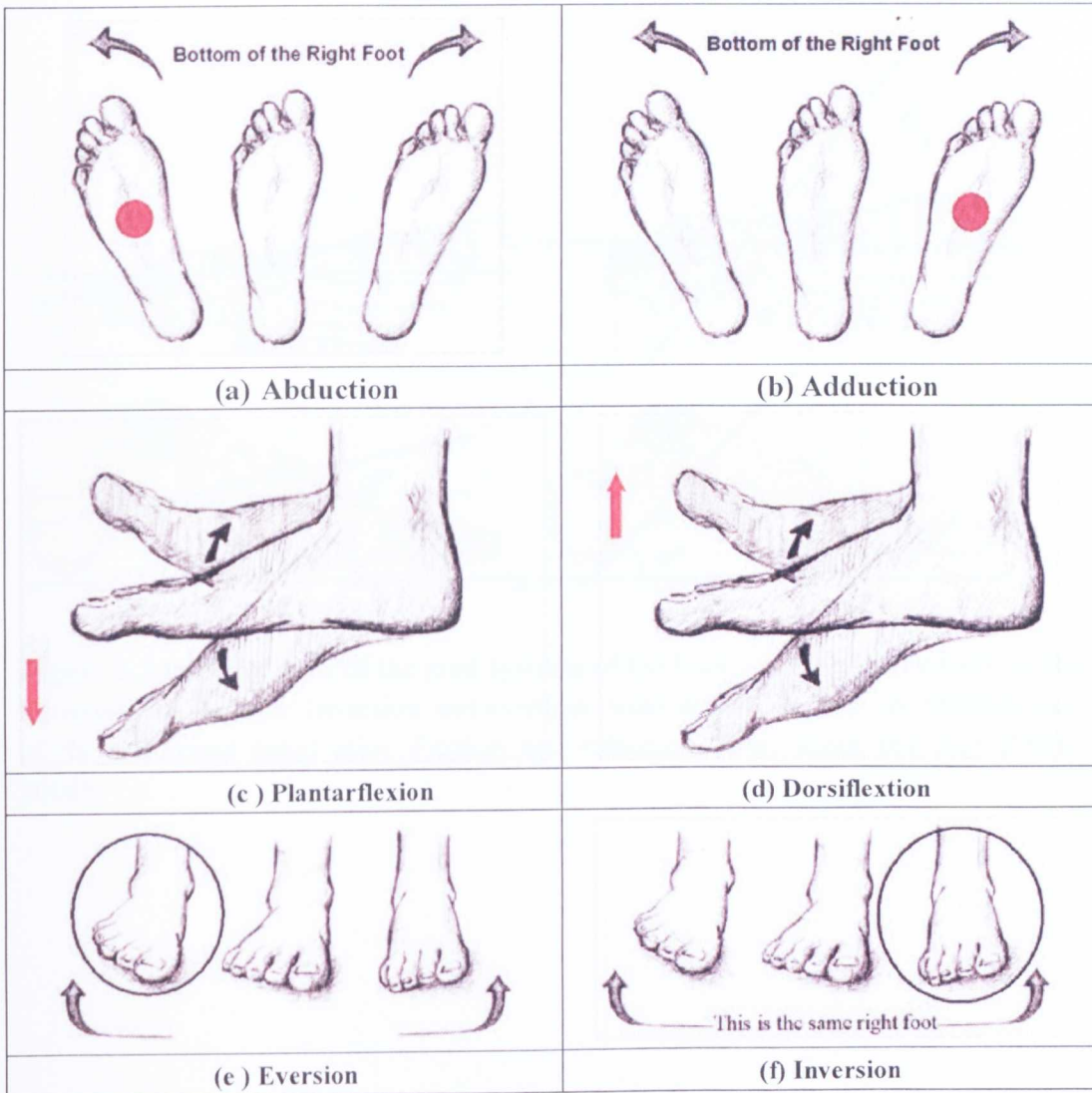
Figure 2.6 Typical movements of the foot in different planes and axes (Mann, 1985).

Figure 2.7 Principal axes of the joint systems of the Foot. (a) Longitudinal axis of the transverse tarsal joint. Inversion and eversion occur about this axis. (b) Oblique axis of the transverse tarsal joint. Flexion and extension occur about this axis (Oatis, 2004).

| (a) Avulsion fracture | (b) Jones fracture | (c) Diaphyseal fracture. |
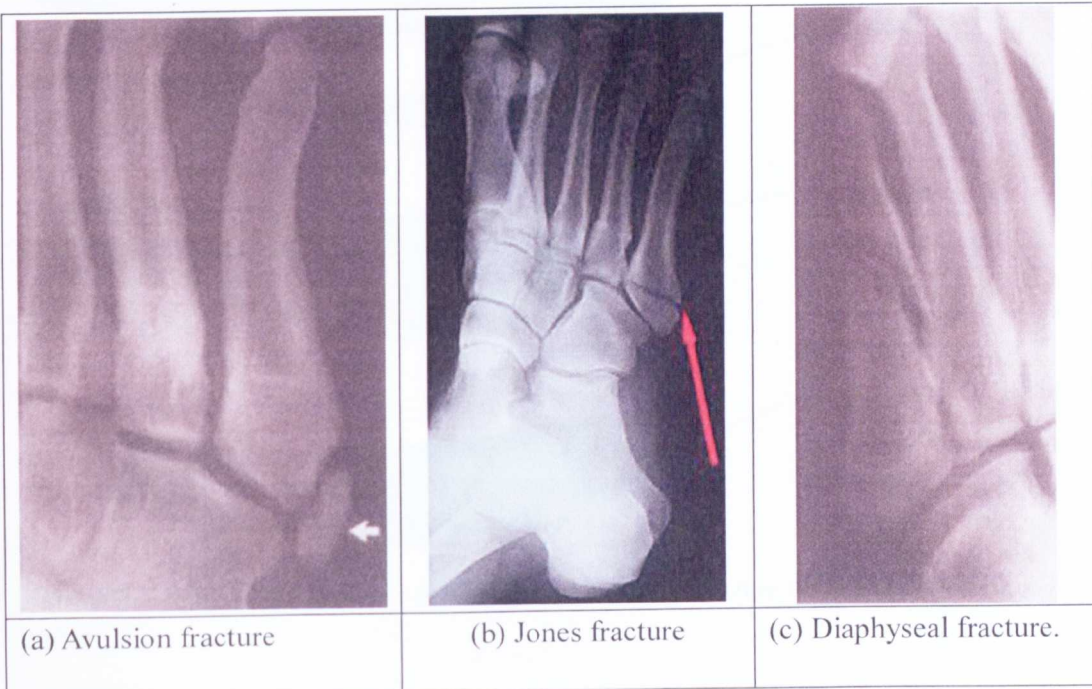
Figure 2.8 CT images showing main fracture types of the fifth metatarsal.

Figure 2.9 Schematics to show the structure of the sport shoe design (Nigg et al., 2006)

Figure 2.10 Example of a flat PPT (open-cell polyurethane foam) insole (A) and a custom made insole used in the study (B). A digital representation of the custom-molded insole with specific characteristics emphasised is shown in (C)(Bus et al., 2004).
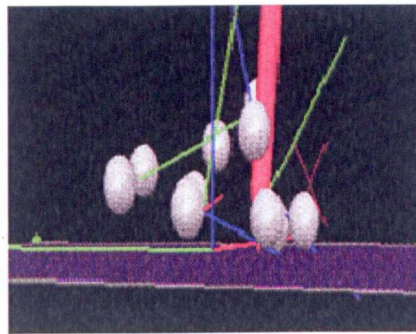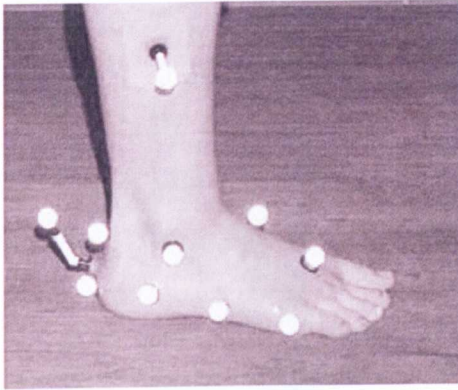
(a) Typical motion analysis system with marker.	**(b)** Typical images showing the movement of the ankle and foot.
(c) Force Platform for jumping tests.	**(d)** Typical reaction force curve in running.
(e) In-shoe pressure system	**(f)** Typical results showing pressure distributions.
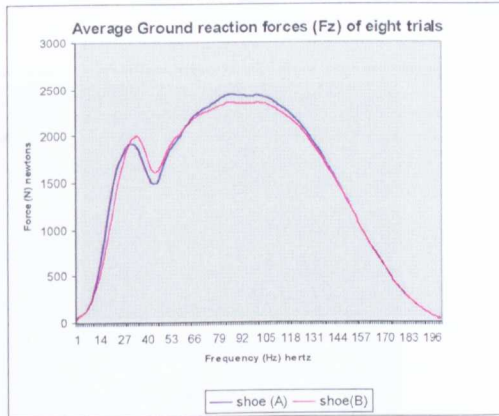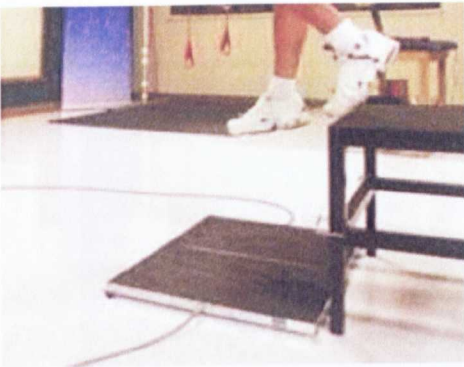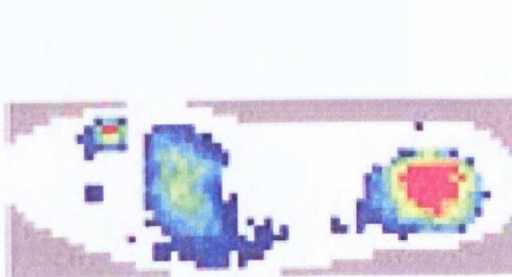
Figure 2.11 Typical experimental biomechanical tests.

Figure 2.12 Typical biomechanical testing methods used for studying foot deformation: (a) skeletal tracking *in vivo* (Arndt et al., 2007); (b) cadaveric test (Nester et al., 2007); (c) stereo camera matching (Kimura et al., 2009).

Figure 2.13 Typical imaging methods to study the internal foot deformation: (a) Fluoroscopy (Gefen *et al.*, 2000); (b) Ultrasound (Cavanagh, 1999); (c) Computed Tomography (Smith *et al.*, 2000), and (d) Magnetic Resonance Imaging (Weaver *et al.*, 2005).

Figure 2.14 Typical examples of FE models in human biomechanics.

Figure 2.15 Use of Finite element modelling in predication of the stresses in the
Achilles tendon (AT) during heel strike and push off (Gu *et al.*, 2008).

Figure 2.16 Typical examples of FE modelling of the human foot movements.

(a) Linearly elastic and isotropic

(b) Elastically non-linear

(c) Viscoelastic
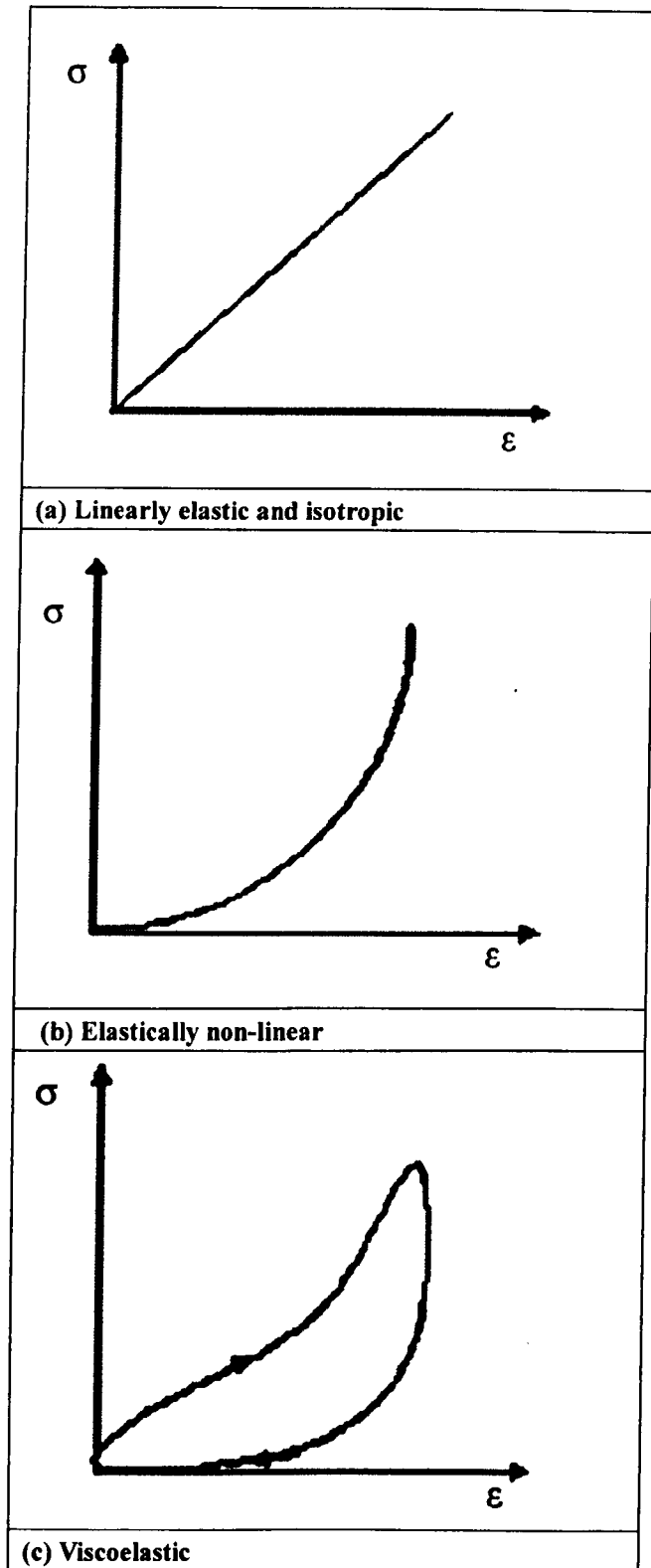
Figure 2.17 Schematics showing linear elastic and non linear elastic material behaviors.

Figure 2.18 *In vitro* testing of the human heel pad *(Ker, 1996).*

Figure 2.19 Test rig in the experimental set-up (Tong et al., 2003).

Figure 2.20 The calculated values for the effective Young's modulus during an entire indention test for the four sites tested on the foot (Klaesner *et al.*, 2001).

Initial screening of the range of E using one result

$v=0$ or 0.495

$E=0.001, 0.01, 0.1, 1, 10$ (N/mm^2)

ABAQUS parametric studies

$v=0, 0.25, 0.499$

$E=0.1, 0.12, 0.13, 0.14, 0.15,$

$0.16, 0.17, 0.18$ (N/mm^2)

Three FE models with the tape

Separation, $t=5, 10,$ or 20 mm

Calculate the error between the modeling and testing results and determine the set of material properties with the minimum average difference
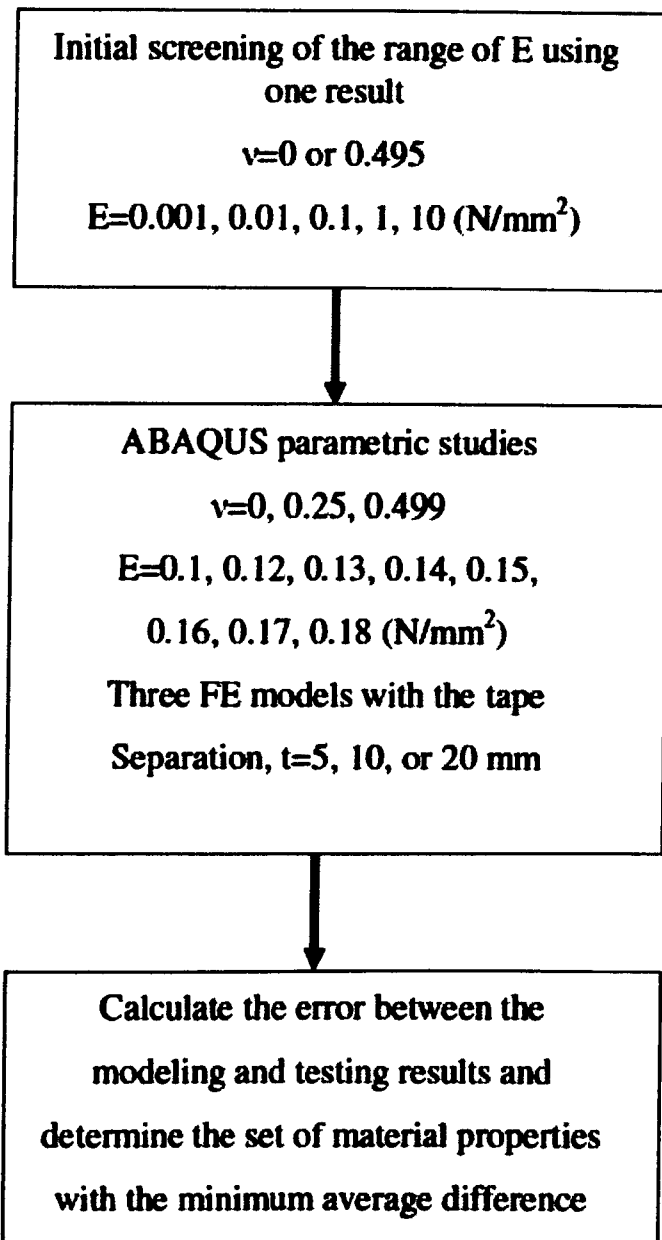
Figure 2.21 The mixed experimental and parametric modelling approach to extract the material properties based on the *in vivo* tensile tests (Ren *et al.*, 2006).

CHAPTER THREE

DEVELOPMENT OF THE FINITE ELEMENT FOOT

MODEL AND APPLICATION IN THE INVERSION

LANDING SIMULATION

3.1 Introduction

This is an integrated approach involving the development of subject specific finite element modelling and biomechanical testing to investigate the deformation of human foot in normal landing and landing with different inversion angles.

The overall research plan for the work is shown in Figure 3.1. In the first part, a subject specific human foot model was developed using 3-D reconstruction techniques based on computed tomography (CT) images in DICOM format in conjunction with computer aided design (CAD) operations. Density segmentation techniques were used to geometrically define key anatomical structures, for example the Achilles tendon, foot bone structure and encapsulated soft tissues. A smoothing technique was applied on to remove the uneven surfaces of some key components caused by the stacking of the medical images. This will ensure that the models are in a stable configuration with minimum error in data transfer, in the mean time, maintaining the dimension accuracy of each part. CAD modelling was used for constructing the geometries of cartilages using the volumes Boolean operations. The finished solid models were then assembled together in a FE package ABAQUS, with detailed material properties. In the second part, the model was used to simulate subject specific *in vivo* indentation tests on the heel pad and the nonlinear material parameters of the soft tissue were determined using parametric studies. The FE foot model was then used to simulate the controlled balance standing tests and the optimum mesh scheme was established by mesh sensitivity tests. The numerically predicted plantar pressure distribution was compared to the experimental results for validation purpose.

The validated model was then used to simulate the forefoot deformation during landing at normal landing and landing with an inversion angles. Subject specific biomechanical data was used to further validate the FE prediction of the landing data. Large subject group biomechanical tests were also performed at normal landing and

inversion landing under controlled testing conditions. The pressure distribution, maximal force and force time integral of the five metatarsals were calculated. The stresses in the soft tissues and the metatarsals under normal landing and inversion landing were predicted and the effect of the inversion angle was established. Finally, the significance of the work was discussed with reference to some clinical observation on metatarsal injuries and potential use of the model is discussed.

3.2 Development of a geometrically detailed 3-D human foot

As shown in section 2.1-2.3, the human foot is a complex structure and an FE model needs to incorporate the necessary details, whilst at the same time achieve optimum computational performances. Figure 3.2 is a flow chart showing the procedure used to convert CT images into solid and FE models. The foot anthropometrical definition was based on images from CT scan of the foot of the subject (28 years old male) using Phillips Brilliance CT equipment (Phillips Medical Systems, Best, Netherlands). The DICOM images generated in the CT scan were then processed with a medical imaging and editing software (MIMICS 10.01, Materialise, Leuven, Belgium) that manipulates density segmentation techniques. The generated primary 3-D models were then exported as geometrical files to a reverse engineering system (Geomagic 9.0, Research Triangle Park, NC, USA) used to smooth each parts before transferring the models into a design program Solidworks 2007 (Solidworks corporation, Massachusetts, USA). Finally, the CAD model was exported to a non-linear FEM/FEA package (ABAQUS 6.8, SIMULIA, RI, USA). Details of each stages and key procedural parameter/operation used are detailed below:

3.2.1 CT images and processing

The model was constructed based on CT scan of the left foot of the subject (male, normal arch, age 28 years, height 176 cm and weight 72 kg). The subject has no clinical history of foot instability, any neurological or musculoskeletal disorders. Coronal CT images were taken with space intervals of 1.25mm in the neutral unloaded position, and a field of view of 137.5mm (110 slices in total). Figure 3.3 shows typical CT slice for the forefoot, midfoot and the hind foot regions. These DICOM image generated from the CT scan are constituted by pixels with different gray intensities. The different intensity fields correspond to different material densities presented at the anatomic foot structure. The 3-D reconstruction of each bone segment was accomplished with manual editing operations using density masks. Every

acquired CT slice is subdivided into a matrix of up to 1024 × 1024 volume elements (voxels) and each voxel has been traversed during the scan by numerous X-ray photons and the intensity of the transmitted radiation measured by detectors. From these intensity readings, the density or attenuation value of the tissue at each point in the slice can be calculated. Specific attenuation values were assigned to each individual voxel. The viewed image was then reconstructed as a corresponding matrix of picture elements (pixels). Each pixel was assigned a numerical value based on the average of all the attenuation values contained within the corresponding voxel, this can be then used in the image. Segmentation process to develop the model for each key part as detailed in the next section.

3.2.2 Volume Segmentation (image analysis)

Image segmentation is a critical procedure in developing the foot model, in which each anatomical structure or the region of interest was delineated and separated from the surrounding structures form individual part. In this process, each CT scan image was partitioned into multiple regions (sets of pixels), according to a given criterion such texture or intensity. If the domain of the image is given by I, then the segmentation problem is to determine the sets or masks $S_k \subset I$ whose union is the entire image I. Thus, the sets (masks) that make up a segmentation must satisfy

$$I = \overset{K}{\underset{k=1}{U}} s_k \qquad (3.1)$$

Where for $S_k \cap S_j = 0$ for $k \neq j$, and each S_k is connected. Ideally, a segmentation operation could identify those sets that correspond to distinct anatomical structures or regions of interest in the image.

Figure 3.4 illustrates the procedure used in the segmentation process of bones in a typical CT slice. A thresholding operation based on the grey scale represented by Housfield units was used to separate each bone from other structures and define the area of encapsulated soft tissue. The thresholding value was selected/established

based on the grey scale bar of different structures as shown in Figure 3.4b *(Bushong, 2000)*. In order to cover all the cortical and trabucular bone at the foot bone structure and exclude the cartilage regions, a lower limit of 250HU and an upper limit of 1000Hu were defined. The soft tissues region was generated accounting a lower limit of -200Hu and an upper limit of 1000HU. Following this procedure, the bone structure in this slice can be clearly separated from the surrounding tissues (Figure 3.4c).

3.2.3 Region growing and 3-D construction

Figure 3.5 shows the procedure in the next stage of image processing region growing and 3-D construction of individual parts. Due to the effect of imaging noise, further segmentation of the density masks is normally required which allows the posterior generation of independent geometrical files and 3-D models. In this work, some manual operations to eliminate residual pixels nominally at cartilages regions were conducted. Cavity fill operations were performed for eliminating the voids at the density masks to obtain independent and smoother primary models. For a better visualisation of internal boundaries in the density masks, polylines were generated using the "Cavity Fill from polylines" tool (Figure 3.5) in order to eliminate mask's internal voids.

The region growing process involved the segmentation of each individual part by assigning each part to one mask, distinguished with different applied mask's colours. To achieve this geometrical separation the adjacent masks must not be connected with any residual pixel. These operations were performed on all slices generated at the CT scan. For the final foot model, 30 different regions have been defined including the bones and soft tissues.

In the construction process of the final model, the generated region masks were used to develop the models for each bone and encapsulated soft tissue volume. The

reconstruction is based on 3-D interpolation techniques that transform the 2-D images (slices) in a 3-D model (Figure 3.5c). For this reconstruction case, gray values interpolation was used in conjunction with an accuracy algorithm for achieving a more accurate dimensional representation of the foot structure. Shell and triangle reduction, respectively, were used for eliminating small inclusions and reduce the number of the mesh elements of the FE model. Each region was then reconstructed to form the bones, Achilles tendon and encapsulated soft tissues volume that geometrically defines the foot structure. Each model was exported as an *.STL file allowing for future CAD operations.

3.2.4 3-D CAD modelling

The *.STL files generated detailed in the previous section was then imported into a data editing software Geomagics (Geomagic, Inc., Research Triangle Park, NC, USA) for smoothing the surfaces. This operation is necessary to increase the quality of the computational mesh generated. As illustrated in Figure 3.6, another operation to convert the geometry into Non-Uniform Rational B-Splines (NURBS) format was also performed in this stage. The NURBS curves were created by the use of a regression analysis technique following a procedure commonly used in image processing. Through the procedures, the points are connected in a format that was compatible with the finite element modelling software. It is important to develop a good NURBS geometry so that a high quality meshes can be generated.

All the major foot bones geometry information has been summarised in Table 3.1. All the parts smoothed from Geomagics were processed using Solidworks 2007 (Solidworks corporation, Massachusetts, USA) to form solid models for each foot part. The cartilages that were not reconstructed in the segmentation process were then modeled in order to connect the bones and fill the cartilaginous space. Plantar fascias, between the medial calcaneal tubercle and proximal phalanges of the toes, were created consider the anatomical locations in reference to anatomy books (*Platzer,*

2002). After these modelling process, volume boolean operations were performed to achieve a volume of soft tissues that corresponds to the subtraction of the bone, fascias and tendon structures. This approach, guarantees the perfect alignment of the models exterior surfaces, which is very important to the future finite element model generation. The finished solid models were then imported and assembled in the non-linear FE package ABAQUS (SIMULIA, RI, USA).

Table 3.1 The geometry data of major foot bones.

First proximal phalange		X:24.1 (mm) Y:33.0 (mm) Z: 21.3 (mm)	First distal phalange		X:22.0 (mm) Y:22.3 (mm) Z: 8.9 (mm)
Second proximal phalange		X:17.8 (mm) Y:28.5 (mm) Z: 21.3 (mm)	Second distal phalange		X:10.8 (mm) Y:16.1 (mm) Z: 13.8 (mm)
Third proximal phalange		X:16.9 (mm) Y:26.8 (mm) Z: 7.5 (mm)	Third distal phalange		X:9.0 (mm) Y:13.2 (mm) Z: 12.5 (mm)
Fourth proximal phalange		X:15.7 (mm) Y:25.3 (mm) Z: 7.4 (mm)	Fourth distal phalange		X:8.9 (mm) Y:13.5 (mm) Z: 11.2 (mm)
Fifth proximal phalange		X:12.7 (mm) Y:23.9 (mm) Z: 7.5 (mm)	Fifth distal phalange		X:9.4 (mm) Y:12.5 (mm) Z: 10.0 (mm)
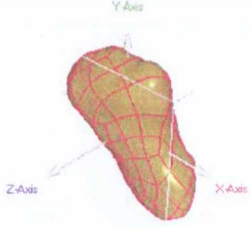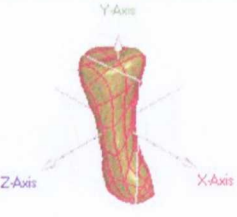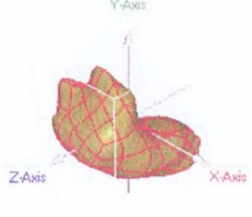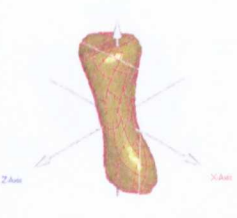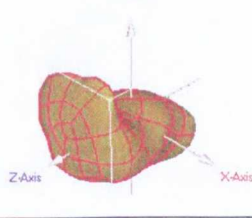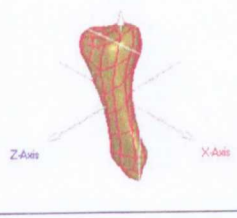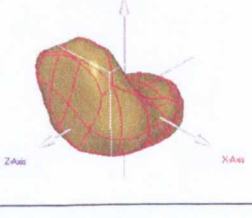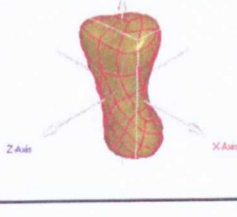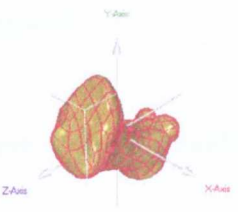
First metatarsal		X:29.3 (mm)	Second Metatarsal		X:19.4 (mm)
		Y:54.4 (mm)			Y:47.8 (mm)
		Z: 52.4 (mm)			Z: 56.3 (mm)
Third Metatarsal		X:19.8 (mm)	Fourth Metatarsal		X:17.5 (mm)
		Y:45.0 (mm)			Y:44.8 (mm)
		Z: 51.2 (mm)			Z: 47.5 (mm)
Fifth Metatarsal		X: 22.9 (mm)	First Cuniform		X: 24.5 (mm)
		Y: 49.7 (mm)			Y: 40.8 (mm)
		Z: 43.8 (mm)			Z: 30.0 (mm)
Second Cuniform		X: 19.6 (mm)	Third Cuniform		X: 23.9 (mm)
		Y: 25.9 (mm)			Y: 26.5 (mm)
		Z: 28.8 (mm)			Z: 25.1 (mm)
Cuboid		X: 29.4 (mm)	Navicular		X: 41.5 (mm)
		Y: 32.9 (mm)			Y: 34.1 (mm)
		Z: 32.5 (mm)			Z: 25.0 (mm)
Calcaneus		X: 47.2 (mm)	Talus		X: 41.9 (mm)
		Y: 76.5 (mm)			Y: 59.8 (mm)
		Z: 41.2 (mm)			Z: 38.8 (mm)
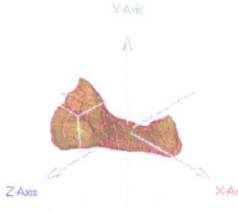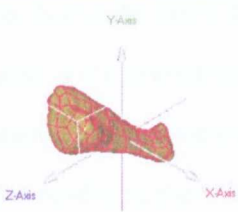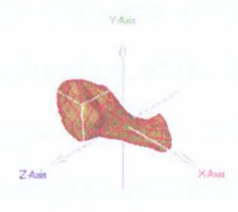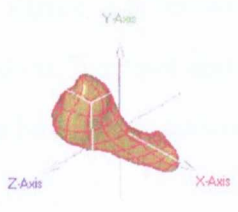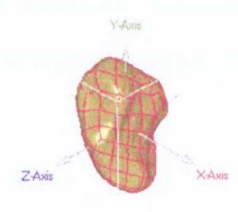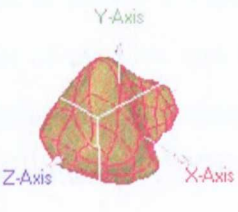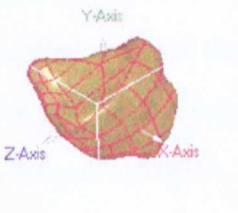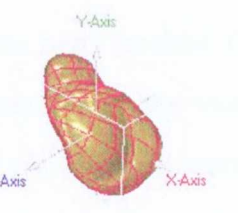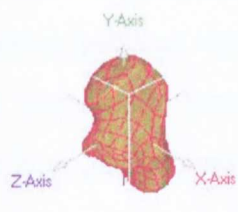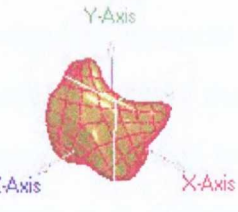
3.3 FE foot model

3.3.1 Structure of the FE model

Figure 3.7a&b shows the bony structure and the soft tissues of the final solid model of the foot. To assess the accuracy of the structure, cross-sectional cut of the foot model at different planes were compared to the original CT images. As shown in Figure 3.8 (a) and (b), the model at the midsection of the foot showed good agreement with the CT images. Figure 3.9 shows the details of the foot structure including bones, cartilage, tendons, ligament and soft tissue. These would provide essential geometrical details for the building an accurate FE foot model.

The FE model, as shown in Figure 3.10, consisted of 28 bony segments, including the distal segment of the tibia and fibula and 26 foot bones: calcaneus, talus, navicular, cuboid, 3 cuneiforms, 5 metatarsals and 14 components of the phalanges. The bone and cartilage structures were bonded together forming a unique structure with different material regions. The plantar fascia is one of the major stabilization feature of the longitudinal arch of the human foot and sustains high tensions during the weight, and the Achilles tendon is also important in transfering the muscle force applied in the calcaneus region. Both Achilles tendon and plantar fascia were boned to the bone through the definition of mesh tie kinematic constraints. Truss elements that have only tension functions capability were also used to simulate ligaments bearing a tension load. Tetrahedral elements which are more versatile to capture the irregular shapes of the bone structure and the encapsulated soft tissues, were used to mesh the model. The foot model is to be used to predict deformation at different loading conditions including heel soft tissue indentation testing, balance standing, normal landing and landing at inversion angles. Corresponding loading and the boundary conditions for each specific condition are detailed in each of the sections.

3.3.2 Material properties of the different foot structures

A significant difficulty for anatomical models resides in selection of the biological material properties, which are most often dependent on the nature of the loading condition, e.g., the loading rate (*Gefen et al., 1999*). The materials properties used must balance the prediction accuracy required and the efficiency of the use of the computational resource and time. All the material constants were listed in Table 3.2. All the data were selected from established literatures. In this work, the bones were treated as an elastic materials, the Young's modulus and Poisson's ratio assigned as 7300MPa and 0.3, respectively (*Gefen et al., 2000*). The soft tissues modeled with different material properties included the cartilage (*Athanasiou et al., 1998*), ligaments (*Siegler et al., 1988*), tendon (*Mow et al., 2000*) and the plantar fascia (*Cheung et al., 2004*).

Table 3.2 Material properties of different parts used in the finite element model.

Component	Young's modulus (MPa)	Poisson's ratio	Element type
Bone	7300	0.3	Tetrahedral solid
Cartilage	1	0.4	Tetrahedral solid
Plantar fascia	350	0.4	Tetrahedral solid
Tendon	1200	0.4	Tetrahedral solid
Ligament	260	0.4	Tension-only truss

3.3.3 Material property of the foot soft tissue

The encapsulated soft tissue is an important part, its deformation has direct influence on the pressure distribution which is a key factor in biomechanical tests. In addition, it is known that the thickness and the properties of the tissue may vary significantly between subjects. So it is essential to use a realistic nonlinear material model and subject specific values. The hyperelastic material model was used to represent the nonlinear and nearly incompressible nature of the encapsulated soft tissue. A second-order polynomial strain energy potential was adopted with the form

$$U = C_{10}(\bar{I}_1-3)+C_{01}(\bar{I}_2-3)+C_{20}(\bar{I}_1-3)^2+C_{11}(\bar{I}_1-3)(\bar{I}_2-3)+C_{02}(\bar{I}_2-3)^2+\sum_{i=1}^{N}\frac{1}{D}(J-1)^{2i} \quad (3.2)$$

where U is the strain energy per unit reference volume; C_{ij} and D_i are material parameters (Table 3.3); J is the volume ratio; I_1 and I_2 are the first and second deviatoric strain invariants. This materials model could effectively capture the nonlinear materials behavior of the material and has been used in other studies *(Cheung et al., 2005; Tao et al., 2009)*. The material property of the soft tissue is an important factor, which is known to be influenced largely by age, sickness, and temperature *(Ledoux and Blevins, 2007)*. In order to assess the validity and tuning of the parameters to be used in subject specific study, an *in vivo* indentation test was carried out on the same subject, who volunteered for the CT scanning. The parameters were predicted from the set which best match the experimental results. Details of the test and results are briefly presented in the next section and the final material parameters are listed in Table 3.3.

Table 3.3 The coefficients of the hyperelastic material used for the encapsulated soft tissue

C_{10}	C_{01}	C_{20}	C_{11}	C_{02}	D_1	D_2
0.08556	−0.05841	0.03900	−0.02319	0.00851	3.65273	0.00000

In vivo **heel pad testing and material parameters identification**

Figure 3.11 (a) shows the testing frame, the position of the indenter and the human heel. In the test, the subject put one foot on top of a rigid platform. The spherical indenter (R=4mm) was moved upward through a hole in the platform to compress the heel pad. An adjustable locking collar with a diameter much larger than the hole was used as one of the mechanical stopper to ensure the indenter will be stopped upon contact with the platform. The system used an actuator (LinMot PS01-23x160) as the driving system, which was mounted on a flexible supporting frame to allow tests in both vertical and horizontal directions. A sensitive load cell (model: LCMS-D12TC-10N) was attached to the moving head of the actuator to monitor the forces during the test. The indentation tests were performed using a spherical indenter made of stainless steel. Indenters with radius 4mm sizes have been used and the force indentation depth data were obtained, which were then used in the inverse analysis.

Figure 3.11 (b) shows the part of the FE foot model of the indentation test. The loading and boundary conditions of the indentation test were developed in the ABAQUS simulating the testing conditions. Hybrid element formulation was used to assure the almost-incompressible constrain for the soft tissue non-linear elastic mechanical behaviour. Rigid element was implemented to define the indenter as the indenter is much stiffer than the soft tissues. Finer meshes were applied in the regions underneath and around the indenter to increase the accuracy of the model. The foot-indenter interface was defined through contact surfaces, to allow the load transmission and relative movement between those two surfaces. In the contact pair, the heel pad surface area was defined as the slave surface and the rigid indenter as the master surface. The friction coefficient between the foot and indenter was set to 0.5 (Erdemir et al., 2005). Sensitivity tests were performed on the influence of mesh size, boundary conditions, and frictional condition, in order to ensure the FE model is accurate with an optimum requirement on computational resources.

The tester was validated against testing on samples (EVA foams) with known material parameters obtained from standard compression and simple shear tests before testing on human subjects (result not shown). Tests on the subject with or without foot trap were compared and showed no significant effect. All the tests were performed under comparable ambient relative humidity (30-35% RH) and temperature (20-23 ^{0}C). The typical testing data in the form of force indentation depth data of the subject with both the loading and unloading curves is shown in Figure 3.12. Figure 3.13 shows the repeated tests on the same subject. There was some scatter of the data but, in general the repeatability was reasonable for *in vivo* tests. Figure 3.14 compared the force-displacement curve from FE prediction with optimised material properties and the experimental results averaged over six repeated tests. The parametric parameters identification process was not shown to perverse clarity of the report. The close agreement with between the numerical and experimental data suggests the heel pad tissue data is valid.

3.4 Biomechanical tests of balance standing and FE simulation

3.4.1 Testing conditions

Figure 3.15 shows the equipment and setup of the balance standing test. In the test, the subject stands on the pressure platform in a neutral state. One purpose of the test is studying the internal deformation of the foot structure in balance standing. Another purpose is to provide biomechanical data for validating foot FE model. Balance standing is a position which is relatively easier to control for the subject than other tests. This will also train the subject up for more complex landing tests.

The plantar pressure data was measured through the Novel emed-x system (Novel GMBH, Munich Germany), which is an automated, digitized pressure platform that analyses pressure, force, and area data along the surface of the foot during static or dynamic movement (Figure 3.15). The resolution of this system is 0.25 sensors/cm^2, and the sensor area of the platform measures 475 mm $\times$ 320 mm, with a total of 6080 sensors, and a pressure range of 10–1270 KPa. Data analysis was conducted with the Novel Database Pro software package (version 11.38, Novel GMBH). In order to achieve a detailed description of foot loading during standing, peak pressure and maximum force were investigated. Before each test, the procedures were explained in detail to the subject who agreed to participate and signed an institutional review board-approved consent form. The subject was familiarized with the procedures and asked not to be concerned with the platform during the standing test.

3.4.2 FE modelling of the balance standing tests and results

Figure 3.16 shows the loading and boundary conditions of FE model for the balance standing tests. To simulate the testing condition, a horizontal rigid plate was modeled in order to represent the ground support (Figure 3.16), which is an effective approach used in biomechanics studies. The foot-ground interface was defined through contact

surfaces, which will allow the load transmission between ground support and foot model. The surfaces interaction definition, allows the generation of a contact pressure field at the foot plantar area. A small-sliding tracking approach associated with a node to surface contact formulation was defined to model the tangential interaction behaviour. The foot plantar surface area was defined as the slave surface and the rigid ground support, as the master surface. An Augmented Lagrange constrain enforcement method was implemented in the definition of the interaction normal behaviour. The friction coefficient between the foot and the plate was set to 0.5 *(Erdemir et al., 2005)*.

A vertical force is applied at the ground support of reference point. Achilles tendon loads are applied at the end of the distal surface of the tendon. However, the value of the Achilles tendon force is not easy to be experimentally measured. For this reason, some analytical assumptions concerning the Achilles tendon load are made in the bibliography, which estimates the Achilles tendon load to be ranging between one half to two thirds of the weight applied on the foot. The study of *Simkin (1982)*, who calculated that the Achilles tendon force should be approximately 50% of the body load during standing was considered for some foot computational models analysis in the literature *(Cheung et al., 2005; Gefen, 2002)*. The vertical reaction force of approximately 370N measured from the Novel emed platform was applied in the ground reference point. Meanwhile, a magnitude of 185N was calculated for the Achilles tendon force, following the model of *Simkin (1982)*. The upper surfaces of the soft tissues, tibia and fibula were fixed in all degrees of freedom (DOF) through the analysis time via a kinematic constrain, while the boundary conditions applied at the reference point load, allowed uniquely the plate movement in the vertical (upper) direction.

Due to complex structure of biological systems, the modelling results were often sensitive on the size of the elements used. The element size has to be sufficiently small to produce accurate results, in the mean time, over meshed models should be

avoided, which may cause significant waste of computer resource and degrade the efficiency of the analysis. In this work, the mesh size has been systematically varied and the effect of mesh densities on the deformation foot positions was studied. As shown in Figure 3.17, the average mesh size of the model was decreased from 9mm to 3mm, the numerical force displacement (movement of the plate) curves were poltted in Figure 3.18 for comparison. It clearly shows that, with reduced mesh size (e.g. mesh 2) of the foot model, the force displacement curves become less sensitive to the mesh density. It also shown in the curve, the mesh size effect is not significant in the initial contact stage before the displacement reaches about 2.8mm with increased deformation or strain level.

Figure 3.19 compares the plantar pressure distribution under normal standing from the Novel emed measurement of the same subject and the FE model. The measurement was conducted on the same subject who volunteered for the CT scanning with which the FE model has been constructed. The plantar pressures measured for this subject during bare foot standing was used to calculate the centre of pressure on the foot and compare the FE predicted plantar pressure distribution in order to validate the model. As shown in Figure 3.19 (a) and (b), the numerically predicted pressure distribution pattern (b) showed reasonable agreement with the experimental result (a). The model predicated peak pressure of 157 kPa and 121 kPa, at the heel region and forefoot region, while the corresponding peak pressure measured by Novel emed were about 175 kPa and 115 kPa in these two regions. The contact areas predicted by the FE model was about 73 cm^2, compared to about 75 cm^2 from Novel EMED measurement during balanced standing.

Results of the FE analysis were presented in terms of *von Mises* equivalent stresses ($\sigma_{v.M}$), which weight the effect of all principal stresses (σ_1, σ_2, σ_3) according to the relation:

$$\sigma_{v.m} = \left\{ \tfrac{1}{2} \left[(\sigma_1 - \sigma_2)^2 + (\sigma_2 - \sigma_3)^2 + (\sigma_3 - \sigma_1)^2 \right] \right\}^{\frac{1}{2}} \quad (3.3)$$

Figure 3.20 depicts the *von Mises* equivalent stresses in the foot bones predicted by the FE simulation and the predicted peak stresses in specific foot bones are tabulated in Table 3.4. The *von Mises* equivalent stresses, which weight the effect of all principal stresses, is commonly used as a indicator of stress level in biomechanical research. As shown in the figure, during balance standing, relatively high stress were predicted at the mid-shaft of metatarsals especially in the second metatarsal. The subtalar joints junctions together with the dorsal junction of the calcaneal-cuboid joint also sustained high stresses. The stresses values were in reasonable agreement with some published works *(Gefen et al., 2000; Cheung et al., 2005)*.

Table 3.4 Peak *von Mises* stresses in the foot bones during balanced standing

Bone	Peak stress (MPa)	Bone	Peak stress (MPa)
1st *Metatarsal*	2.02	Talus	2.83
2nd *Metatarsal*	6.35	Calcaneus	3.03
3rd *Metatarsal*	4.38	Navicular	1.21
4th *Metatarsal*	1.86	Cuboid	1.32
5th *Metatarsal*	1.92	Medial cuneiform	0.52
1st *Toe*	0.42	Middle cuneiform	1.36
2nd *Toe*	0.56	Lateral cuneiform	1.98
3rd *Toe*	0.38	5th Toe	0.08
4th *Toe*	0.12		

3.5 Biomechanical landing tests and results

3.5.1 Experimentals, subjects and testing scheme

The landing test was designed to investigate the characteristics of reaction force and the plantar pressure distribution in vertical landing. During the test, the subject performs a vertical jump then lands on the pressure platform. As shown in Figure 3.21, both normal landing and controlled landing with an inversion angle have also been studied. The difference in pressure distributions between different landing conditions for the same subject would potentially provide important information on the foot deformation during inversion landing. The testing program has also been performed on large group to establish a statistically reliable trend. The FE model validated based on the subject specific data was then used to predict the effect of biomechanical factor (inversion) on the pressure and the stresses of the metatarsals in the forefoot.

Ten healthy young adults volunteered to participate in this study (Table 3.5). All subjects signed informed consent documents prior to participation. All the subjects were free from musculoskeletal injury requiring medical attention for at least 2 years by self-report. None had ever had foot or ankle injury requiring surgery or casting, and all were currently active in collegiate sports.

Table 3.5 Details of the subjects.

Subject	Age (yrs)	Height (m)	Mass (kg)
1	22	1.83	86
2	21	1.74	78
3	22	1.73	76
4	22	1.68	62
5	24	1.79	68
6	21	1.75	65
7	22	1.76	69
8	22	1.80	76
9	20	1.72	65
10	23	1.78	70
Mean(±std dev):	21.9(±1.10)	1.76(±0.04)	71.5 (±7.37)

Novel EMED-x system (Novel GMBH, Munich, Germany) was used to measure the plantar mechanical data in this study. The subjects were asked to create varying the landing position (normal and inversion, Figure 3.21) with barefoot from a box (30cm in height). Each subject was familiarized with the testing procedure by self-selected pace landing from the box several times. In the test, the subjects were instructed not to look down at the platform but to look ahead at a fixed position distant to the platform. Data were collected from six trials, conducted at 3 minute intervals, on the same day for each subject.

Five metatarsals region in the forefoot was divided using the EMED Automask software (Figure 3.22). Using the EMED software, peak pressure, mean pressure, maxim force and force-time integrals, for the various masks were then generated and transferred to a spreadsheet for descriptive statistical reporting.

3.5.2 Biomechanical testing results

Figure 3.23 shows the typical peak pressure distribution of the foot during the whole landing process, while Figure 3.24 display the typical highlight of pressure distribution over forefoot, which experienced the highest pressure during landing. As shown in the figure, the high pressure zone over the forefoot was concentrated in the medial region during the normal landing, while lateral side played a major role during landing at an inversion angle.

Mean values of plantar pressure measurement recorded from the six trials of 10 subjects were obtained and analyzed. During normal landing (Figure 3.25), the second metatarsal had the highest mean pressure among the five regions, with a general decline in peak pressure from the third metatarsal to the first metatarsal, the fourth metatarsal and the fifth metatarsal. For the inversion landing condition, the highest mean pressure was under the fourth metatarsal, with a general decline in peak pressure from the fifth metatarsal to the third metatarsal, the second metatarsal and the

first metatarsal (Figure 3.26). Peak pressure and mean pressure values showed similar trend during normal landing at five regions of metatarsals studied, with biggest difference in the first metatarsal approximately 50% higher than mean pressure (Figure 3.25). The big difference also happened in the first metatarsal region under inversion landing, which experienced 221% higher than the mean pressure (Figure 3.26).

Figure 3.27 shows the maximal force value under normal and inversion landing conditions. The highest force value was found in the second metatarsal and third metatarsal zone during normal and inversion landing, respectively. The fifth metatarsal was the most sensitive area with significant in loading change between these different landing positions, in which the maximal force increased up to from 43N at the normal landing condition to 180N at the inversion landing position, representing an increase of 319%.

The force time integral in the normal landing was highest in the second metatarsal region, followed by the first and third metatarsal regions (Figure 3.28). But the difference in these three regions was not significant, and was approximately in the same level. Observed values of force time integral in the inversion position, the third metatarsal region showed to be the highest, followed by the fourth and second metatarsal regions (Figure 3.28). Comparing to the normal landing, the fifth metatarsal experienced biggest variation and was reduced up to 61%, and the third metatarsal seems approximately not affect by the landing position, almost in the same level.

3.5.3 FE modelling and results

As shown in Figure 3.29, the foot–ground interaction during landing was simulated by using a foot-plate system, this approach is commonly used in biomechanical modelling *(Cheung et al., 2005; Goske et al., 2006)*. Metatarsals internal mechanical

state in the normal landing, and inversion position with 10 degrees and 20 degrees would be investigated.

In order to study the stress distribution in the metatarsals at different inversion angles, a normal force of 410 N extracted from a Novel EMED-x system at the initial forefoot contact during landing was applied to the reference point of the supporting plate, which was allowed to move in the vertical direction only. A force of 206 N was exerted on the Achilles tendon for balance intention. The friction coefficient between the foot and plate was set to 0.5 *(Erdemir et al., 2005)*. The superior surfaces of the soft tissue, distal tibia and fibula were fixed throughout the analysis.

Controlled tests with the foot approach the ground with an inversion angle has been conducted by the subject who volunteered for the CT scan. Foot plantar-flexion was controlled through the height from the bottom of the Achilles tendon (mark attached), and the inversion angle was controlled by the pre-casted wedges, with 10degrees tilt angle (Figure 3.30). In both normal landing and inversion landing tests, the plantar pressure data on the same subject was recorded and data was used to validate the FE model.

3.5.4 Simulation results

Figure 3.31 compared the plantar pressure distribution under normal and 10 degrees inversion landing from the Novel EMED measurement and the FE model. As shown in the contour plots, the numerically predicted pressure distribution pattern (b and d) resembles well with the experimental results (a and c). The data clearly demonstrated the difference between normal landing and inversion landing. During normal landing, a peak pressure of 255 KPa was predicted in the FE model at the second metatarsal head region, while the corresponding peak pressure measured by Novel EMED was about 286 KPa in this region. Under inversion landing, the peak pressure of 276 KPa was predicted in the FE model at the lateral metatarsal head region, while the

corresponding peak pressure measured by Novel EMED was about 292 KPa in this region.

The modelling results from models for normal landing, inversion angle of 10 and 20 degree were compared. The predicted force-displacement data (i.e. movement of the plate) was shown in Figure 3.32. Under identical load, the movement of the plate increased when the foot position was changed from s normal landing to inversion landing in the model. There was an 26% increase in peak vertical deformation with 10 degree inversion landing than that for the normal landing position; while the only 10% increase of peak vertical deformation with 20 degree inversion in comparison to that for 10 degree inversion.

Figure 3.33 shows the distribution of the *von Mises* equivalent stress (VMS) within the metatarsals during landing at different inversion angles. It clearly shows that both the overall pattern of VMS distribution and the stress concentration position are strongly influenced by the inversion angle. As the inversion angle increased from the normal landing position to 20 degrees, the position of the peak VMS shifted from the second metatarsal to the fifth metatarsal. Figure 3.34 plots the peak VMS within the five metatarsals at different inversion angles. Under the normal landing condition, a large proportion of the forces are sustained by the middle metatarsal; the highest VMS is 6.65 MPa at the neck of the second metatarsal, followed by the third (5.83 MPa), the fourth (5.36 MPa), the first (3.69 MPa), and the fifth (2.21 MPa). The VMS distribution varied significantly when the plate approached the foot from an inversion position. The lateral metatarsals began to play a major role in load bearing with the peak VMS point moved to the fifth metatarsal. The peak VMS position within each metatarsal also shifted with increase of the inversion angles. As shown in Figure 3.33, the forces on the lateral fourth and fifth metatarsals at an inversion landing position are significantly higher than that with the normal landing. The FE modelling results suggests that the inversion angle has a significant effect on the load bearing function, plantar pressure distribution and stresses in the metatarsals. Large group tests and

modelling are required in future works to quantify the effects of the inversion angles following the modelling procedure developed in this work.

3.6 Discussion

3.6.1 Use of combine subject-specific biomechanics and numerical modelling approach in studying abnormal landing

FE analyses and biomechanical studies are complimentary techniques to characterise complex biomechanical behavior of the foot and its components. In general, experimental investigations could provide clinically relevant data (e.g. plantar foot pressure, plantar soft-tissue deformation, and various foot deformities) with regards to normal and pathological foot conditions. These studies, however, were not able to assess foot structure as well as internal stress and strain states. The capability of the computational model to predict the internal stress within the bony and soft tissue structures makes it a valuable tool to study the biomechanical behaviour of the foot structure and supporting systems. Once it was verified by experimental data, models could offer detailed information and predict the effects of some key variables as shown by previous works of FE modelling on the mechanics of the lower limb system *(Tao et al., 2009; Goske et al., 2006; Gu et al., 2005; Barani et al., 2005; Erdemir et al., 2005; Chen et al., 2003; Lewis, 2003; Syngellakis et al., 2000; Lemmon et al., 1997; Chu and Reddy, 1995; Shiang, 1997)*. However, there have been very limited detailed studies of using foot FE modelling to evaluate the foot internal structure response during abnormal foot movement. The normal gait with an idealised position of the foot may not truly represent the complex loading situation that the foot experiences in real loading conditions. It is essential to investigate the foot internal structures' mechanical response in abnormal position that was a common factor associated with many foot injuries *(Gruneberg et al., 2003; Willems et al., 2005)*. In this work, this challenging and important problem has been successfully investigated through subject specific FE modelling and biomechanical tests. The FE model developed represents a detailed model based on subject specified dimensions and materials properties used for simulating the deformation of the human foot. The numerical results were directly compared to biomechanical tests, which was

commonly used to assess the accuracy and validity of FE models *(Gefen et al., 2000; Chen et al., 2001)* under controlled conditions. As shown in Figure 3.19, the predicted plantar pressure distribution is comparable to the Novel emed measurement. The stress level predicted for normal landing conditions also agreed with other FE model predications in standing and walking *(Gefen et al., 2000; Cheung et al., 2005)*. The validated model can then be used to achieve objective and quantitative evaluations of the internal deformation of the foot structures.

3.6.2 Effects of varying soft tissue stiffness on the foot plantar pressure

The plantar pressure distribution is an important characteristic in foot mechanics, which is directly linked to some clinical foot problems (such as ulcers). As shown in Figure 3.19, the predicted plantar pressure distribution was in general comparable to the pressure platform measurement. The high pressure regions were confined to the areas beneath the heel and the medial metatarsal heads. This is in good agreement with the commonly observed formation of plantar foot ulcers at the medial forefoot and heel regions of diabetic patients *(Mueller et al., 1994; Raspovic et al., 2000)*. Despite the fact that it is widely used in biomechanics studies, there is limited understanding on the potential effect of the material properties on the plantar pressure. The material properties of the structure were known to be dependent on the subjects or medical conditions. In the soft tissue material sensitivity study (Figure 3.35), the developed FE model was able to predict the effect of varying bulk soft tissue stiffness on the peak plantar pressure of the foot during balance standing. The result showed that the increase in plantar stiffness could lead to an intensified peak plantar pressure. This suggests that stiffer plantar soft tissue will decrease the ability of the foot to accommodate and assimilate the plantar pressures, which can be a possible factor for igniting plantar foot pain and further tissue breakdown and ulcer development. Some of the FE foot model reported in the literature used a much higher stiffness value for the soft tissue stiffness *(Chu and Reddy, 1995; Jacob and Patil, 1999; Chen et al., 2001)*. The value could not fit the *in vivo* indentation tests of the subject, which may

potentially have overestimated the actual plantar soft tissue stiffness, and reduced the adapting ability of the plantar soft tissue to the supporting surface. This will lead to inaccuracy in predicting the plantar pressure and contact area. One significant improve in this work is the use of subject specific testing results from the *in vivo* indentation tests, which could provide much more reliable data for the biomechanical simulation.

3.6.3 Metatarsals response in inversion landing

Fracture of the metatarsal is one of the most common foot injuries, some of these were directly associated with the foot orientation during landing *(Ekrol and Court-Brown, 2004)*. The confined positions, long and narrow shaft structure of these metatarsals and the high plantar pressure underneath the metatarsal heads are probably the direct cause of stress concentration and frequent sites of stress fracture. The present study showed the stress distribution (load supporting) in the metatarsals was significantly different between normal and inversion landing conditions. The changes of the stress conditions with increasing inversion angles were found to vary between each metatarsal. The stress in the lateral metatarsals increased, while medial metatarsals stress decreased, with increasing inversion angles. Peak stress concentration was found to be near the proximal part of the fifth metatarsal during inversion landing.

Both the stress distribution and peak stress could directly affect metatarsals injuries. As shown by the results (Figure 3.33), the stresses level in the second metatarsal was the highest among the metatarsals under the normal landing condition, which takes up a large percentage of the force. This agrees with the finding that the second metatarsal was the most common of the lessor metatarsal heads to become injured *(Weinfeld et al., 1997)*. The modelling results showed that the lateral metatarsal suffered higher forces than the medial ones at an inversion landing position. As shown in Figure 3.33, the forefoot contact force was concentrated beneath the lateral metatarsal heads with

an increased inversion angle. The VMS value in the first metatarsal decreased 71%, while the stress in the fifth metatarsal increased 262% as the foot landing position changed from normal to landing at 20 degrees (Figure 3.36). Results on other inversion angles showed a similar trend. During inversion landing, the forefoot was subjected to a large adduction force and there is a scale limitation of deformation the foot can undertake to invert more, this made the proximal part of the fifth metatarsal acted as a fulcrum causing high stress, which may cause the bone injury. The increased stress level in the lateral metatarsals under inversion condition, in particular in the fifth metatarsal, may potentially be a factor contributing to the high occurrence of lateral metatarsal injuries during inversion reported in clinical studies (*Ekrol and Court-Brown, 2004; Labella, 2007*). For example, the clinical study by *Ekrol and Court-Brown (2004)* found that 67.2% cases among 355 patients with metatarsal injuries were in the fifth metatarsal. This suggests that the prediction of VMS using the current model is viable method to predict the effect of the inversion angle on the stresses in the metatarsals.

3.6.4 Limitation of the work and future development

The FE model developed represents a detailed model based on subject specified dimensions and materials properties from *in vivo* tests. The numerical results were directly compared to biomechanical tests, which was commonly used to assess the accuracy and validity of FE models *(Gefen et al., 2000; Chen et al., 2001)* under controlled conditions. The current model aimed at to investigate the general effect of the inversion angle on the foot deformation, the modelling approaches developemnt are sufficiently accurate and in the mean time efficient in terms of the use of computational resources. There is still several limitations which can be improved to suit more detailed biomechanical studies. For example, homogeneous and linearly elastic material properties were assigned to the bone, cartilage and ligamentous structures. This can be improved by including detailed structures of the structure of interest through submodelling or multiscale modelling based on the current model

establsihed to be able to direct predict the bone damage processes. Another factor to be considered is the boundary and loading condition. In this work, only the Achilles tendon loading was considered while other intrinsic and extrinsic muscles force were not simulated. The load bearing characteristic of foot under different maneuver requires the incorporation of detailed muscular loading, which will be the future development of the FE model. In addition, the current work used a rigid ground in the simulation to set the limit of the effect of the inversion angle (extreme condition as injury is the main concern). The foot-ground model could be improved using a system including the foot-mat-ground three parts, in order to further investigate the effect of the foot contact part material and thickness effects to the inversion landing movement, providing some protective design for reducing foot inversion injury. The FE model established has also laid a good frame work to include viscoelastic material properties of the soft tissue in future studies.

```
┌─────────────────────────────────┐
│ Development of 3-D FE human      │
│ foot model based on subject      │
│ specific CT images               │
└─────────────────────────────────┘
                  │
                  ▼
┌─────────────────────────────────┐        ┌──────────────────────────────────────┐
│ In vivo continuous indentation   │◄──────►│ Simulation of in vivo heel            │
│ tests of the human heel pad      │        │ indentation test and estimate of the │
└─────────────────────────────────┘        │ soft tissue properties by parametric  │
                                            │ studies                               │
                                            └──────────────────────────────────────┘
                  │
                  ▼
┌─────────────────────────────────┐        ┌──────────────────────────────────────┐
│ Biomechanical testing of barefoot│◄──────►│ Biomechanical test of human          │
│ balance standing                 │        │ balance standing. Plantar pressure    │
└─────────────────────────────────┘        │ distribution character investigation  │
                                            └──────────────────────────────────────┘
                  │
                  ▼
┌─────────────────────────────────┐        ┌──────────────────────────────────────┐
│ Biomechanical testing of barefoot│◄──────►│ Development of FE models for          │
│ normal/inversion landing          │        │ simulation of landing at difference   │
└─────────────────────────────────┘        │ inversion angles.                     │
                                            │ Prediction of the pressure and foot   │
                                            │ deformation.                          │
                                            │ Prediction of the effect of inversion │
                                            │ angles on the stresses in the         │
                                            │ metatarsals and the effect of         │
                                            │ materials properties                  │
                                            └──────────────────────────────────────┘
```

Figure 3.1 Flow chart showing the structure of the work for finite element model development and biomechanical testing to study the foot deformation in normal and inversion landing.
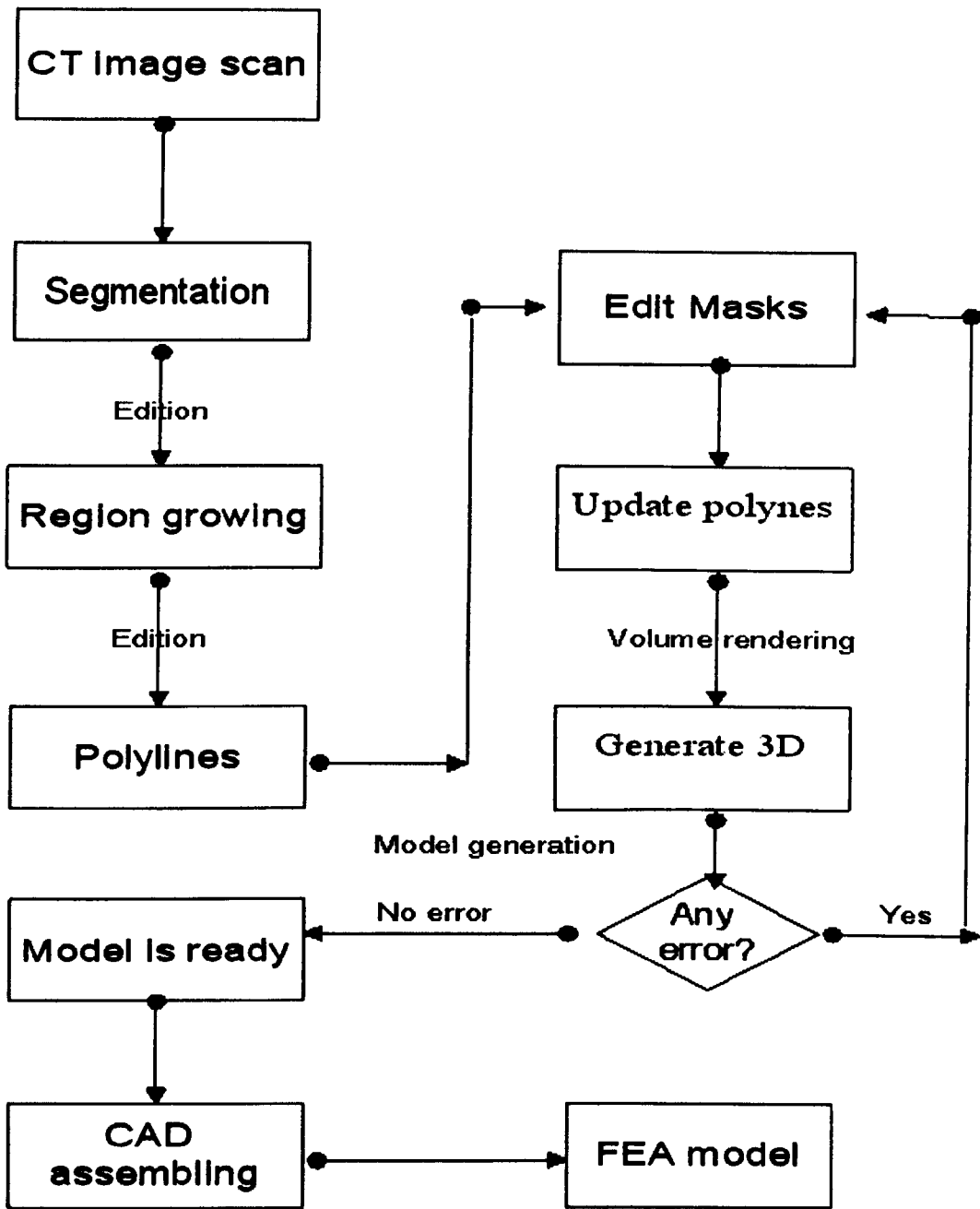
Figure 3.2 Flow chart showing the procedure used to convert CT images into solid and finite element model of the human foot.
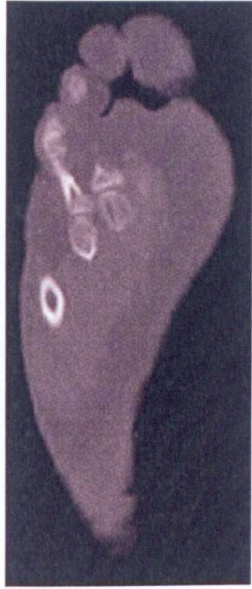
(a) Forefoot (slice number 18)

(b) Midfoot (slice number 46)

(c) Hind foot (slice number 66)

Figure 3.3 Typical CT scan slices of the foot in the forefoot, midfoot and the hind foot.
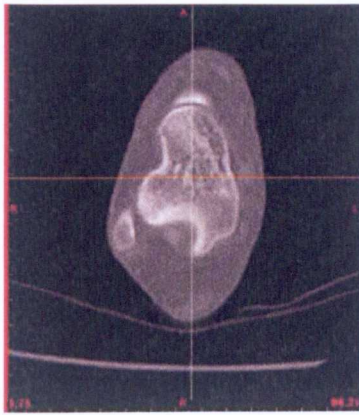
(a)Typical CT slice (Talus position)

Air   Water

|_____|_____|_____|_____|
−1000   −500   0   +500   +1000
                                    Soft tissue   Bone
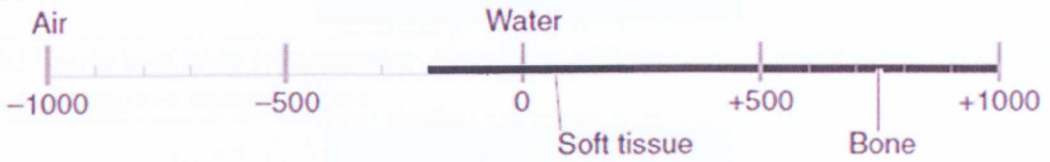
Bone	+250 ⟶ +1000
Soft tissue	−200 ⟶ +1000
Water	0
Air	−1000

(b) The Hounsfield scale of CT numbers used in this work.
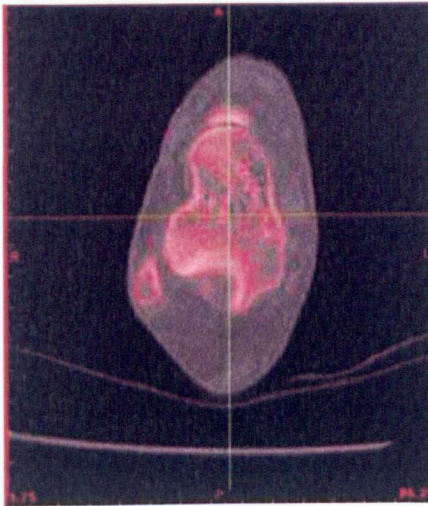
(c) Image after segmentation of the bones

Figure 3.4 Segmentation processes of the structures based on the grey scale. (a) original image; (b) scale of CT numbers used for segmentation of the bones; (c) image after segmentation of the bones.

(a) Example of bone segmentation. Notice that still some extra pixels inside the masks, which requires manual edition.
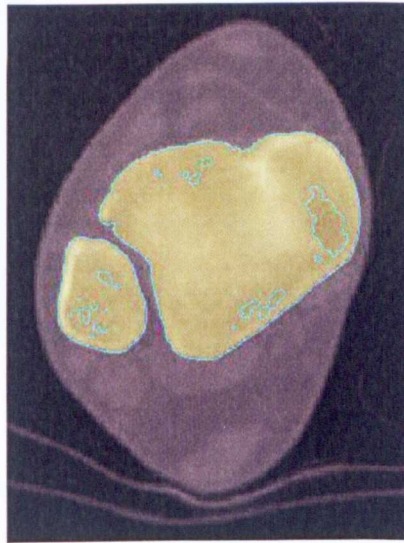
(b) Cavity Fill from polylines tool used to identify gaps, and missing pixels.
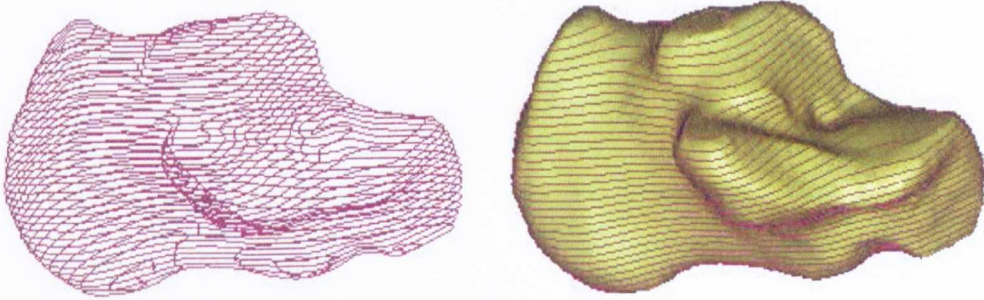
(c) Example of 3-D reconstruction based on the 2-D polylines data.

Figure 3.5 Typical segmentation, cavity filling process and 3-D reconstruction based on the 2-D polylines data.

STL file input

surface smooth

NURBS fit

Grid generation
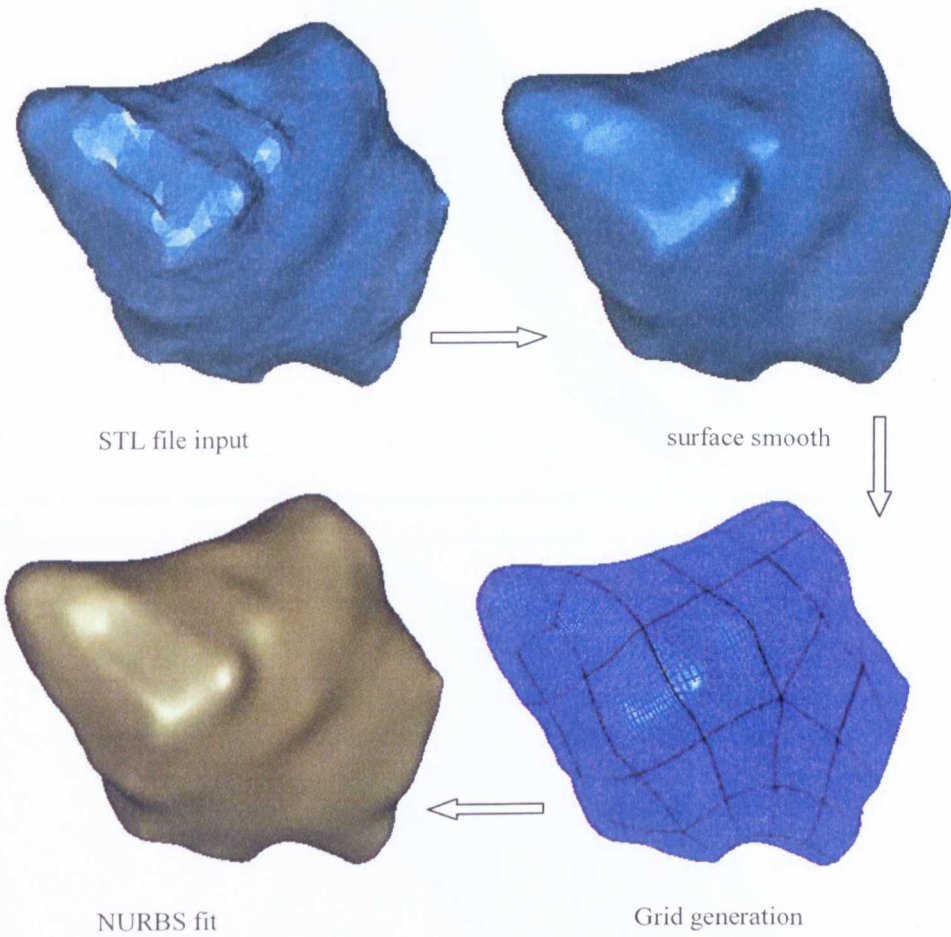
Figure 3.6 Surface smoothing processes for generating the CAD model using reverse engineering approach.
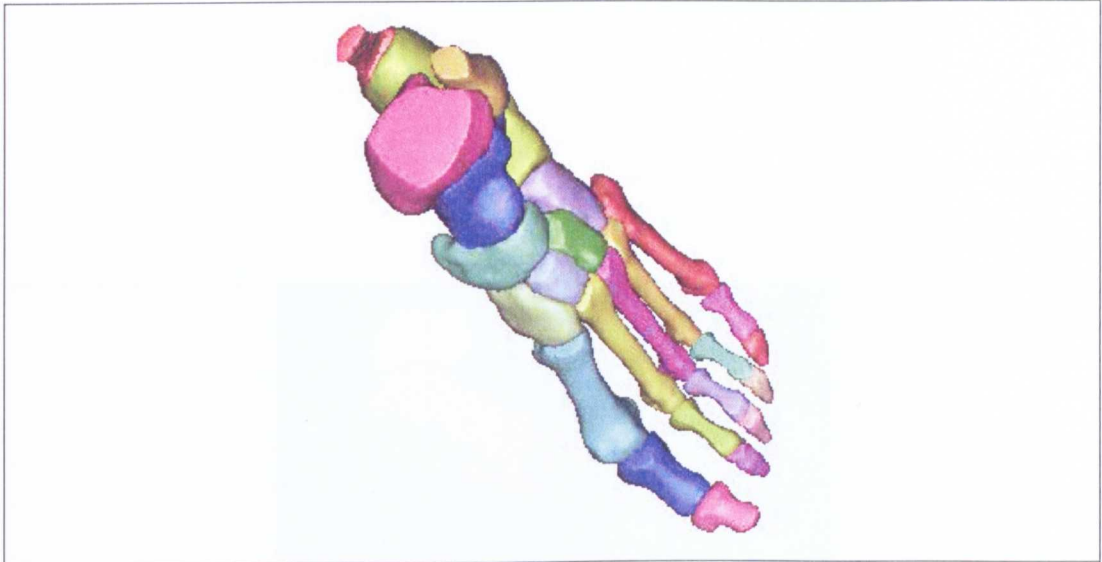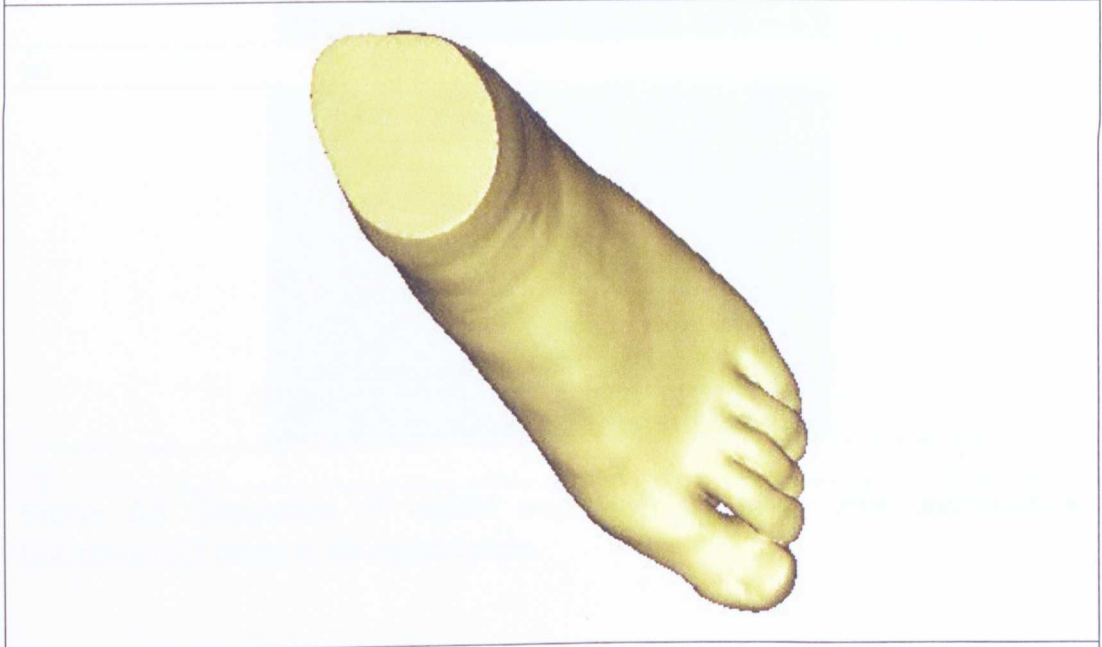
Figure 3.7 3-D assembling of the foot models.   (a) Bone structure assembly; (b) Soft tissue model.
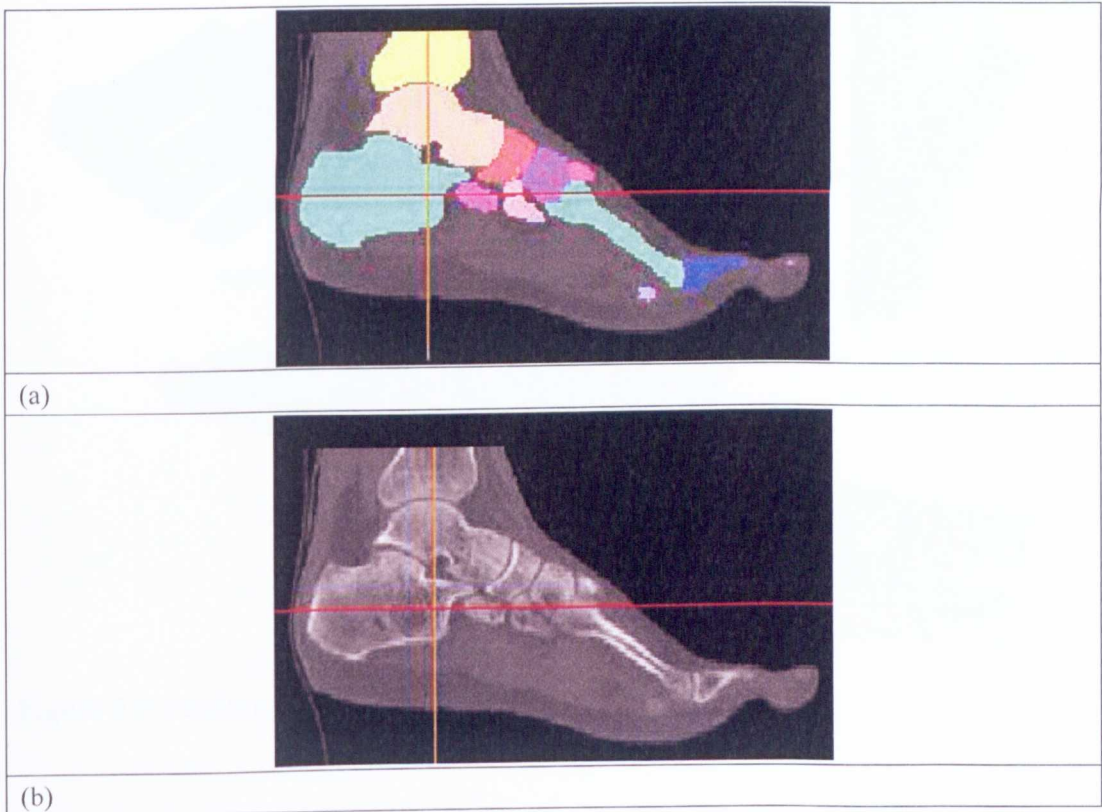
Figure 3.8 Comparison of sagittal model. (a) CT image after segmentation; (b)Original CT image in the sagittal plane.
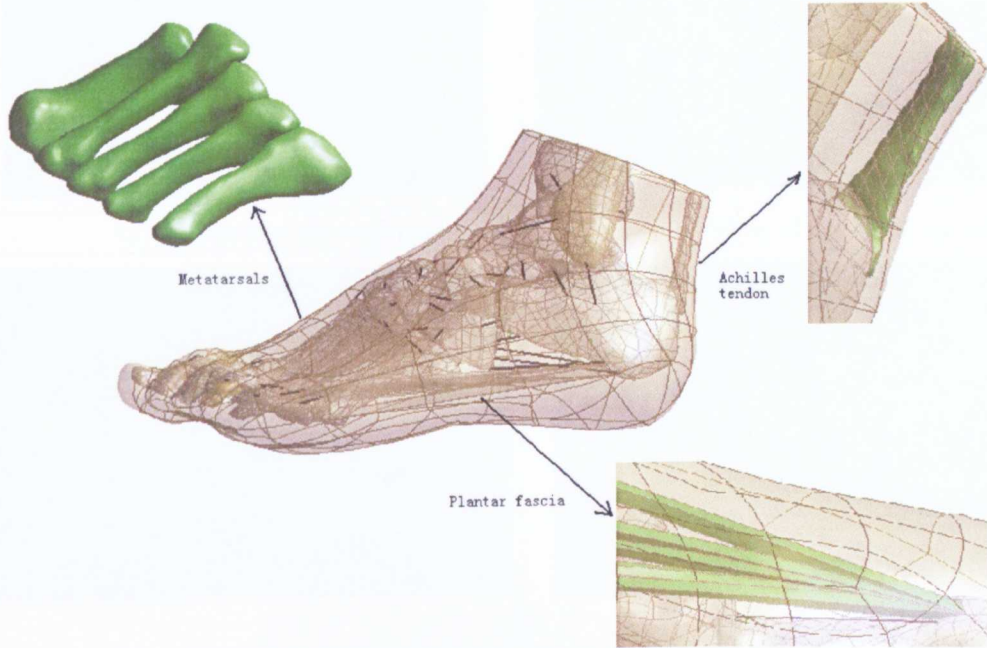
Figure 3.9 Details of the main tendons in the foot model.

(a) Meshes of the soft tissue	(b) Meshes of the bone structure
(c) Meshes of the Achilles tendon and plantar fascia	(d) Meshes of the cross-section of the foot
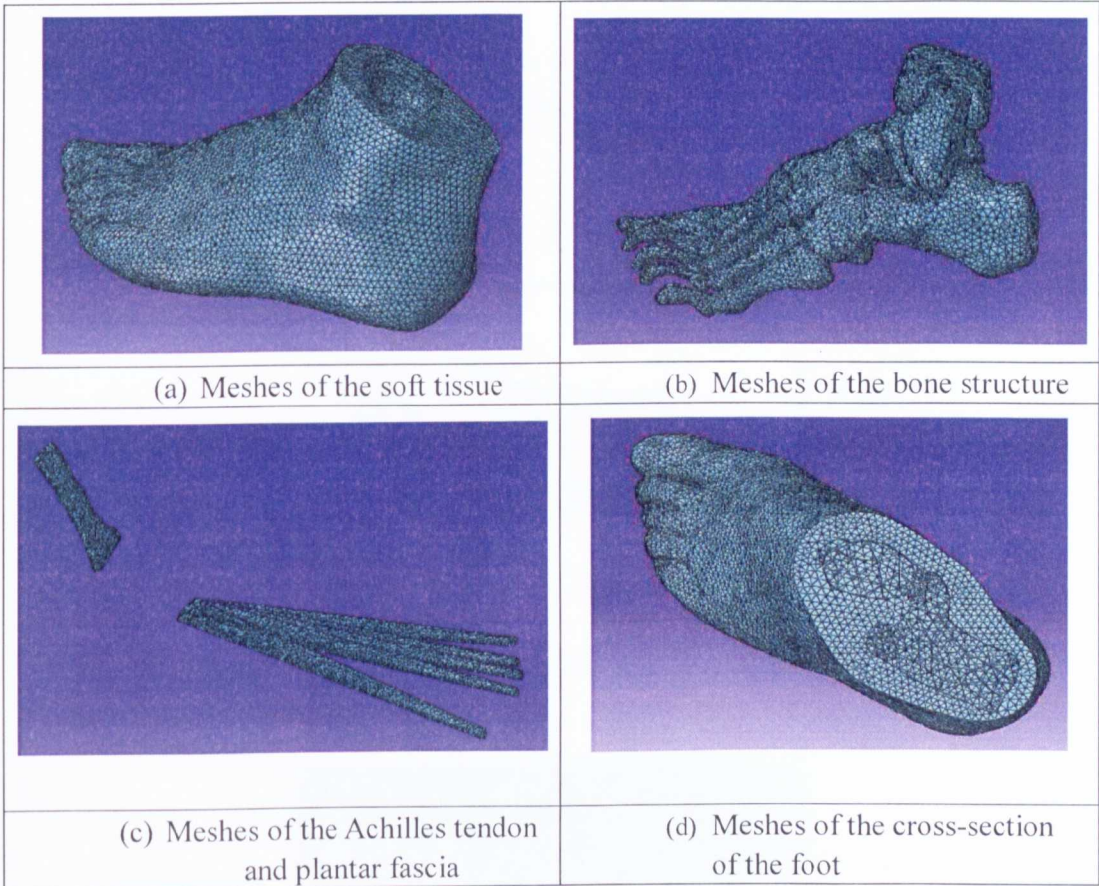
Figure 3.10 FE models of the foot and meshes in typical sections of the assembly.
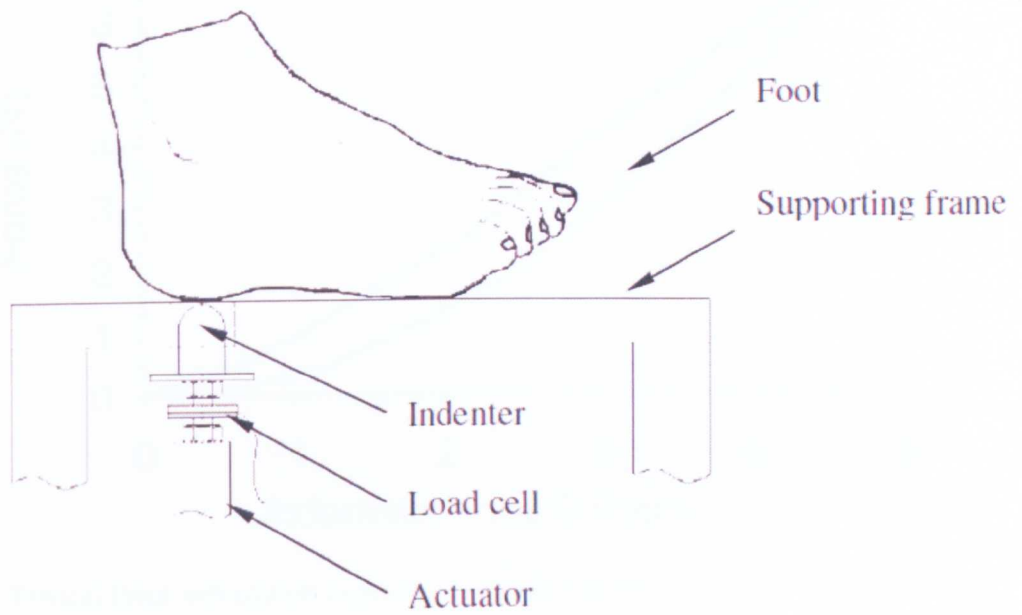
(a) Set-up of the *in vivo* indentation testing on the human heel pad
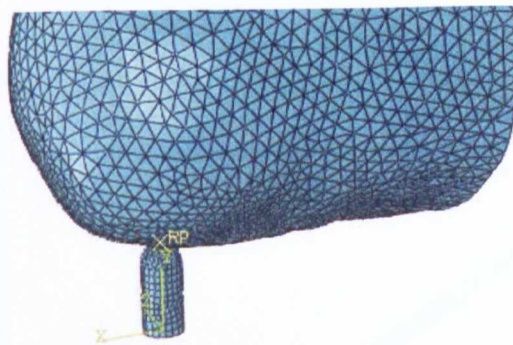
(b) FE models of the *in vivo* indentation test.

Figure 3.11 *In vivo* indentation test and simulation of the human plantar soft tissue.
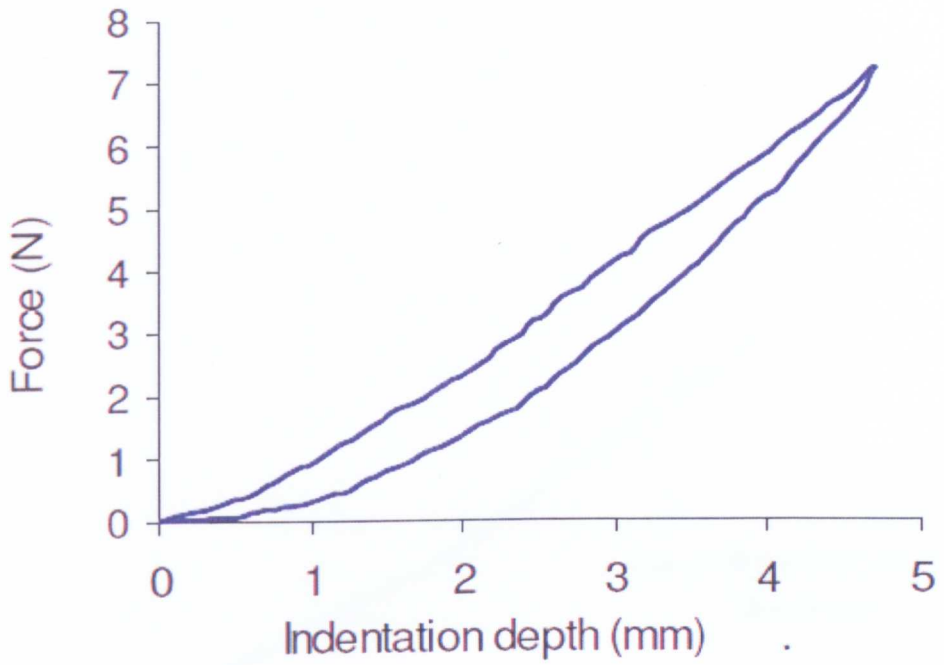
Figure 3.12 Typical force indentation depth curves of *in vivo* test.
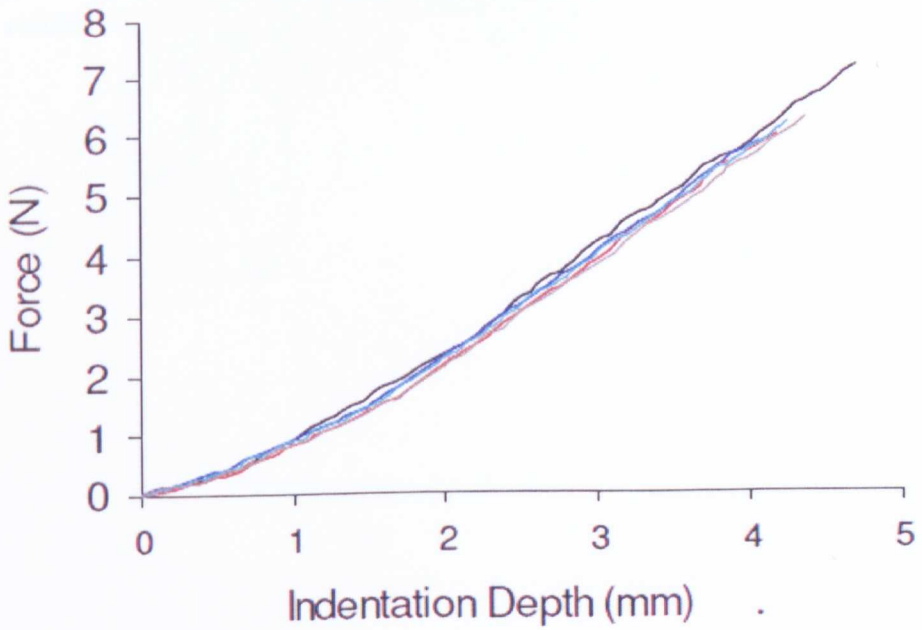
Figure 3.13 Typical force indentation depth curves showing the repeatability of *in vivo* test.
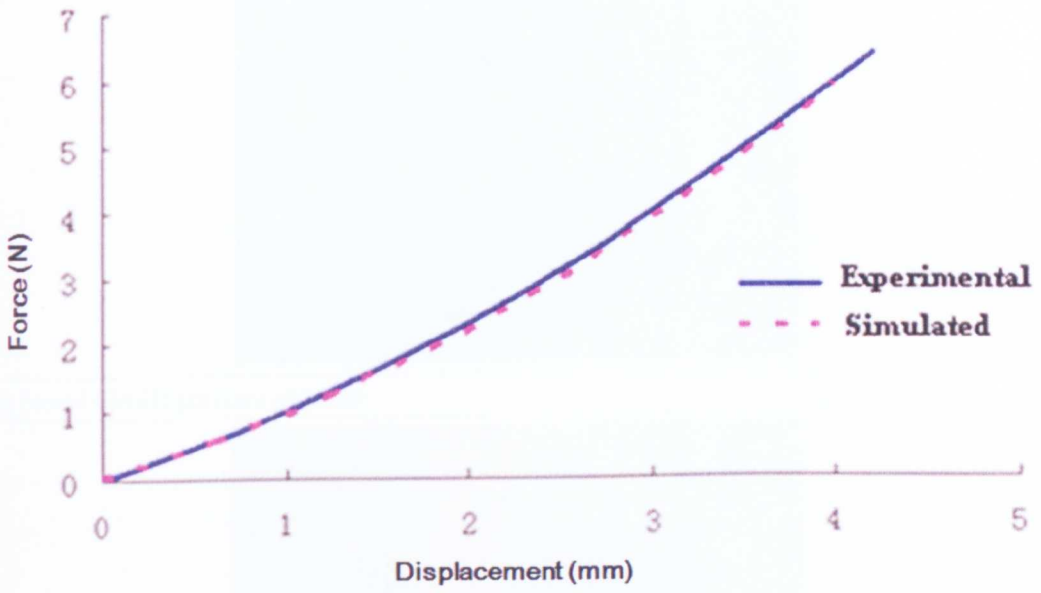
Figure 3.14 Comparison of force-displacement curve between experiment and simulation results.
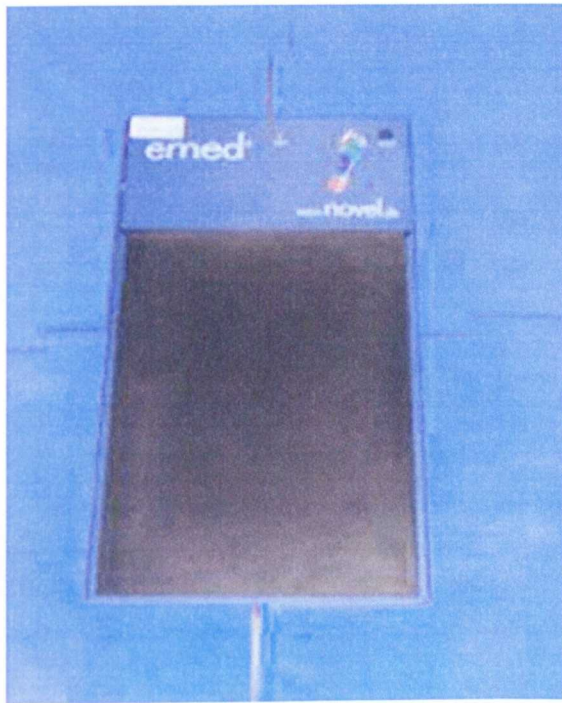
(a) Novel EMED pressure platform
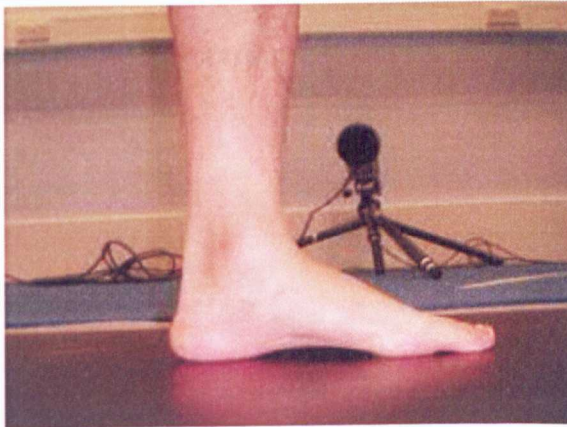
(b) Balance standing test

Figure 3.15 Experimental facilities and setup for the balance standing test.
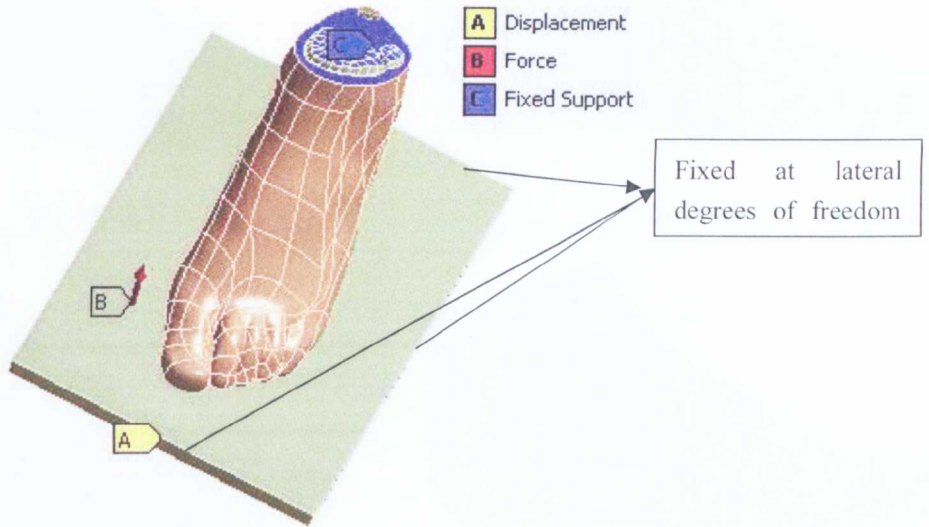
Figure 3.16 Loading and boundary conditions used in the FE model for simulating the balance standing condition.

(a) Mesh 1   (b) Mesh 2

(c) Mesh 3   (d) Mesh 4
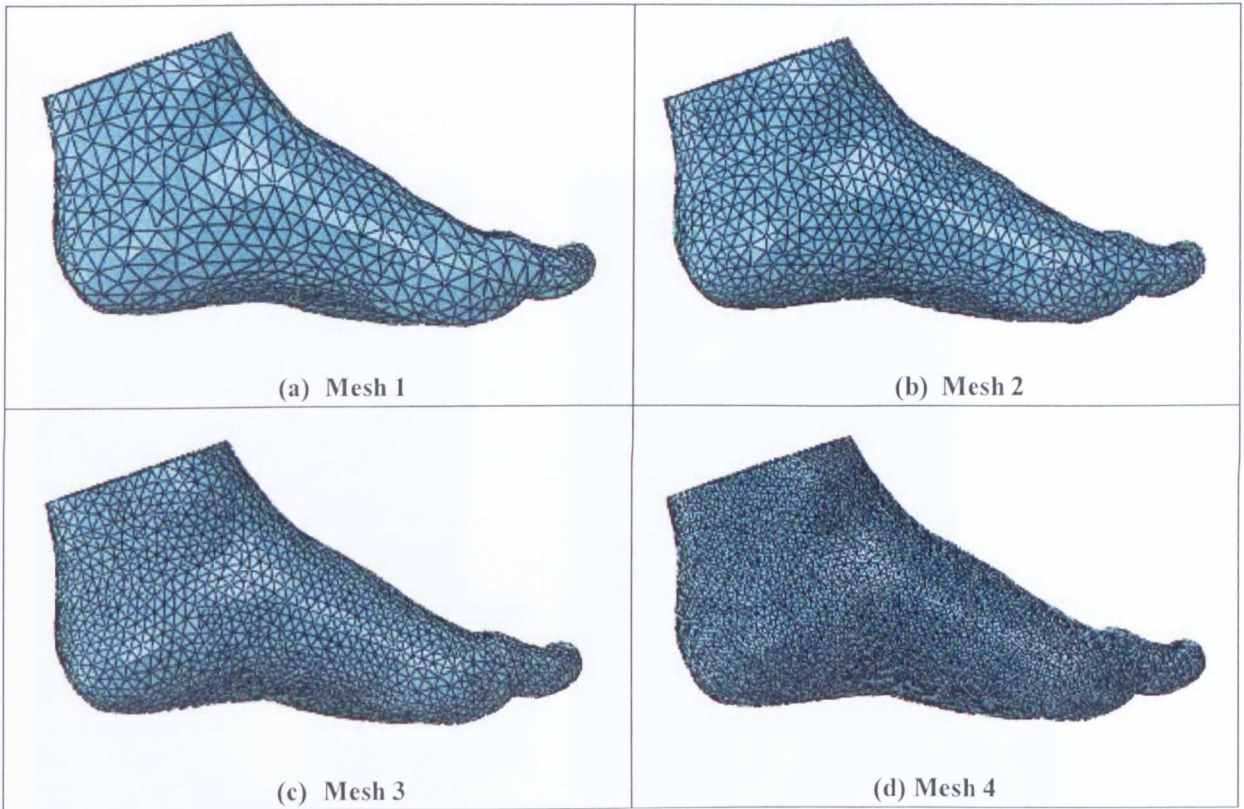
Figure 3.17 Models with different mesh sizes.
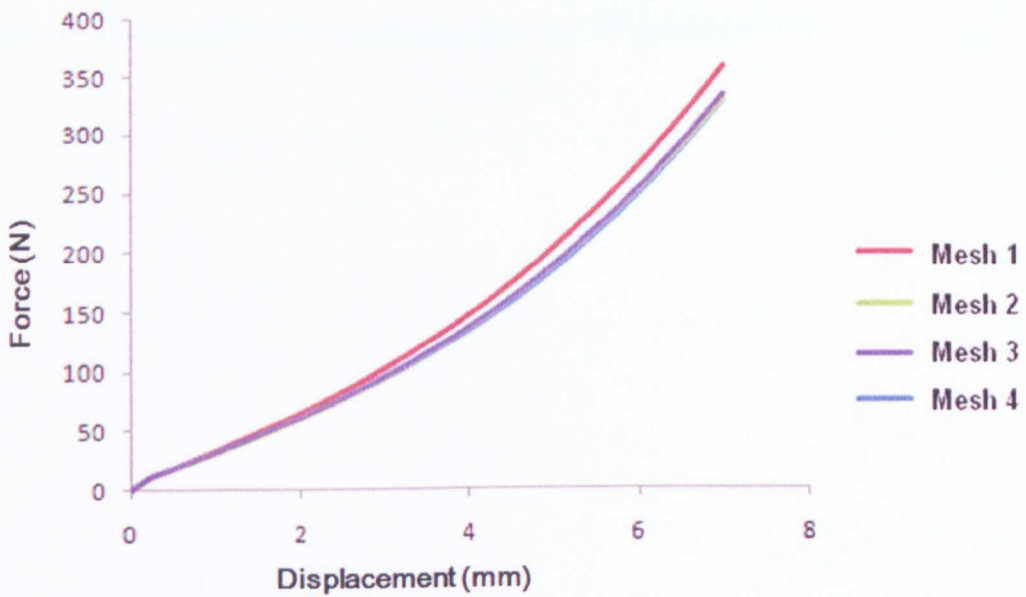
Figure 3.18 Simulated force-displacement curve during balance standing condition and mesh size effect.
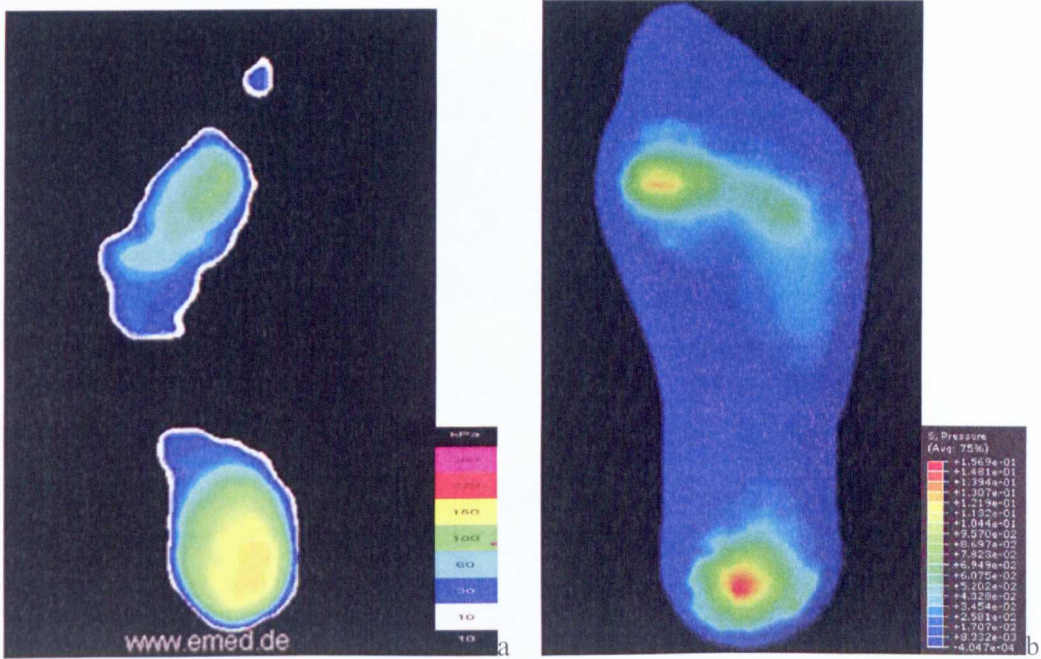
Figure 3.19 Plantar pressure distribution under balance standing showing the comparison between Novel emed results (a) and FE predication (b).

Bottom view

MPa
+6.350e+00
+5.803e+00
+5.277e+00
+4.750e+00
+4.224e+00
+3.697e+00
+3.171e+00
+2.644e+00
+2.118e+00
+1.591e+00
+1.065e+00
+5.384e-01
+1.194e-02

Top view
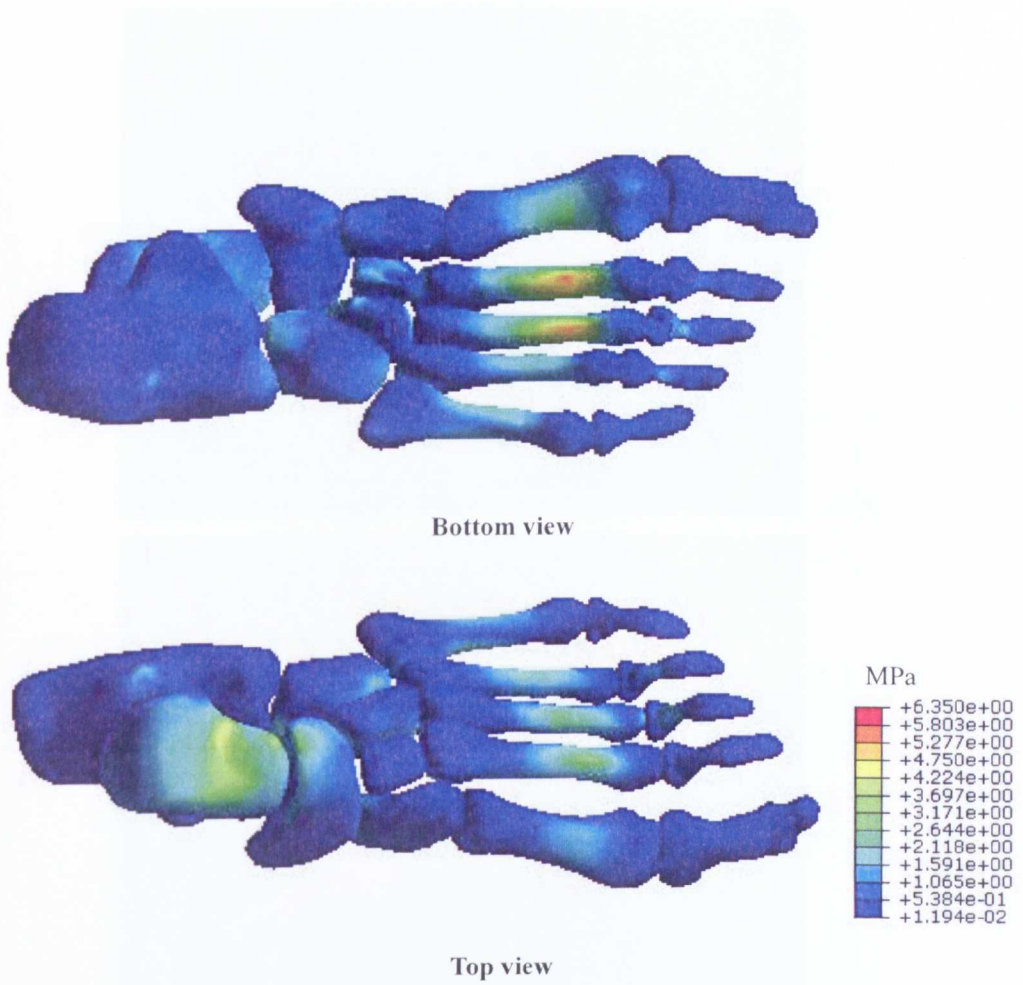
Figure 3.20 FE prediction of *von Mises* stress distribution in the foot bones.
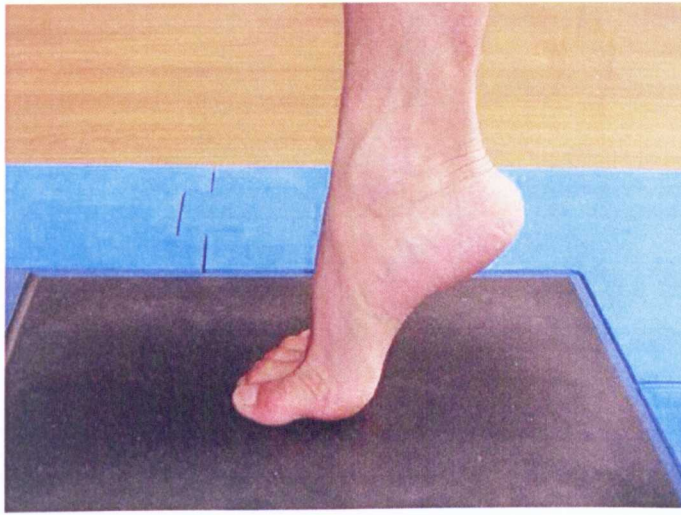
(a)
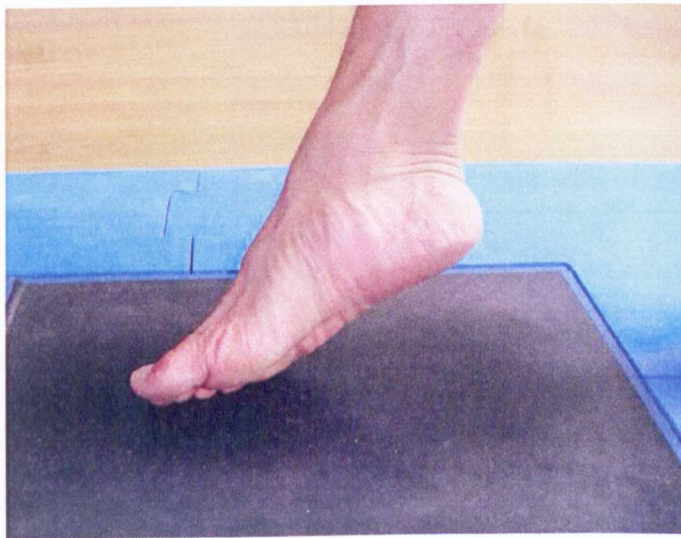
(b)

Figure 3.21: Force platform and foot pressure measurement during different types of landing: (a) Normal landing; (b) Landing at an inversion angle.
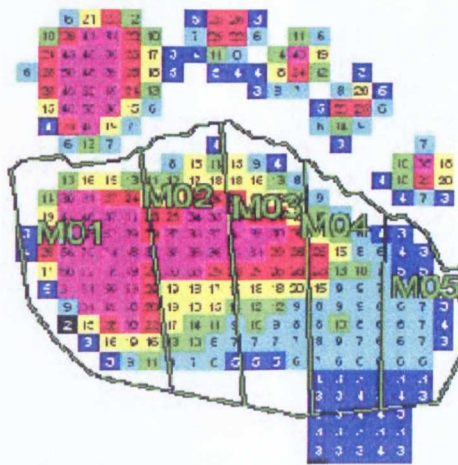
Figure 3.22 Division of the metatarsal regions (M01-M05).
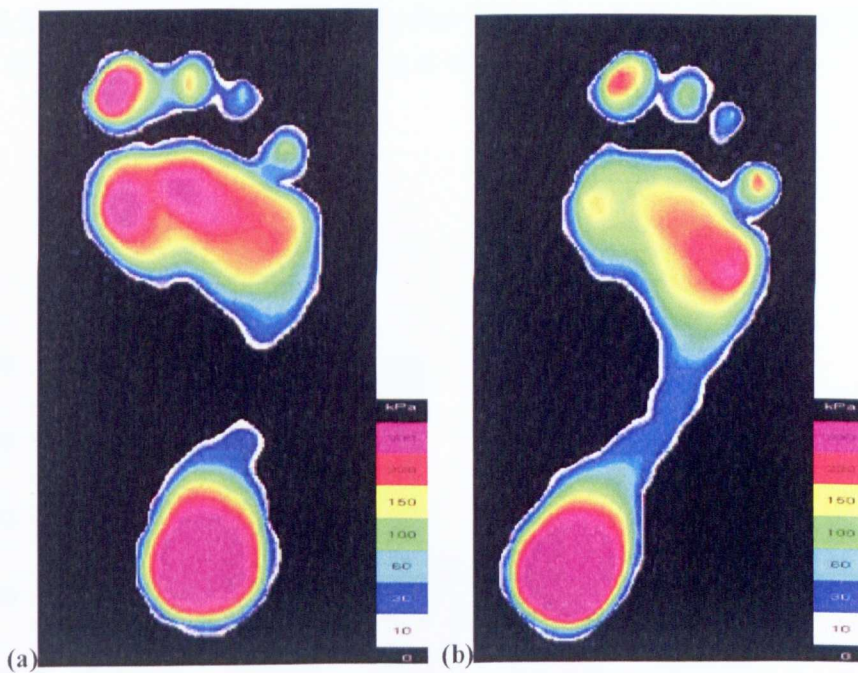
Figure 3.23 Typical whole foot pressure distribution during landing: (a) Normal landing. (b) Inversion landing.
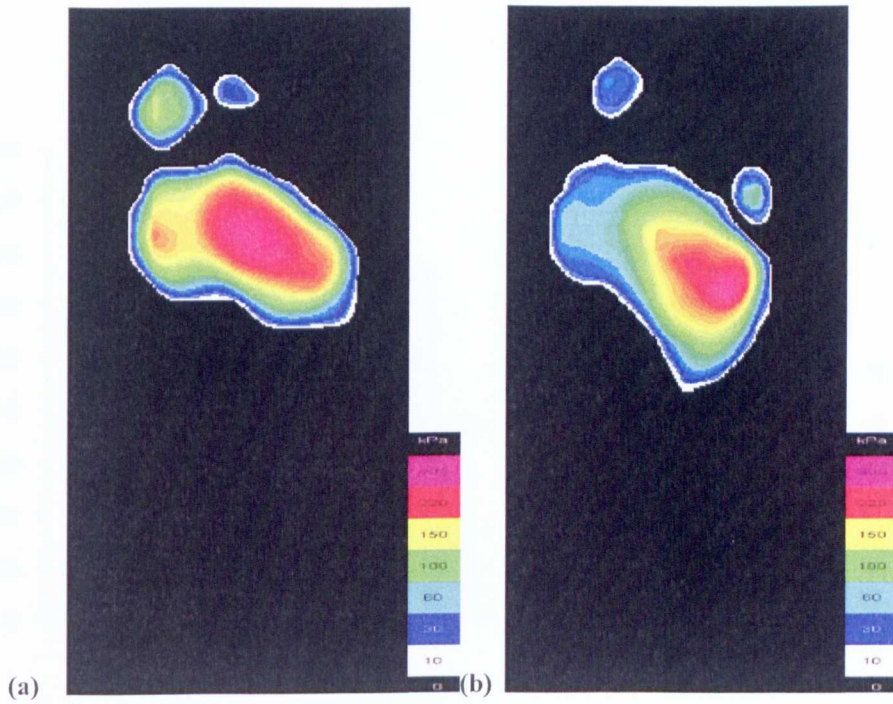
Figure 3.24 Typical peak pressure of the forefoot region during different type of landing. (a) Normal landing. (b) Landing at an inversion angle.
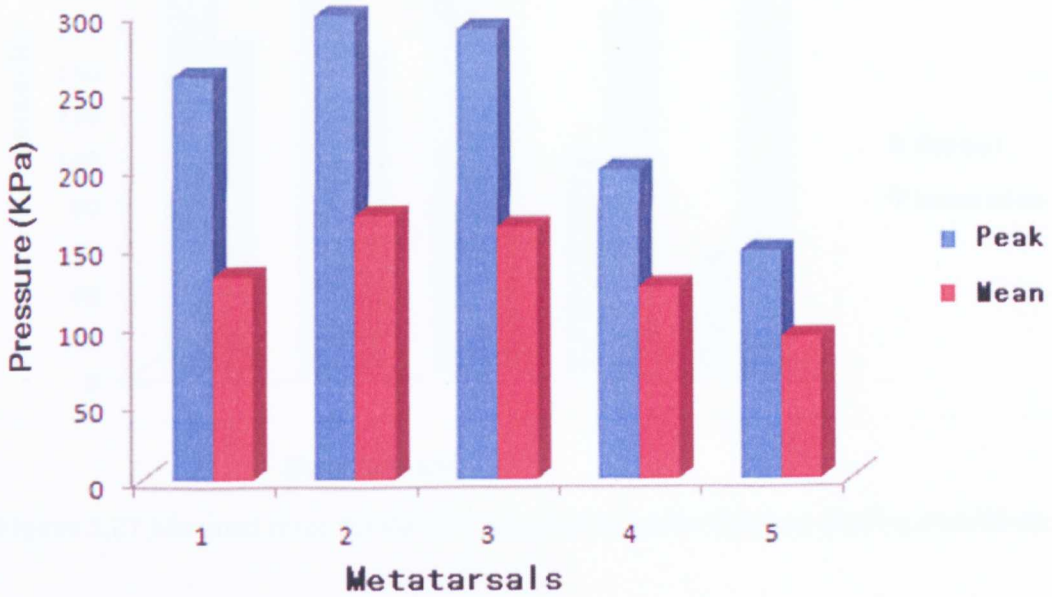
Figure 3.25 Maximum and mean pressures of the five metatarsals regions in the forefoot during normal landing.
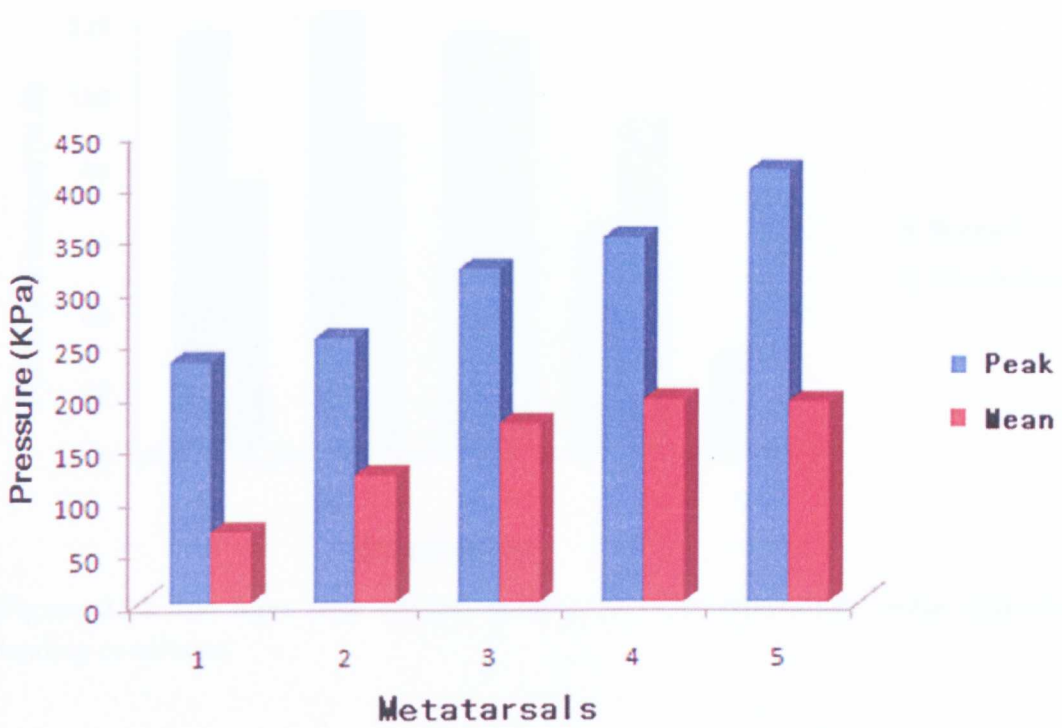
Figure 3.26 Maximum and mean pressures of the five metatarsals regions in the forefoot during inversion landing.
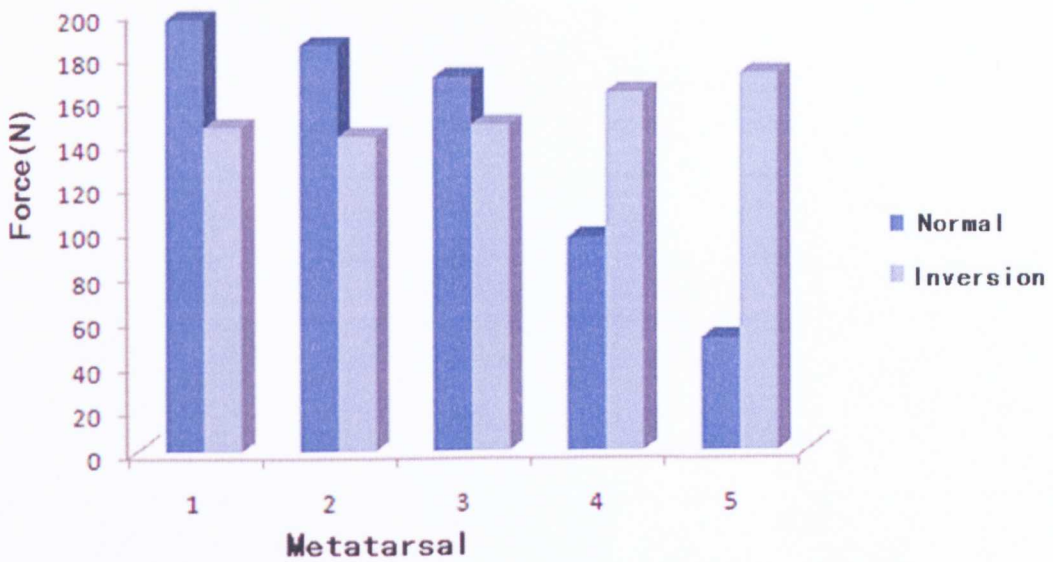
Figure 3.27 Maximal force for the five metatarsals under different landing conditions.
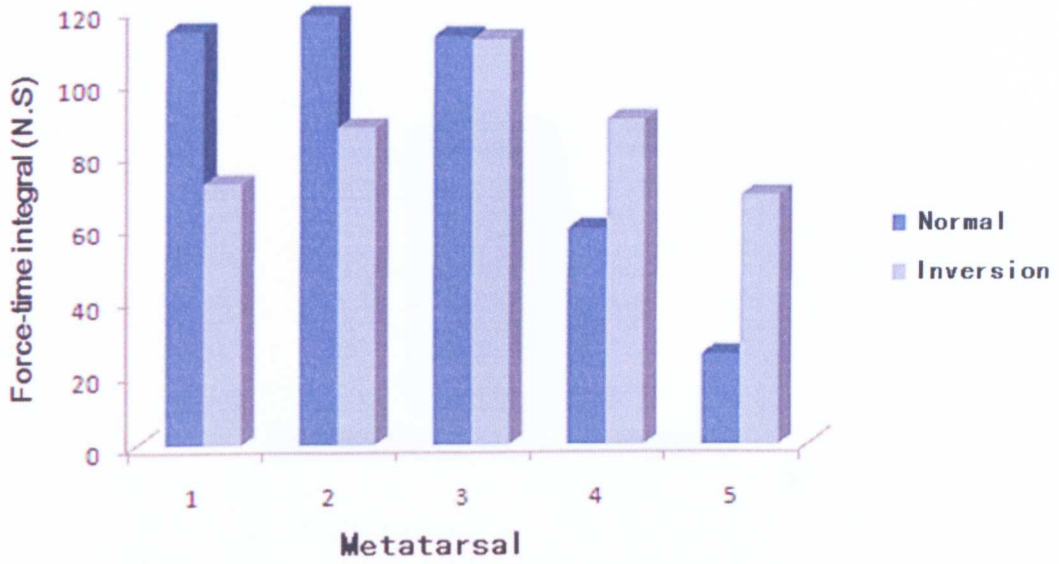
Figure 3.28 The force time integral value of the five metatarsals under different landing conditions.
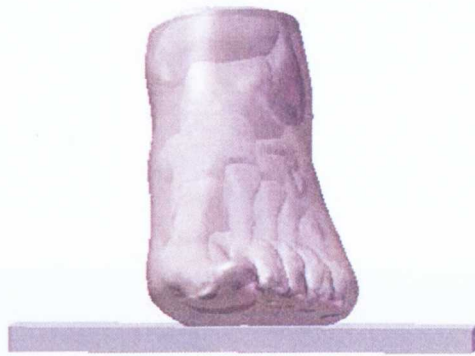
Figure 3.29 Different landing conditions to study the effect of inversion angle in the FE modelling: (a) normal landing; (b) 10 degree inversion; (c) 20 degree inversion.
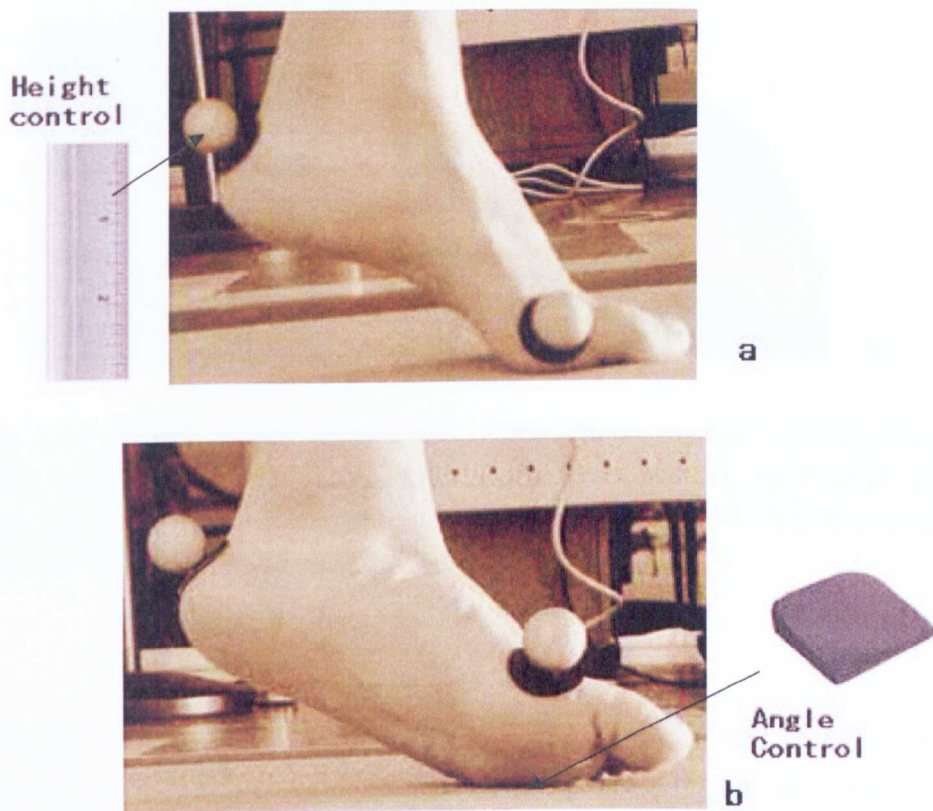
Figure 3.30 Testing method and foot control of the biomechanical test of inversion landing.
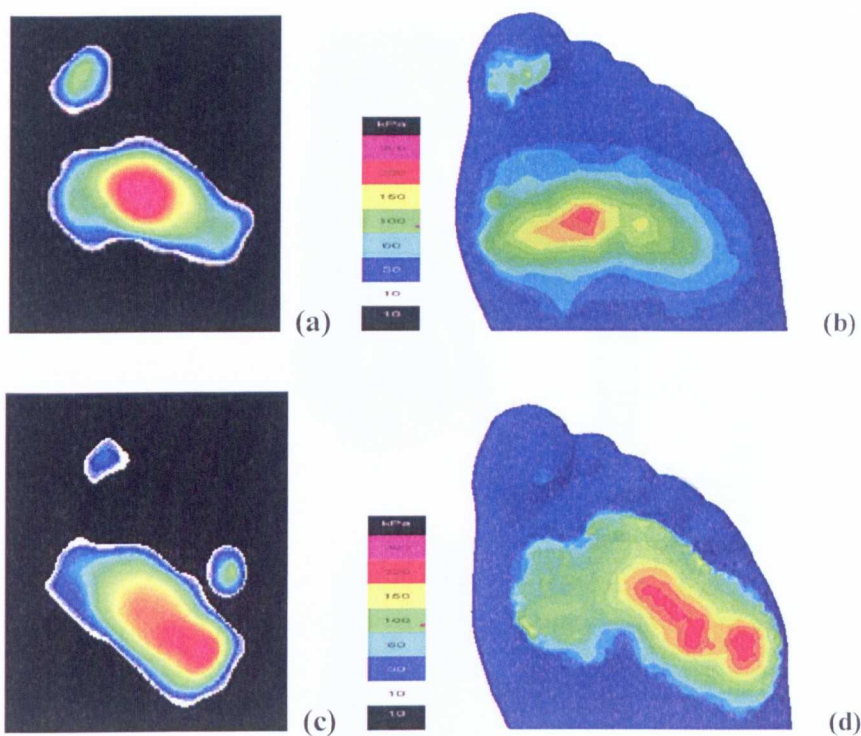
Figure 3.31 Subject specific comparison of the plantar pressure distribution under different landing conditions from experimental tests and FE modelling. Normal landing: (a) Novel emed measured; (b) Finite element predicated; 10 degree inversion landing: (c) Novel emed measured; (d) Finite element predicated.
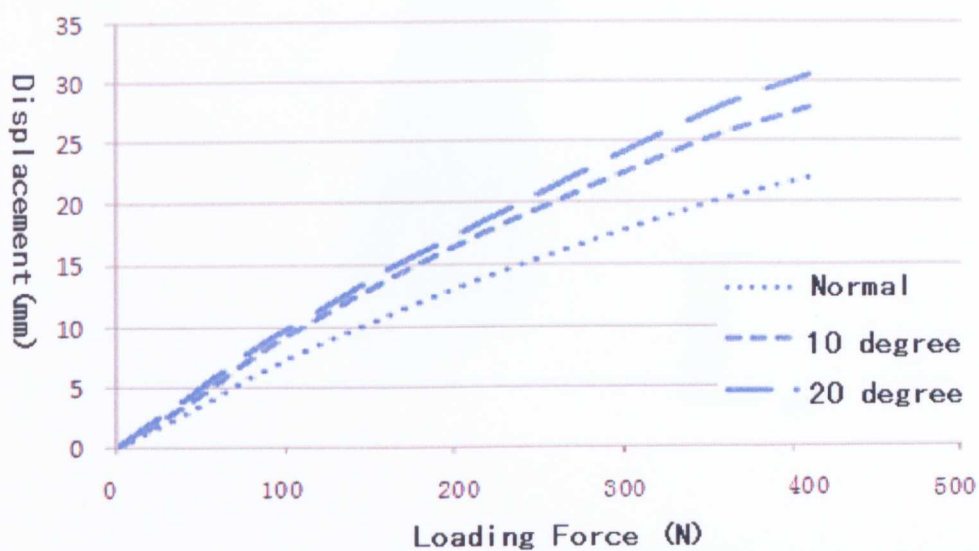
Figure 3.32 Numerical results of the force-displacement (plate movement) data during different landing conditions.
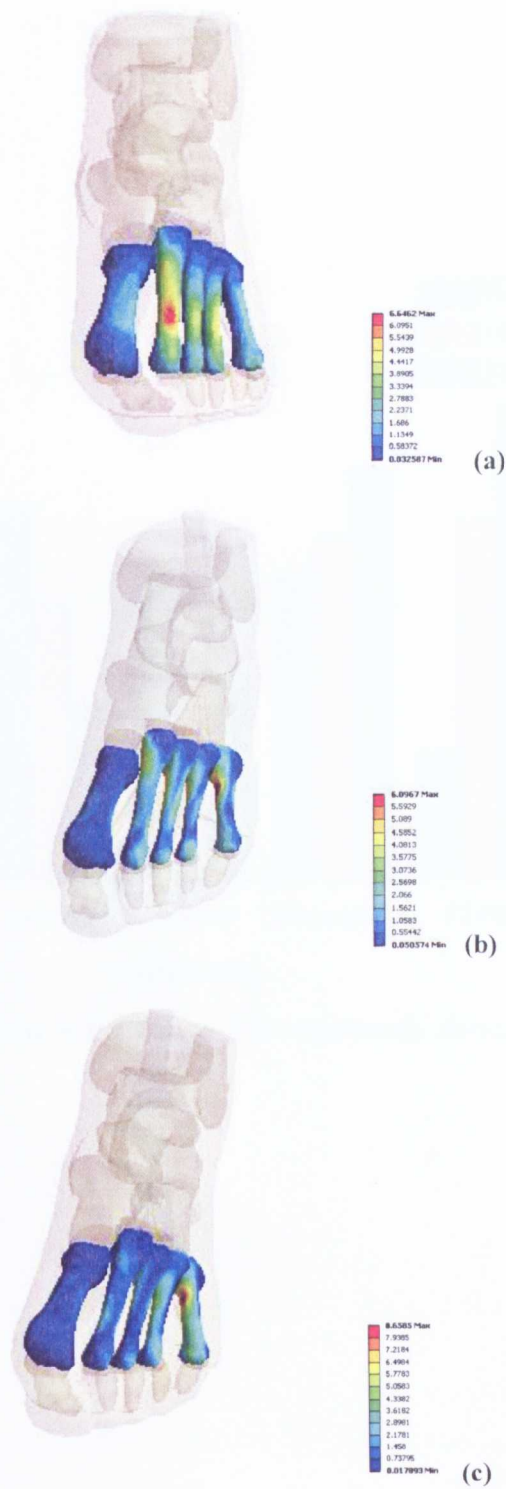
Figure 3.33 Stress distribution in the five metatarsals (MPa): (a) normal landing; (b) 10 degrees inversion; (c) 20 degrees inversion.
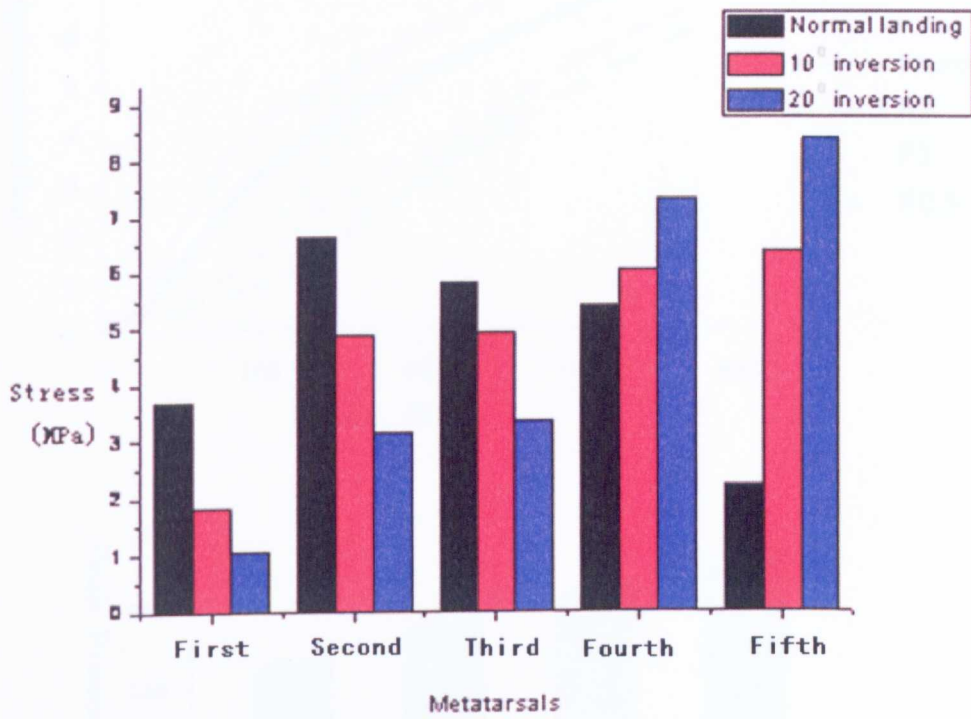
Figure 3.34 The peak stress value of the five metatarsals during different landing conditions.
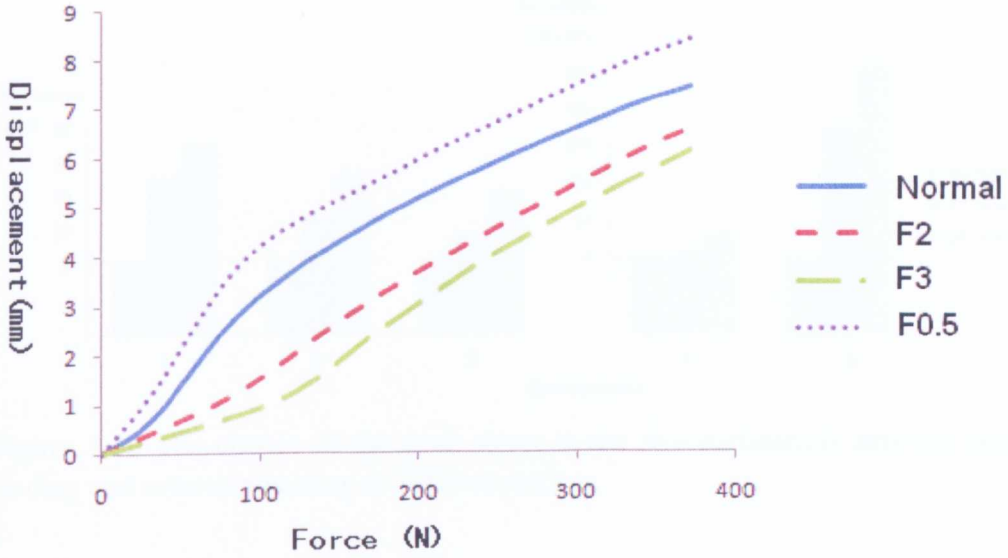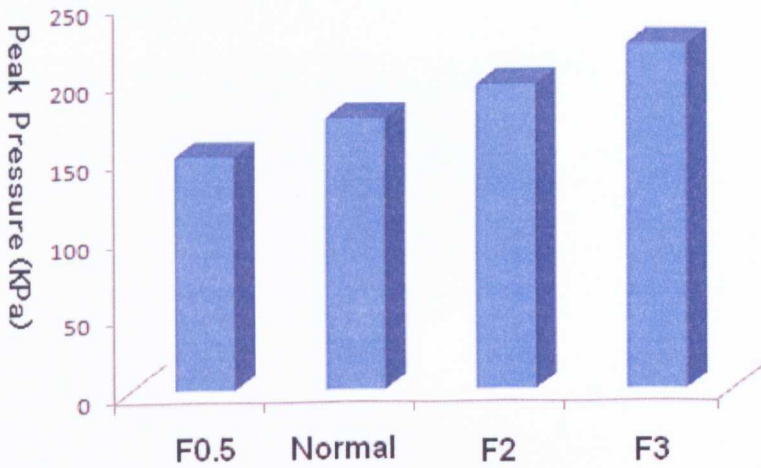
Figure 3.35 (a) Simulated force-displacement curve during balance standing condition under different soft tissue stiffness; (b) Peak plantar pressure value of foot with different soft tissue stiffness. (F0.5, F2 and F3 correspond to simulation with half, two, and three times of stiffness of the normal soft tissue.)
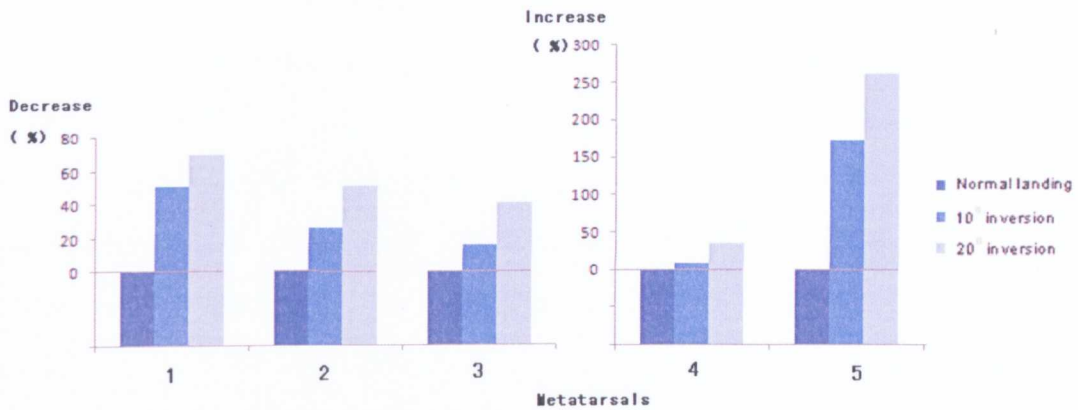
Figure 3.36 The change of the peak stress in the five metatarsals between normal landing and inversion landing at different angles.

CHAPTER FOUR

NUMERICAL INVESTIGATION OF THE EFFECT OF

SUBJECT SPECIFIC MIDSOLE INSERT FOR HEEL

PLANTAR PRESSURE RELIEF

4.1 Introduction

Heel pad of the foot, plays an important role for load bearing and providing protection to the underlying tissue and bones *(De Clercq et al., 1994)*. It normally experiences significant amount of load during the normal activities, which could cause heel pain as one of the most common foot complaints *(Reiber et al., 1992)*. The high pressure of the heel region was also related to many foot problems such as heel spurs *(Aldridge, 2004)*, plantar warts *(Schon et al., 1993)* and plantar ulcers *(Busch and Chantelau, 2003)*. Recent developments of experimental and numerical biomechanics have greatly improved the understanding of the relationship between load and tissue damage and provide design criteria for optimal pressure relieving strategies that may lead to measures for the enhancement of both tissue resistance and repair *(Zheng et al., 2000; Erdemir et al., 2005)*.

It is generally accepted that the primary cause of foot ulcer is prolonged external mechanical loading on soft tissues. Therefore, many research and design optimisation works have been focused on the development of preventive measures that reduce or relieve these loads, in particular the heel pressure. Footwear design with special structures and/or materials has become the most effective way to relieve high plantar pressure *(Hennig and Milani, 1995; Li et al., 2000; Hennessy et al., 2007)*. However, most of these works were based on generic design optimisation without considering the structural difference of the subject. A subject based design approach of the sole structure could potentially further improve the pressure distribution by combing the imaging data of the subject with computational modelling.

Computer simulation such as FE methods has become a successful way for studying the effectiveness of shoe design on the internal foot mechanics. Combined with experimental approach, it could predict the load distribution between the foot and different supports and offer important information such as the internal stress and strain of the whole foot. In addition, FE analysis technique could allow efficient parametric

evaluations of the outcomes of shape modifications and other design parameters changes of footwear without the prerequisite of fabricated footwear and replicating patient trials. Computational modelling of the human foot and footwear has been successfully adopted to the product design optimisation *(Lemmon et al., 1997; Saunders et al., 2003; Erdemir et al., 2005; Goske et al., 2006)*. Most of the works on heel pressure relief have been focused solely on the generic design improvement without considering the bone structure, such as the calcaneus. As the first bone attached to the heel pad, it could have a directly effect upon the pressure distribution. It was well documented that the calcaneus bone has a fundamental importance in bearing loads during body support or locomotion *(Gefen and Seliktar, 2004)* and its architecture is also a significant factor influencing the functional patterns of the mechanical heel pressure distribution *(Rosenbaum et al., 1995)*.

The work reported in this chapter represents a detailed analysis of a new concept of subject specific midsole design using under calcaneus area (UCA) plug for heel plantar pressure relief, together with details for the manufacturing, X-ray imaging based positioning and biomechanical testing procedures. The comparison between biomechanical testing and FE modelling results were compared for validation purpose. The numerical results with three plug materials of different hardness (in comparison to the midsole EVA foam) were compared to establish the effect of material properties and thicknesses of the UCA plug on the plantar pressure distribution and peak pressure level during the heel strike phase of normal walking.

As shown in Figure 4.1. In the first stage the dimension of the calcaneus was measured based on the CT images and circular midsole plugs with a relative dimension to the calcaneus area were designed. The midsole material and the softer insole materials used for the plug were tested using a continuous indentation tester and the nonlinear materials parameters were identified through parametric studies. In the second part, midsole were manufactured according to foot profile of the subject. UCA plugs of different relative size to the width of the calcaneus were designed and

manufactured. The midsole were scanned to assess the position of the plug with respect to the calcaneus using an X-scanner, modification of the position was made until the UCA was properly positioned underneath the calcaneus bone. In the next stage, biomechanical tests were performed to measure the plantar pressures during heel strike in walking. A FE model was developed to simulate the biomechanical tests with corresponding loading and boundary conditions. The validated model was then used to establish the effect of the design attributes (materials, size and thickness) of the UCA plug on the pressure distribution. Limitations of the work, future developments and potential applications of the design concept were discussed with regard of some clinical problems associated with the human heel pad.

4.2 Subject specific midsole design, manufacture, materials characterization and biomechanical tests

4.2.1 Concept of the midsole UCA plug for heel pressure relief

As shown in Figure 4.2, the work involves the development of subject specific midsole with tailored made outer contour and UCA plugs in the heel region. The design was done in Solidworks 2007 (Solidworks Corporation, Massachusetts, USA). The contour of the midsole was obtained form the plantar shape of the subject who underwent the CT scanning for the development of the foot FE model. The contour was then extruded to a predefined thickness to form the base model of the midsole. The solid model was then input to the computerized numerical control milling machine (Bridgeport CNC Hardinge Inc. NY, USA) to fabricate the midsole from a sheet of EVA foam (Figure 4.3).

The position of the calcaneus and its dimension was measured from the foot model. The maximum diameter of the cacaneous bottom part was around 32mm. UCA plug with different sizes (95%, 80%, and 65% of the dimension of the calcaneus bone) were manufactured from foams of different hardness. The thickness of the UCA plug were ranged from 5, 10 and 15 mm, representing 1/3, 2/3 and 3/3 of the thickness of the midsole.

4.2.2 X-ray scanning for positioning the UCA plug

An Dual energy X-ray absorptiometry (DEXA) equipment was used to check the position of the UCA plug with regard to the position of the calcaneus bone. The DEXA machine differentiates components based on the differential attenuation by tissues of levels of x-rays, a mental papers was glued around UCA hole of midsole. As shown in Figure 4.4, during the scanning process, the subject standed on the scanner, with the x-ray sources mounted beneath a table and a detector overhead. The subject puts the foot on the sole, stretching the ankle backwards in order to keep the hind-foot directly under the detector. As shown in Figure 4.5, the image could clearly demonstrate the UCA position with respect to the calcaneus. The position of the foot

with respect to the plug was then marked with a marker pen for repositioning. The midsole with the correct/modified UCA position were then used for the future biomechanical tests and FE modelling.

4.2.3 Indentation tests of the foam samples and material parameters identification

The UCA midsole inserts were made of plastazote foam, commonly used in sole fabrication. Three foams with different hardness material, with Shore A hardness 10, 20 and 30, were selected designated as soft, medium, hard UCA insert in comparison to the EVA midsole (Shore A hardness 50). Figure 4.6(a) shows the set-up of the indentation tests. The indentation tester was the same system as the *in vivo* heel test but the test were perform with the indenter moving downward driven by the actuator. The indentation system was mounted on a strong supporting frame and allows tests in both vertical and horizontal directions. A sensitive load cell (model: LCMSD12TC-10N) is attached to the moving head of the actuator to monitor the forces during the test.

The indentation tests were performed using a spherical indenter made of stainless steel. As shown in Figure 4.6 (b), the indentation curves of the insert materials and the EVA midsole materials were considerably different. The curves has followed a similar trend but the indentation resistance is significant different. The acquired foam parameters were determined from a parametric studies *(Ren et al., 2006)* to fit the force-displacement curve as "calibrated" against test data on the same foam. The foam model used was the hyperfoam material model, in which the strain energy function (U) is represented by Eq.(4-1):

$$U = \sum_{i=1}^{N} \frac{2u_i}{\alpha_i^2} \left[\lambda_1^{\alpha_i} + \lambda_2^{\alpha_i} + \lambda_3^{\alpha_i} - 3 + \frac{1}{\beta_i} (J_{el}^{-\alpha_i \beta_i} - 1) \right] \qquad (4-1)$$

Where λ_i are the principal stretches, N is the order, J_{el} is the volume ratio and μ, α and β are material specific parameters.

In this process, an FE model has been developed simulating the foam tests (as shown in Figure 4.7(a)). A parametric study was developed which allows systematical change of the material properties. The nonlinear material parameters were then determined by selecting the parameters which produced an indentation curve best match the experimental data, as sown in Figure 4.7(b). The coefficients of the hyperfoam model were listed in Table 4.1.

Table 4.1 UCA inserts and midsole material coefficients

	μ	α
plastazote soft	0.63	32.3
plastazote medium	0.90	26.1
plastazote hard	1.31	28.3
Normal EVA	1.96	26.0

4.2.4 Biomechanical tests

To compare the interaction between the foot and the midsole with UCA plug, a plantar pressure measuring system was used in controlled biomechanical tests to measure the centre of pressure, total ground reaction forces and foot-shank position with the midsole of UCA. Heel-strike step, involving heel pad play a major support function in the heel area, was selected in the biomechanical tests. The in-shoe plantar pressure during the heel-strike was measured using the Novel-Pedar in-sole system (Novel GMBH, Munich Germany) sampling at 50Hz (Figure 4.8). The Pedar measurement system has been proven to be an accurate, reliable, and a repeatable measure of loading force and peak plantar pressure *(Murphy et al., 2005; Putti et al., 2007)*. The insole consisted of an array of 99 sensors that were evenly distributed over the insole with a spatial resolution of approximately 0.391 cm^2/sensor. The plantar loading parameters were transmitted from the Pedar transmission device to a laptop

computer via Bluetooth technology. Prior to data collection, the pressure measurement insole was calibrated according to the company specifications. In the biomechanical tests, six trials were collected for each heel-strike condition and then the average load of vertical loading force during controlled heel-strike was extracted as the loading condition in the FE model. The pressure distribution of controlled loading was used to validate the FE models.

4.3 FE modelling of heel strike in walking

4.3.1 Foot-sole CAD modelling

Figure 4.9 shows the FE foot model and the design of the midsole. As the main focus of the FE modelling is the effect of the UCA plugs, much finer meshes have been used in hind foot region. The optimum FE mesh was determined by a converging process in which the mesh density was gradually increased, until the deviation of the predicted peak pressure values with further element size change was within 3% variation (Figure 4.10). The geometry of the sole structure was based on the realistic structure of the midsole and the UCA plugs. The thickness of the midsole was 15mm. Series FE models has been developed with different UCA designs with different sizes with the diameter varied between 65%, 80%, and 95% of the width of the calcaneus (Figure 4.9). The thickness for the UCA insert selected was 5, 10, and 15mm, as the maximal midsole thickness was 15mm in this model. As detailed in section 4.2.3, the material parameters of the foams (Table 4.1) were inversely predicted from continuous indentation tests.

4.3.2 Loading and boundary condition

The foot-sole and sole-plate interface was simulated using penalty contacts with a friction coefficient of 0.5 *(Erdemir et al., 2005)*. The bones and soft tissues were bonded together forming a unique structure with different material regions through the definition of mesh tie kinematic constraints. The plate was assigned as a rigid body to simulate the ground support. The upper surfaces of the soft tissues, distal part of tibia and fibula were fixed throughout the analysis, while the plate was allowed to move in the vertical (upper) direction. A loading force of 386N, which was determined from subject specific biomechanical, was exerted at the reference point of the plate. The data of plantar pressure from FE models of different UCA plugs were compared to establish the effectiveness of the design on pressure relief.

4.4 FE simulation results

4.4.1 Comparison of the FE results and the biomechanical pressure measurement

Figure 4.11 shows the comparison between the plantar pressure distribution under heel strike from the Novel pedar measurement and the FE model with a 10mm thick hard UCA plug with a size of 95% of the width of the calcaneus. As shown in Figures 4.11 (a) and (b), the numerically predicted pressure distribution pattern (b) showed good agreement with the experimental results (a). The FE model predicated a peak pressure of 172 KPa at the center of heel region, while the corresponding peak pressure measured by Novel pedar was about 158 KPa. The close agreement of the distribution pattern and the peak pressure value suggests that the FE model is sufficiently accurate.

4.4.2 Effect of the UCA plug on the pressure distribution

As shown in the Figure 4.14, the pressure levels with an UCA insert is significantly lower than the peak plantar pressure with pure EVA midsole, the peak value of which was 201KPa. This suggests that an UCA insert could effectively achieve a pressure relieve. The pressure reduction in comparison with pure EVA foam for three plug materials (designated soft, medium and hard) with different thicknesses were listed in Table 4.2. As shown in the data, the maximum peak plantar pressure reduction with these three different plug materials 18% (soft), 22% (medium) and 19% (hard). As shown in the pressure data of UCA sizes, a larger UCA plug could be more effective for peak pressure relief. The most effective design was found to be with the UCA insert of a foam with a medium hardness and a size of 95% UCA.

Table 4.2 Percent reduction in peak pressures with UCA plugs of different materials and sizes

Material	Thickness (mm)	UCA size 65%	80%	95%
P-soft	5	7%	16%	17%
	10	8%	18%	18%
	15	8%	18%	18%
P-middle	5	9%	13%	16%
	10	10%	15%	22%
	15	10%	16%	22%
P-hard	5	10%	10%	11%
	10	11%	14%	18%
	15	11%	14%	19%

As shown in the data, the thickness of the insert also played an important role in pressure reduction. The most significant changes was found to be with the hard insert materials, the thicker the plug, the more effective it was in relieving pressure. For example, increasing the thickness of the insert with 80% UCA from 5mm to 15mm improved the pressure reduction from 10% to 14% of pressure level with a pure EVA (Figure 4.12). Typical pressure distributions with different plug thickness were shown in Figure 4.13. It is clearly illustrated that the peak pressure with thinner plug was much higher (the dark red region in Figure 4.13(a)). The thickness of soft plug, on the other hand, had a minimal effect on pressure reduction, as illustrated by the limited improvements in pressure reduction for the soft thin plug compared to the soft thick plug. In addition, the soft insert also caused an increase of the pressure at the perimeter of the insert. As shown in Figure 4.14, the pressure at the edge is much higher than the pressure at the central region. This edge effect may have adverse effect on the soft tissues

4.5 Discussion

In this study, a detailed subject specific foot model has been developed and successfully used to investigate the effect of UCA midsole plug on the pressure distribution. The numerical results of pressure distribution, with a UCA plug, was in good agreement with the plantar pressure measurement, which suggests that the FE modelling is valid and suitable to be used for subject specific footwear modification/development. The work showed that the UCA plug could improve the pressure distribution and its effectiveness is associated with the size of the plug relative to the size of the calcaneus bone, thickness of the plug and the hardness of the material used. The effect of the UCA size on the pressure level/distribution were found to be more sensitive for medium material, but the effect was less obvious in the soft plug with a size between 80% and 95% of UCA. The present study also showed that the thickness of the plug was also an effective variable in reducing peak plantar pressure for the medium hardness materials but showed limited effect when the material was too soft. These findings have opened up a new way of plantar pressure management though composite midsole with a UCA plug.

A variety of sole products are frequently used to relieve plantar pressures through material, thickness, and conforming parameter modification of the insole under the heel or the metatarsal areas *(Viswanathan et al., 2004, Bus et al., 2004, Tsung et al., 2004, Goske et al., 2006)*. In these works, the peak plantar pressure was chosen as the output variable for validation and evaluation of insole design because of its widespread use in footwear-related research works *(Erdemir et al., 2005, Goske et al., 2006, Cheung and Zhang, 2008)*. Although the insole design is a good approach for the peak pressure relief, there is certain limitation on the thickness and sizes. In the study by *Goske et al., (2006)* flat insole design with optimum material and thickness could reduce the peak pressure by 24.1% from the peak pressure for the barefoot condition during the heel-strike stage. However, high thickness value of insole would cause the foot itself feeling too tight due to the upper part was not adjustable. The

work reported in this project showed that the use of UCA midsole plug is another effective way for pressure relief. The simulations results suggest that for midsole plug to be successful in reducing the peak pressure, large plug with medium material will be the most effective option. The maximum pressure reduction was up to 33.6% comparing to the barefoot peak pressure during heel-strike stage on a solid ground, the effect is more significant than the reduction achieved by insole under comparable condition as reported by *Goske et al., (2006)*. In addition, midsole part could provide enough design space for the complex structure be manufactured during the moulding process of the midsole. The work has been focusing on the assessing the feasibility of the concept, one area requires further investigation is incorporating a more detailed representation of the material properties including the viscoelastic properties of the materials to assess it longer term effect. The sole material in FE studies were represented by hyperfoam strain energy function *(Erdemir et al., 2005; Goske et al., 2006)*, which is a practical way for comparing different design concepts. *Even-Tzur et al. (2006)* have reported that the peak heel pad stresses and strains could be affected by the viscoelastic properties of the foam material. Especially after long-term used sole material, the shock-absorption ability could be markedly reduced due to the foam micro-structural damage, which would lead to an increase of the peak plantar pressure *(Verdejo and Mills, 2004)*. The frame work establish in this work will enable future work to investigate the effect of these factors in future works.

FE study considers both human musculoskeletal and footwear structures is expected to take an active role for the evaluation and design for footwear and related components. More complex footwear structure could be evaluated through the current FE method to fulfill the needs of modern footwear research and industries. Inclusion of comprehensive assembled footwear model consisting of upper structure will also be one important step forward for realistic biomechanical simulations of foot-shoe interface. The mechanical properties change of the human tissue in different ages would be solved using FE methods to design the products for enhancing its functional performance to the general public. The ability of the developed FE model for the

pressure relieve during walking was justified in this study. Further investigations on the biomechanical effects of different functional design on different sports, like football and tennis, can be used to refine the design principles of footwear in terms of appropriate structure and material of the sole or upper in order to fit specific functional requirements of the subject and individual foot structure.

In this work, the FE model was developed based CT images of the foot and the assembly between the foot and the midsole with an UCA plug. In general, the numerical results showed a reasonable agreement with the experimental data. However, some limitation of the model in this study may influence the simulation result and need to be addressed in future studies. In this work, the material property of heel pad was simplified as one layer, and muscle force have not been directly considered in the simulation. The outsole layer and insole layer was not included in the model to suit the experimental condition and to focus on the effect of the midsole plug. The conformity of the sole layer, which was an important factor to reduce the peak pressure *(Goske et al., 2006, Cheung and Zhang, 2008)*, need to be further investigated as another design factor. Due to the model being created from only one subject, the optimised design of the pressure-relieving may also be highly individualized. Therefore, current FE simulations for the response of the general population deserve further computational and experimental investigations. Future work is required to explore these issues based on a larger group of cohorts. With further improvement and development of the FE model, it can be directly used for subject footwear design based on the hind foot structure to fit specific functional requirement. In a longer term, the approach can be developed into a tool for to provide systemic guidelines for clinicians to prescribe optimised footwear to improve pressure relief, comfortness or gait performance.
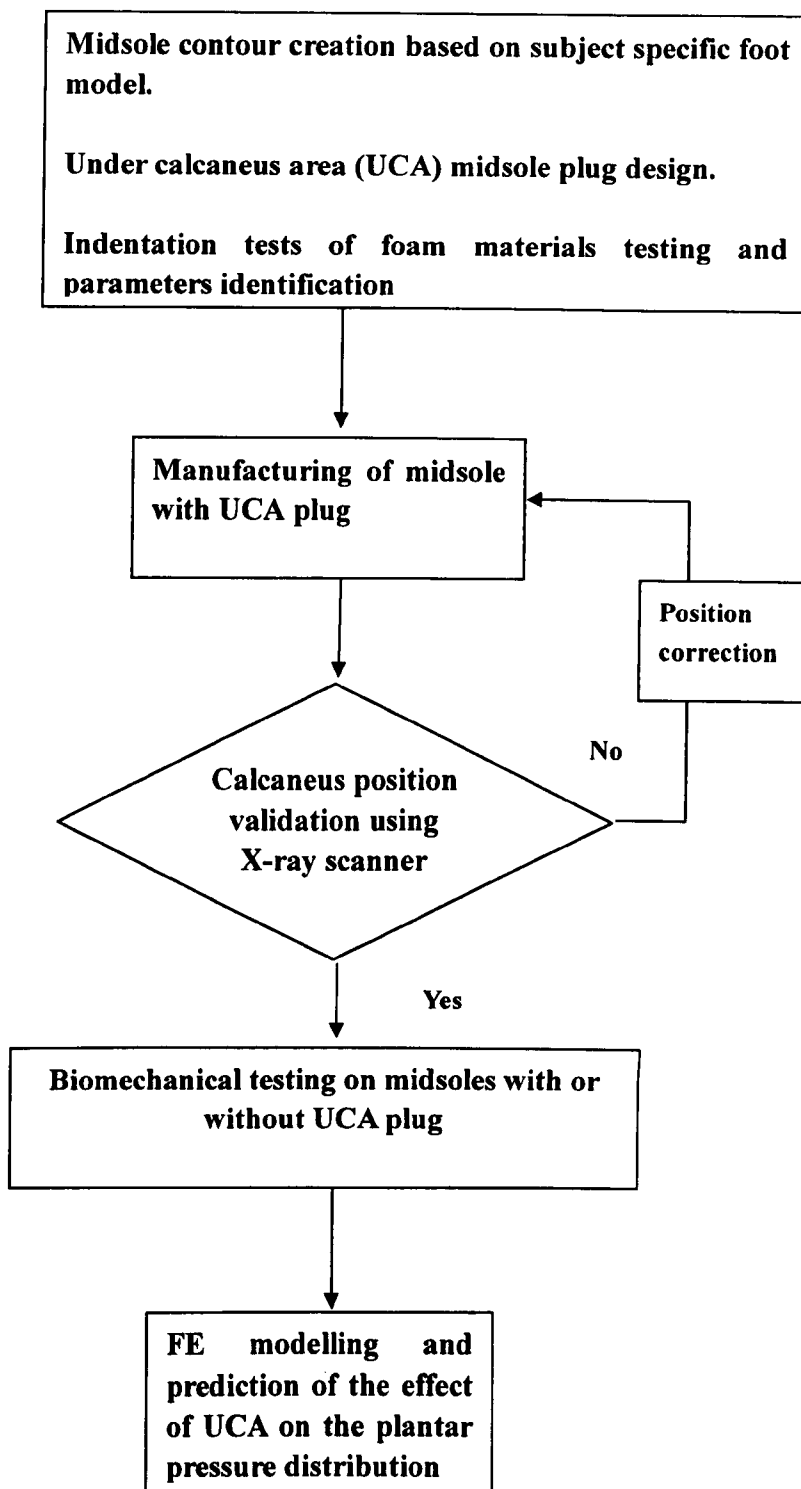
Figure 4.1 Flow chart showing main works in the development of the image based midsole plug, fabrication and FE modelling.
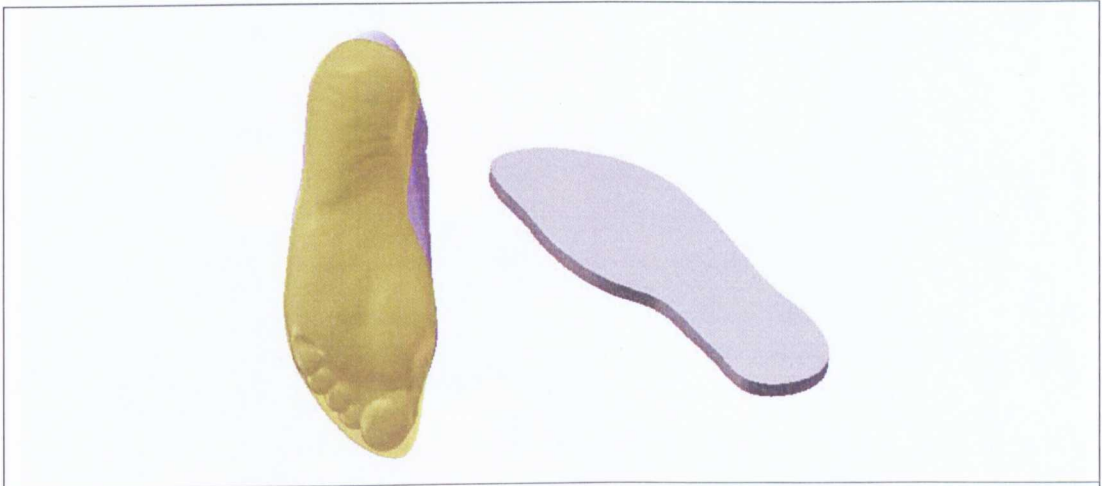
(a) Midsole outer contour design based on the foot model.

27.61

34.92

Centre of
calcaneus
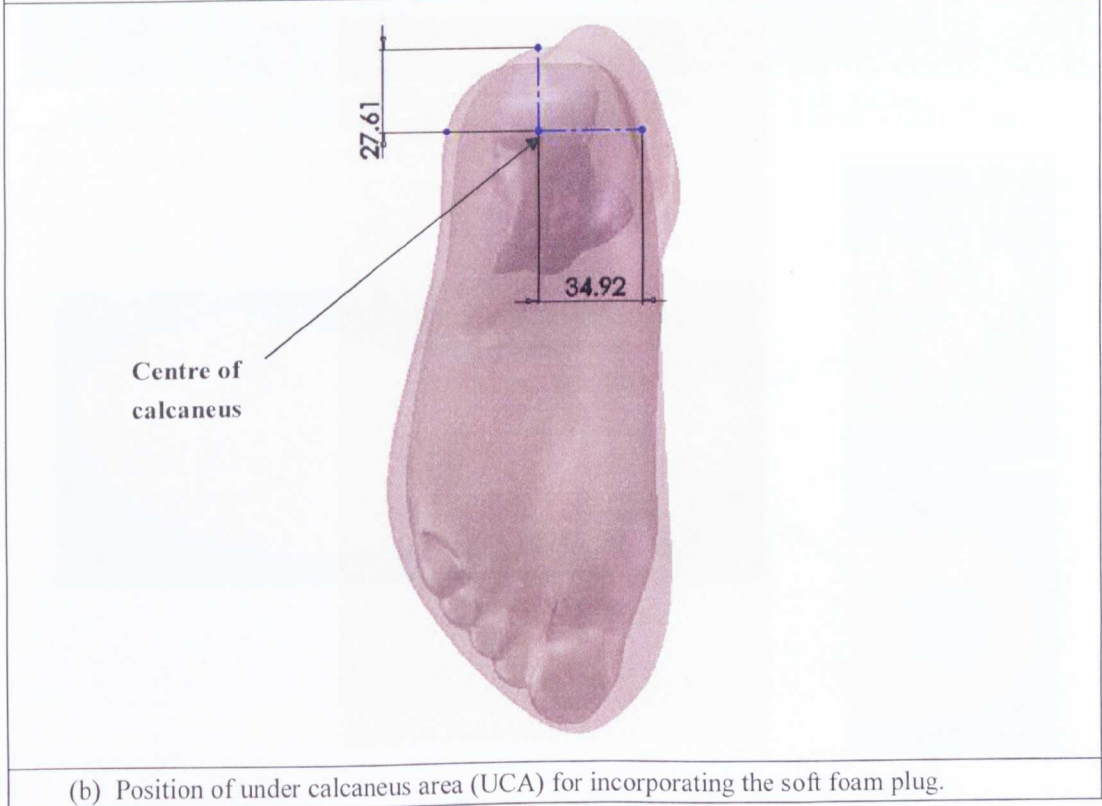
(b) Position of under calcaneus area (UCA) for incorporating the soft foam plug.

Figure 4.2 Concept of subject specific midsole design in Solidworks.

(a) CNC milling machine for the manufacturing the midsole with a UCA area.
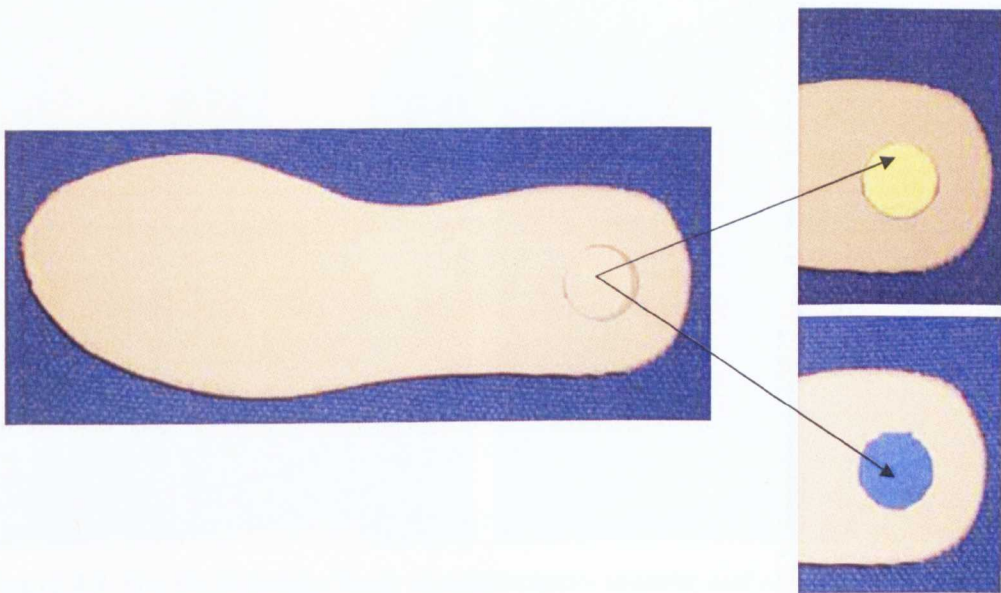
(b) Images showing the midsole and UCA of different materials.

Figure 4.3 Manufacture of the midsole with UCA plug of different materials.
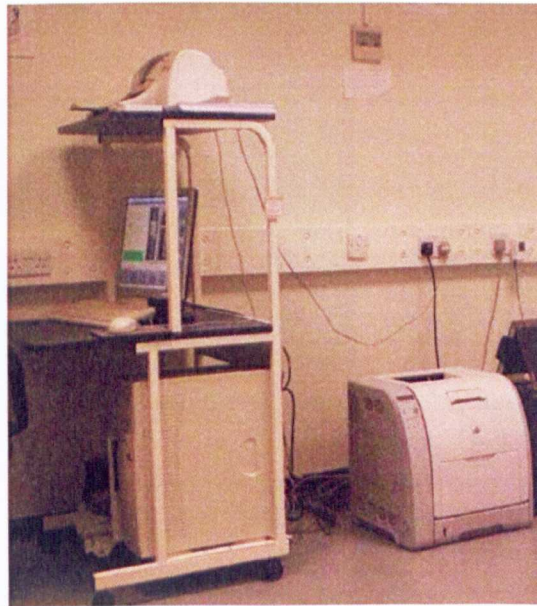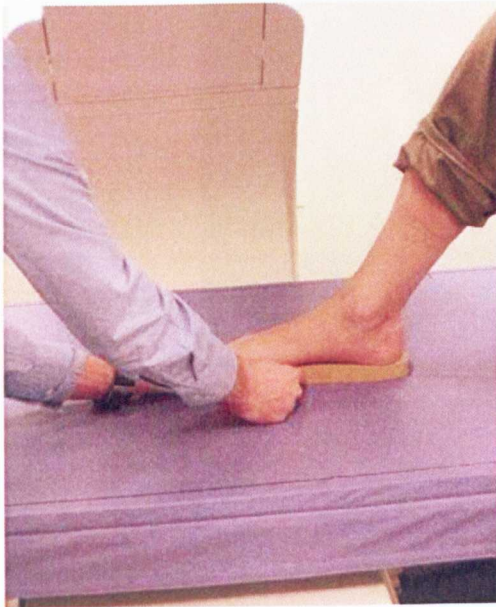
Figure 4.4 The Dual energy X-ray absorptiometry scanner and setup for plug accurate positioning of the UCA plug.
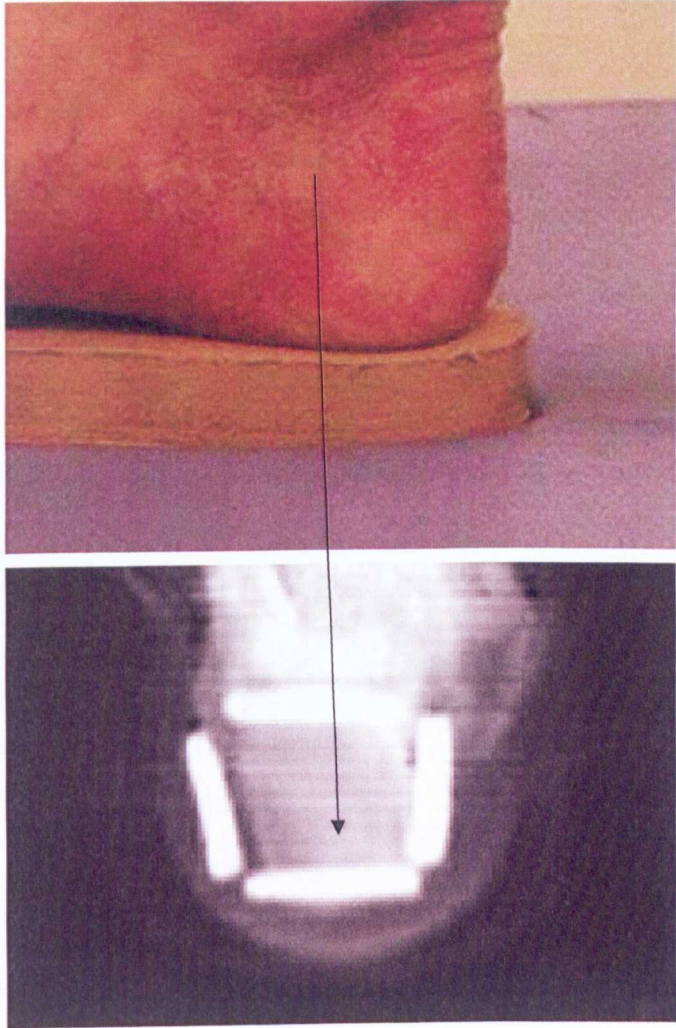
Figure 4.5 Typical DEXA image showing the relative position of the UCA plug and the calcaneus.
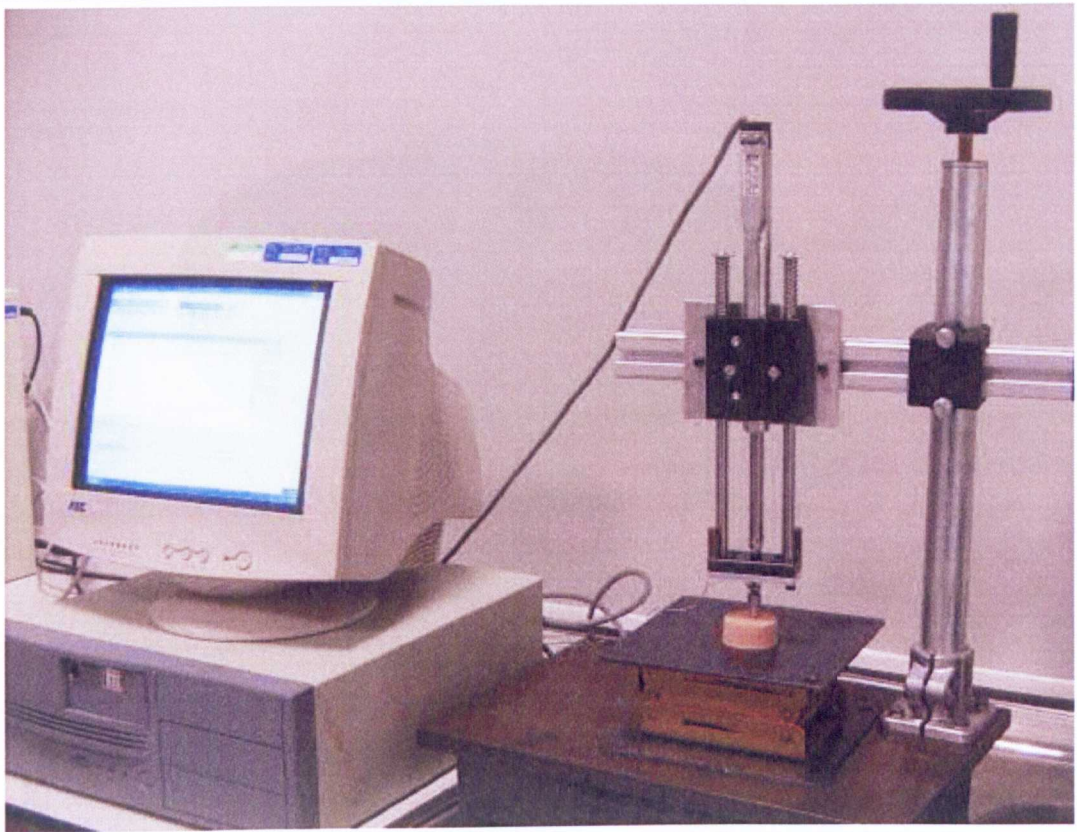
(a) Setup of the indentation tests of foams.
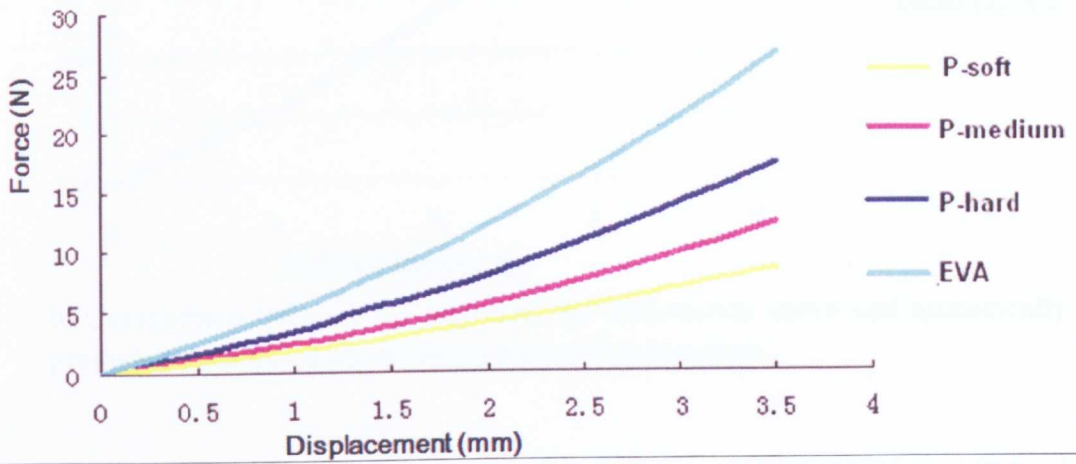
(b) Typical force-displacement data of the midsole EVA foam and UCA plug materials.

Figure 4.6 Typical indentation testing data of the different sole materials.
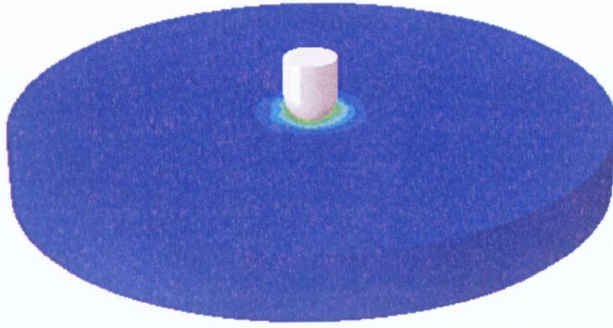
a. FE model of the indentation test.
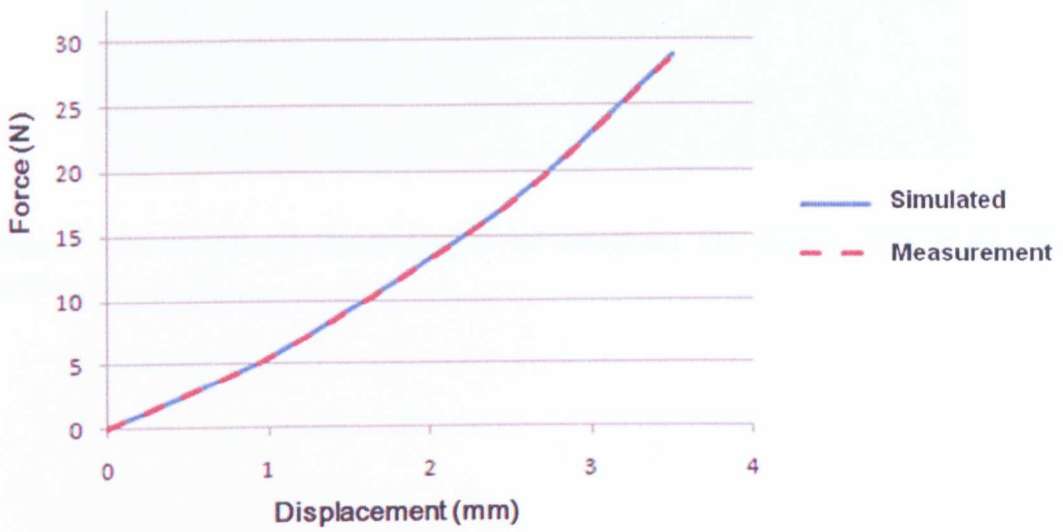
b. Comparison between the experimental indentation curve and numerically predicted data based on the fitted material parameters.

Figure 4.7 FE model of the indentation tests and the comparison of the experimental and numerical results.
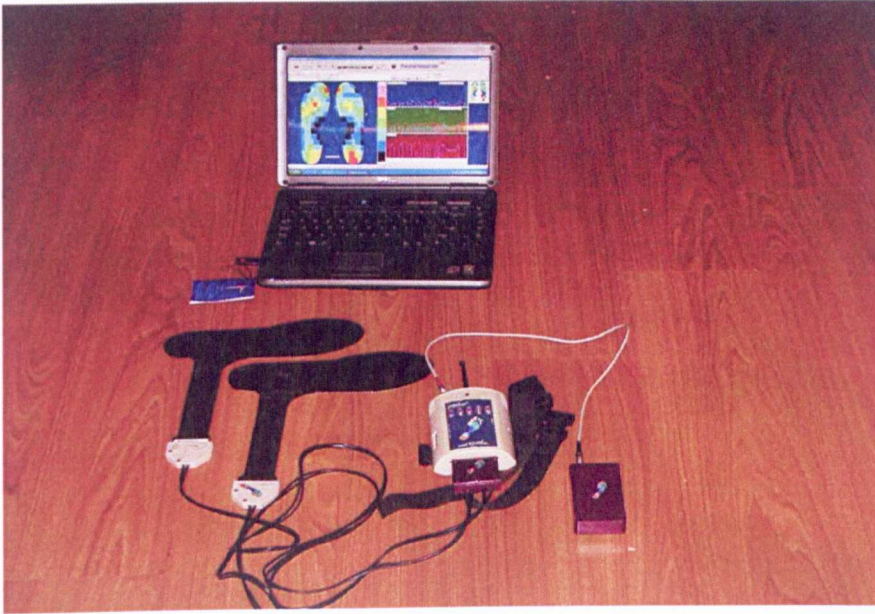
Figure 4.8 Novel-Pedar insole system for measuring the plantar pressure in heel strike.
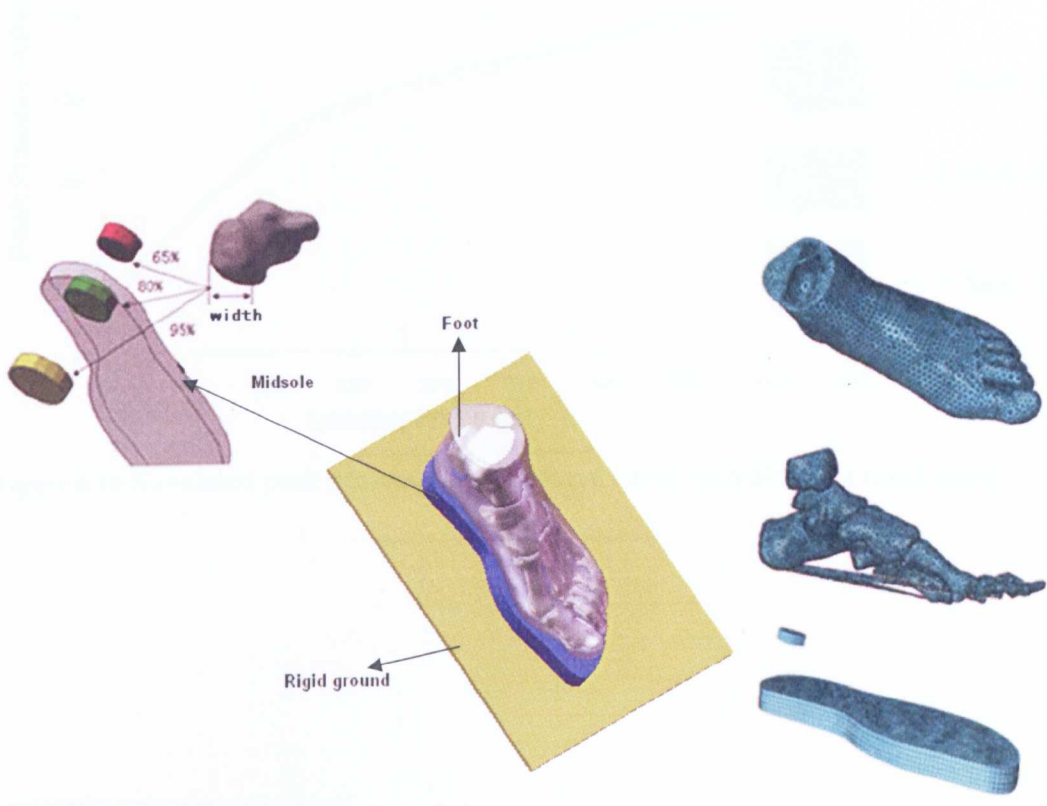
Figure 4.9 A schematic illustration of the FE model for simulating the heel strike with different UCA plugs.
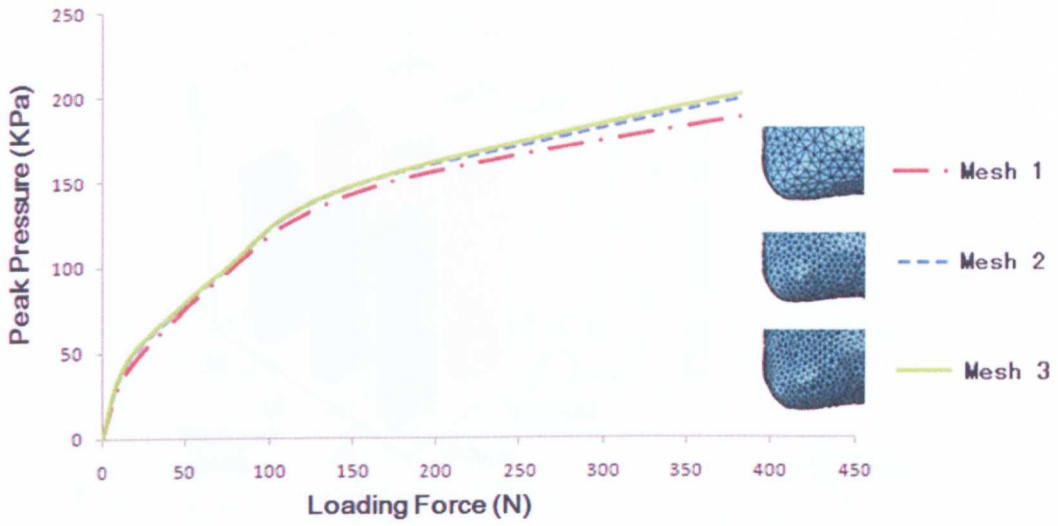
Figure 4.10 Simulated peak pressure-loading force curve with different mesh sizes.
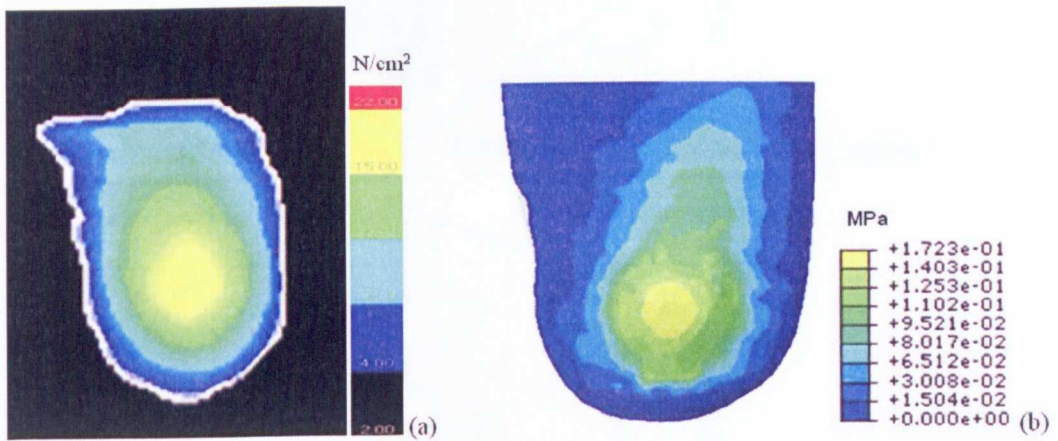
Figure 4.11 Plantar pressure distribution with plastazote hard plug (thickness=10mm, size: 95% UCA) during heel-strike. a: Novel-pedar measurement; b: Finite element predicted.
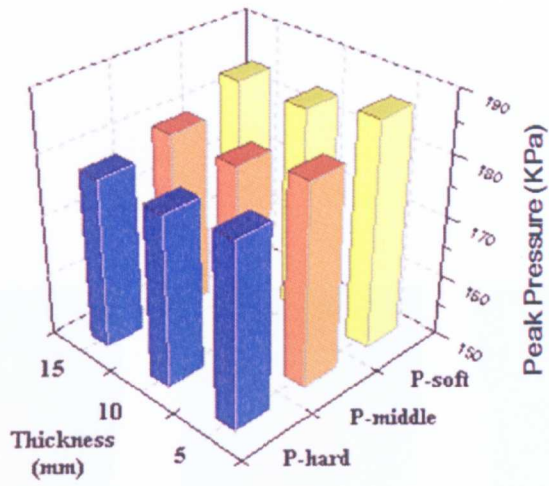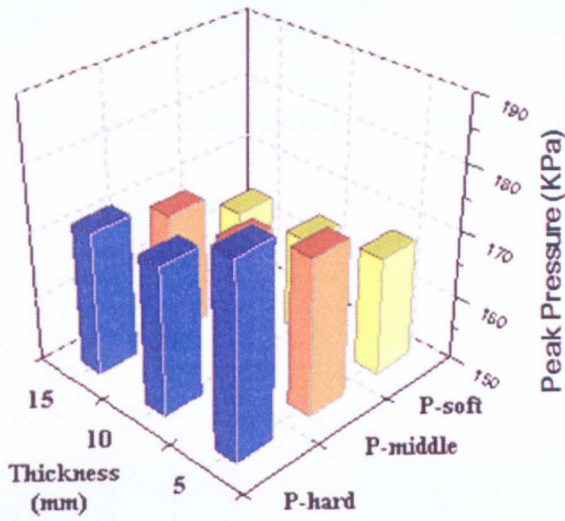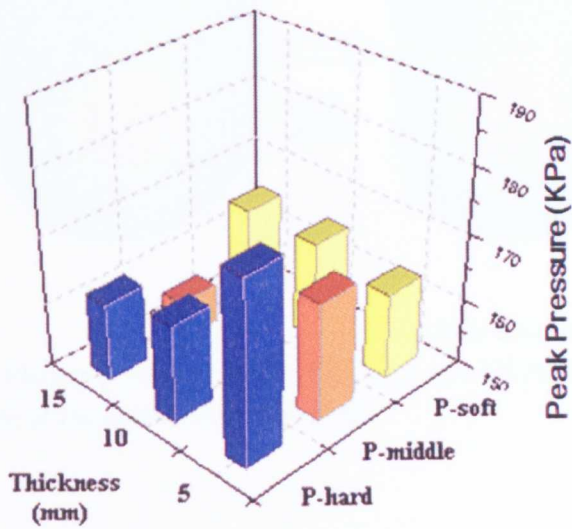
Figure 4.12 Simulated peak pressures for different midsole plugs at heel strike of walking.

a:5mm   b:10mm   c:15mm
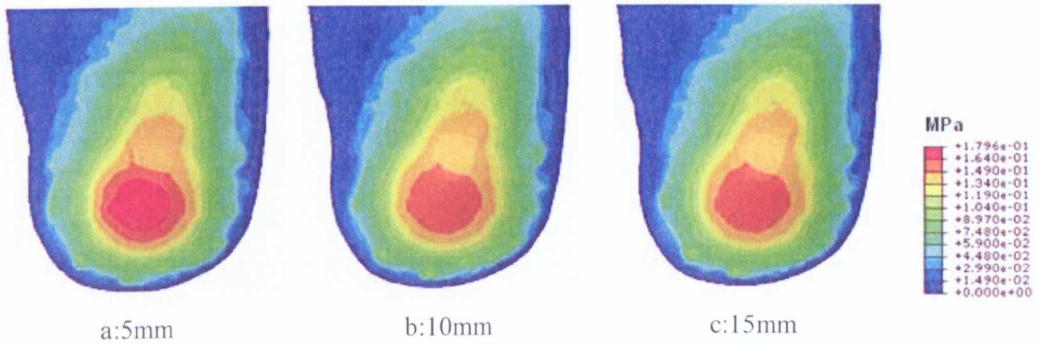
Figure 4.13 Plantar pressure distribution for a 80% UCA plug with three different thicknesses.

Pure EVA   15mm thickness of 65%UCA
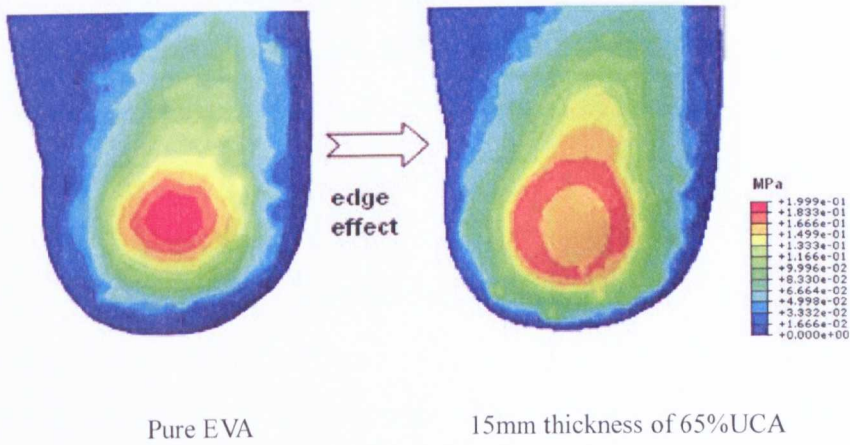
Figure 4.14 Plantar pressure distribution for a soft UCA plug showing the edge effect (high pressure at the perimeter of the plug).

CHAPTER FIVE

CONCLUSIONS AND FUTURE WORKS

5.1 Conclusions

In this study, a subject specific 3-D finite element (FE) foot model has been developed based computer tomography (CT) images and validated with subject specific biomechanical tests. The model was successfully used to study the foot deformation during normal/inversion landing and to develop a new midsole design concept of using under calcaneus area (UCA) plug for heel pressure relief. The FE model incorporated realistic structures and material properties of the soft tissues, which was validated by *in vivo* indentation tests. The plantar pressure was assessed in controlled balance standing tests and the data was used to validate the FE model and establish the optimum loading conditions and meshing scheme through mesh sensitivity tests. The validated model, combined with specially designed biomechanical tests, was then used to simulate the deformation of the forefoot in landing and to predict the effect of materials and sizes of the UCA on the plantar pressure distribution.

Combined with controlled biomechanical tests, the FE model was successfully used to predict the stresses in the metatarsals during normal and inversion landing. Subject specific biomechanical tests have been performed and the data were used to validate the FE model. Tests with a large group subjects in landing were also performed. The pressure distribution, maximal force and force time integral of the five metatarsals were calculated. The test results showed the major loading was mainly focused on the medial side of the forefoot during normal landing, while the loading character changed to the lateral side when the landing position changed to an inversion position. The fifth metatarsal region was found to be the most sensitive area with a significant load increase in an inversion landing. The numerically predicted plantar pressure distribution showed good agreement with data from controlled biomechanical tests. The stresses in the soft tissues and the metatarsals were predicted and the effects of the inversion angle (normal landing, 10 degree inversion and 20 degree inversion angle) were established. The modelling results showed that the lateral metatarsals

stress increased while the medial metatarsals stress decreased with the angle of inversion. The peak stress point was found to be near the proximal part of the fifth metatarsal that agrees with reported clinical observation on the metatarsal injuries.

Pressure relief is an active research area in biomechanics research with fundamental importance for footwear development. In this work, a new concept of subject specific midsole design for heel plantar pressure management has been proposed and evaluated. Plugs made of softer materials (in comparison to the midsole EVA foam) with different relative size to the dimension of the calcaneus bone of the subject were incorporated in the heel region of the midsole. FE model has been developed to simulate the biomechanical test with the new midsole and the numerically predicted plantar pressure showed reasonable agreement with the experimental data on the same subject. For each plug size, the effect of material properties and thicknesses of the UCA plug on the plantar pressure distribution and peak pressure level during the heel strike phase of normal walking has been established through parametric studies. The results showed that the UCA midsole insert could effectively modify the pressure distribution and its effectiveness was directly associated with ratio between its dimension to the size of the calcaneus bone of the subject. A medium hardness plug with a size of 95% of the calcaneus has achieved the best performance in peak pressure relief in comparison to the pressure level for a solid midsole, while a smaller plug with 65% of the calcaneus size and an insert with a very soft material showed minimum beneficial effect. This approach established potentially could open up a new way of heel pressure relief from the traditional approach by using insoles.

This study developed a detailed FE foot model, which took into consideration the nonlinearities of material properties, large deformations and interfacial slip/friction conditions consisted of bony structures, ligaments, Achilles tendon and the plantar fascia embedded in a volume of encapsulated soft tissue. The FE predictions were found to be in a reasonable agreement of experimental measurements under different conditions. The developed FE model can be used in clinical applications to investigate

the foot behaviour of different abnormal movement. Using the ability of the FE model to identify vulnerable skeletal and soft tissue components of the foot, it can be used not only for understanding the development mechanisms of some common disorders like diabetes, arthritis and stress fractures, etc, but also to serve as a tool for development of novel clinical solution and foot treatment approaches. In terms of footwear design, the FE model has opened up a way of parametric evaluations of the effect of the shape and other design parameters of the footwear components without the prerequisite of fabricated product and replicating biomechanical test.

5.2 Recommendations for future works

This work represents an integrated approach effectively combining FE modelling and biomechanical tests. The work on the forefoot deformation during inversion landing has advanced the understanding of this important human movement. The new concept of midsole design has opened up a new way of plantar pressure management in the footwear design. The methodology developed and the outcome of the work has laid a solid platform for future works in the following areas:

The FE model can be developed further to include more shoe components and the ground (such as the mat) for the studies on the inversion landing. The current work has been focusing on work with solid ground which represents an extreme condition in terms of forefoot loading. An improved modelling scheme can be used to further investigate the potential effects of the shoe and the ground on the stresses in metatarsals in different sports. On particular interest is football, as metatarsals failure has been a major problem. The model developed in this project can be incorporated in the assembly of the soccer boots to simulate some typical movement such as landing, cutting, etc. In addition, the current model used homogeneous and linearly elastic material properties for the bone, cartilage and ligamentous structures. This was sufficient for the current work. Future work may include a detailed model of the structure of interest through submodelling or multiscale modelling based on the current model established to be able to provide more detailed info directly link to the bone damage processes.

The concept of design based on the bone structure for a particular function (in this case, heel plantar pressure relief) is a new concept, and it can provide another dimension in subject specific design to the current process focusing on the fitting of the footwear. This approach may be transferred to other areas to target a particular objective or using more complex pug shapes. The concept of subject specific midsole design for heel plantar pressure management is particularly relevant to running shoes

or basketball shoes. Further studies are required to investigate its implication on the manufacturing process. The plug material properties used was selected solely to prove the concept; more detailed works are required to quantify sensitivities of the pressure change on materials properties based on a larger group of cohorts. In addition, the potential use of some functional materials can also be assessed using the validate FE modelling scheme.

Appendix I

Element number for each part in the FE model

Component	Mesh size (mm)			
	9	7	5	3
The first metatarsal	2670	2966	3895	5267
The second metatarsal	1761	2075	2825	3920
The third metatarsal	1458	1674	2233	2608
The fourth metatarsal	1465	1796	2352	3189
The fifth metatarsal	1362	1536	2044	2689
Soft tissue	22044	32375	36190	52504
Achilles tendon	1645	1986	2364	3155
Plantar fascia	1755	2002	2875	3807
Calcaneus	4550	5849	6768	7776
Talus	4192	4565	6670	7014
Cuboid	1757	1992	2991	4178
Navicular	1592	1819	2527	3725
Tibia	3187	3591	5764	6361
Fibula	1315	1575	2426	3428
The first cuneiform	1611	1830	2538	4314
The second cuneiform	1776	2043	2259	3082
The third cuneiform	2083	2431	2799	3680
The first phalange	2807	2941	3268	3516
The second phalange	1015	1167	1353	1611
The third phalange	1082	1095	1179	1381
The fourth phalange	1069	1132	1232	1426
The fifth phalange	1204	1267	1530	1696

Appendix II

Peak pressure values for different midsole plugs at heel strike of walking

Material	Thickness (mm)	UCA size		
		65%(KPa)	80%(KPa)	95%(KPa)
P-soft	5	186.9	168.8	166.8
	10	184.9	164.8	164.8
	15	184.9	164.8	164.8
P-middle	5	182.9	174.9	168.8
	10	180.9	170.9	156.8
	15	180.9	168.8	156.8
P-hard	5	180.9	180.9	178.9
	10	178.9	172.9	164.8
	15	178.9	172.9	162.8

References

Abboud R.J., Rowley D.I., 1996, 'Foot pressure measurement, history and development'. in Surgery of disorders of the foot and ankle, Martin Dunitz, London.

Aerts P., Ker R.F., De Clercq D., Ilsley D.W., McN R.A., 1995, 'The mechanical properties of the human heel pad: A paradox resolved'. Journal of Biomechanics. Vol.28, No.11, pp.1299-1308.

Almekinders L.C., Temple J.D., 1998, 'Etiology, diagnosis, andtreatment of tendonitis: an analysis of the literature'. Medicine and Science in Sports and Exercise. Vol.30, pp.1183–1190.

Ahroni J.H., Boyko E.J., Forsberg R.C., 1998, 'Clinical correlates of plantar pressure among diabetic veterans'. Diabetes Care. Vol.22, pp.965-972.

Akay M., Aslan N., 1996, 'Numerical and experimental stress analysis of a polymeric composite hip joint prosthesis'. Journal of Biomedical Materials Research. Vol.31, pp.167-182.

Aldridge T., 2004, 'Diagnosing heel pain in adults'. American Family Physician. Vol.70, pp. 332–338.

Al-Qattan M.M., 2007, 'Surgical treatment and results in 17 cases of open lacerations of the extensor hallucis longus tendon'. Journal of plastic, Reconstructive & Aesthetic surgery. Vol.60, No.4, pp.360-367.

Altman GH, Horan RL, Lu HH, Moreau J, Martin I, Richmond J. Kaplan D, 2002, 'Silk matrix for tissue engineered anterior cruciate ligaments'. Biomaterials. Vol.23, pp.4131-4141.

Arampatzis A., Morey-Klapsing G., Bruggemann G.P., 2003, 'The effect of falling height on muscle activity and foot motion during landings'. Journal of Electromyography and Kinesiology. Vol.13, pp.533-544.

Arndt A., Wolf P., Liu A., 2007, 'Intrinsic foot kinematics measured *in vivo* during the stance phase of slow running'. Journal of Biomechanics. Vol.40, pp.2672-2678.

Athanasiou K.A., Liu G.T., Lavery L.A., Lanctot D.R., Schenck R.C., 1998, 'Biomechanical topography of human articular cartilage in the first metatarsophalangeal joint'. Clinical Orthopaedics. Vol.348, pp.269–281.

Bader D.L., Bowker P., 1983, 'Mechanical characteristics of skin and underlying tissues *in vivo*'. Biomaterials. Vol.4, pp.305-308.

Barani Z., Haghpanahi M., Katoozian H., 2005, 'Three dimensional stress analysis of diabetic insole: a finite element approach'. Technol Health Care. Vol.13, pp.185-192.

Beaupre G. S., Hayes W. C., 1985, 'Finite element analysis of a three-dimensional open-celled model for trabecular bone'. Journal of Biomechanical Engineering. Vol.107, pp.249-256.

Beillas P., 2004, 'A new method to investigate *in vivo* knee behavior using a finite element model of the lower limb'. Journal of Biomechanics. Vol.37, pp.1019–1030.

Bennell K., Crossley K., Jayarajan J., 2004, 'Ground reaction forces and bone parameters in females with tibial stress fracture'. Medicine and Science in Sports and Exercise. Vol.36, pp.397–404.

Bouten C.V., Westerterp K.R., Verduin M., Janssen J.D., 1994, 'Assessment of energy expenditure for physical activity using a triaxial accelerometer'. Medicine and Science in Sports and Exercise. Vol.26, pp.1516–1523.

Bratteby L.E., Sandhagen B., Fan H., Enghardt H., Samuelson G., 1998, 'Total energy expenditure and physical activity as assessed by the doubly labeled water method in Swedish

adolescents in whom energy'. American Journal of Clinical Nutrition. Vol.67, No.5, pp.905–911.

Briggs P.J., 2005, 'The structure and function of the foot in relation to injury'. Current Orthopaedics. Vol.19, pp.85-93.

Brodsky J.W., Kourosh S., Stills M., 1988, 'Objective evaluation of insert material for diabetic and athletic footwear'. Foot Ankle. Vol.9, pp.111–116.

Burns, J., Crosbie, J., Hunt, A., Ouvrier, R., 2005, 'The effect of pes cavus on foot pain and plantar pressure'. Clinical Biomechanics. Vol.20, pp:877-882.

Bus S.A., Ulbrecht J.S., Cavanagh P.R., 2004, 'Pressure relief and load redistribution by custom-made insoles in diabetic patients with neuropathy and foot deformity'. Clinical Biomechanics. Vol.19, pp.629–638.

Busch K., Chantelau E., 2003, 'Effectiveness of a new brand of stock 'diabetic' shoes to protect against diabetic foot ulcer relapse: A prospective cohort study'. Diabetic Medicine. Vol.20, pp.665–669.

Bushong S.X., 2000, *Computed tomography, Essentials of medical image series*. McGraw-Hill companies, USA.

Cavanagh P. R., 1999, 'Plantar soft tissue thickness during ground contact in walking'. Journal of Biomechanics. Vol.32, No.6, pp.623-628.

Chen W.P., Tang F.T., Ju C.W., 2001, 'Stress distribution of the foot during mid-stance to push-off in barefoot gait: a 3-D finite element analysis'. Clinical Biomechanics. Vol.16, pp.614-620.

Cheung J.T.M., de Vries G., Nigg B.M., 2007, 'Biomechanical effects of midfoot fusion—a finite element study'. Journal of Biomechanics. Vol.40, S2, pp.326.

Cheung J.T.M., Zhang M., 2008, 'Parametric design of pressure-relieving foot orthosis using statistics-based finite element method'. Medical Engineering&Physics. Vol.30, pp.269-277.

Cheung J.T.M., Zhang M., An K., 2004, 'Effects of plantar fascia stiffness on the biomechanical responses of the ankle-foot complex'. Clinical Biomechanics. Vol.19, pp.839-846.

Cheung, J.T.M., Zhang, M., Leung, A. K., Fan, Y. B., 2005, 'Three-dimensional finite element analysis of the foot during standing--a material sensitivity study'. Journal of Biomechanics. Vol.38, No.5, pp.1045-1054.

Chu T.M., Reddy N.P., 1995, 'Stress distribution in the ankle-foot orthosis used to correct pathological gait'. Journal of Rehabilitation Research and Development. Vol.32, pp.349-360.

Cook S.D., Kester M.A., Brunet M.E., 1985, 'Biomechanics of running shoe performance'. Clinical Sports Medicine. Vol.4, pp.619–626.

Crolet J.M., Aoubiza B., Meunier A., 1993, 'Compact bone: numerical simulation of mechanical characteristics'. Journal of Biomechanics, Vol.26, pp.677-687.

Dameron T.B., 1975, 'Fractures and anatomical variations of the proximal portion of the fifth metatarsal'. The Journal of Bone and Joint Surgery. Vol.57, pp.788–792.

Davis I.S., 2004, 'Foot and ankle research retreat: consensus statement'. Journal of Orthopaedic and Sport Physical Therapy. Vol.34, pp.2–4.

De Clercq D., Aerts P., Kunnen M., 1994, 'The mechanical behavior characteristics of the human heel pad during foot strike in running: an *in vivo* cineradiographic study'. Journal of Biomechanics. Vol.27, pp.1213–1222.

De Cock A., De Clercq D., Willems T., Witvrouw E., 2005, 'Temporal characteristics of foot roll-over during barefoot jogging: reference data for young adults'. Gait Posture. Vol.21,

pp.432–439.

Delalleau A., Josse G., Lagarde J.M., Zahouani H., Bergheau J.M., 2006, 'Characterization of the mechanical properties of skin by inverse analysis combined with the indentation test'. Journal of Biomechanics. Vol.39, No.9, pp.1603-1610.

Denoth J., 1986, 'Load on the locomotor system and modelling'. In: Biomechanics of running shoes. Champaign, IL, Human Kinetics.

Dion J.L., Foufllot J.P., Leblanc A., 1982, 'Ambulatory monitoring of walking using a thin capacitive force transducer'. In: Proceedings of the fourth International Symposium on Ambulatory Monitoring and the Second Gent Workshop on Blood Pressure Variability. Academic Press, London, pp.420–425.

Dixon S.J., Creaby M.W., Allsopp A.J., 2006, 'Comparison of static and dynamic biomechanical measures in military recruits with and without a history of third metatarsal stress fracture'. Clinical Biomechanics. Vol.21, pp.412-419.

Donahue S.W., Sharkey N.A., 1999, 'Strains in the metatarsals during the stance phase of gait: implications for stress fractures'. The Journal of Bone and Joint Surgery. Vol.81, pp.1236-1244.

Ekrol I., Court-Brown C.M., 2004, 'Fractures of the base of the 5th metatarsal'. The Foot. Vol.14, pp.96–98.

Erdemir A., Viveiros M.L., Ulbrecht, J.S., Cavanagh, P.R., 2006, 'An inverse finite-element model of heel-pad indentation'. Journal of Biomechanics. Vol.39, No.7, pp.1279-1286.

Even-Tzur N., Weisz E., Hirsch-Falk Y., Gefen A., 2006, 'Role of EVA viscoelastic properties in the protective performance of a sport shoe: Computational studies'. Biomedical Materials and Engineering. Vol.16, pp.289-299.

Finni T., Komi P.V., Lukkariniemi J., 1998, 'Achilles tendon loading during walking: application of a novel optic fibre technique'. European Journal of Applied Physiology. Vol.77, pp.289–291.

Fregly B.J., Sawyer W.G., Harman M.K., Banks S.A., 2005, 'Computational wear prediction of a total knee replacement from *in vivo* kinematics'. Journal of Biomechanics. Vol.38, pp.305-314.

Fritz G.R., Prieskorn D., 1995, 'First metatarsocuneiform motion: a radiographic and statistical analysis'. Foot and Ankle International. Vol.16, No.3, pp.117-123.

Garcia-Gonzalez A., Bayod J., Prados-Frutos J., Losa-Iglesias M., Jules K., Bengoa-Vallejo R., Doblare M., 2009, 'Finite-element simulation of flexor digitorum longus or flexor digitorum brevis tendon transfer for the treatment of claw toe deformity'. Journal of Biomechanics. Vol.42, pp.1697-1704.

Gayle R., Montoye H.J., Philpot J., 1977, 'Accuracy of pedometers for measuring distance walked'. Research Quarterly. Vol.48, No.3, pp.632–636.

Gefen A., Elad D., Shiner R. J., 1999, 'Analysis of stress distribution in the alveolar septa of normal and simulated emphysematic lungs'. Journal of Biomechanics. Vol.32, pp.891–897.

Gefen A., Megido-Ravid M., Azariah M., Itzchak Y., Arcan M., 2001, 'Integration of plantar soft tissue stiffness measurements in routine MRI of the diabetic foot'. Clinical Biomechanics, Vol.16, No.10, pp.921-925.

Gefen A., Megido-Ravid M., Itzchak Y., Arcan M., 2000, 'Biomechanical analysis of the three-dimensional foot structure during gait: a basic tool for clinical applications'. Journal of Biomechanical Engineering. Vol.122, No.6, pp.630-639.

Gefen A., Seliktar R., 2004, 'Comparison of the trabecular architecture and the isostatic stress

flow in the human calcaneus'. Medical Engineering& Physics. Vol.26, pp.119-129.

Gerard J.M., Ohayon J., Luboz V., Perrier P., Payan Y., 2005, 'Non-linear elastic properties of the lingual and facial tissues assessed by indentation technique: Application to the biomechanics of speech production'. Medical Engineering & Physics. Vol.27, pp.884–892.

Giannakopoulos A.E., 2006, 'Elastic and viscoelastic indentation of flat surfaces by pyramid indentors'. Journal of the Mechanics and Physics of Solids. Vol.54, pp.1305-1332.

Giddings V.L., Beaupre G.S., Whalen R.T., Carter D.R., 2000, 'Calcaneal loading during walking and running'. Medicine and Science in Sports and Exercise. Vol.32, pp.627–634.

Gooding G.A., Stress R.M., Graf P.M., Moss K.M., Louie K.S., Grunfeld C., 1986, 'Sonography of the sole of the foot. Evidence for loss of foot pad thickness in diabetes and its relationship to ulceration of the foot'. Investigative Radiology. Vol.21, No.1, pp.45-48.

Gooding G.A., Stress R.M., Graf P.M., Grunfeld C., 1985, 'Heel pad thickness: determination by high-resolution ultrasonography'. Journal of Ultrasound in Medicine. Vol.4, pp.173-174.

Goonetilleke R.S., 1999, 'Footwear Cushioning: Relating Objective and Subjective Measurements'. Human Factors. Vol.41, No.2, pp.241-256.

Goske S., Erdemir A., Petre M., Budhabhatti S., Cavanagh P.R., 2006, 'Reduction of plantar heel pressures: Insole design using finite element analysis'. Journal of Biomechanics Vol.39, pp.2363-2370.

Grimston S.K., Nigg B.M., Fisher V., Ajemian S.V., 1994, 'External loads throughout a 45-minute run in stress fracture and non-stress fracture runners'. Journal of Biomechanics. Vol.27, pp.668.

Gruneberg C., Nieuwenhuijzen P., Duysens J., 2003, 'Reflex responses in the lower leg following landing impact on an inverting and non-inverting platform'. Journal of Physiology. Vol.550, pp.985-993.

Gu Y.D., Li J.S., 2005, 'Finite element analysis of the instep fatigue trauma in the high-heeled gait'. World Journal of Modelling and Simulation. Vol.2, pp.117-122.

Gu Y.D., Li J.S., Lake M.J., Ren X.J., Zeng Y.J., 2008, 'The mechanical response of Achilles tendon during different kinds of sports'. Communications in Numerical Methods in Engineering, Vol.24, pp.2077-2085.

Gu Y.D., Li J.S., Lake M., Ren X.J., 2008, 'Three dimensional finite element analysis of hind foot bones in jumping moment'. Journal of Medical Biomechanics. Vol.23, pp.127-130.

Gunner C.W., Hutton W.C., Burlin T.E., 1979, 'The mechanical properties of skin *in vivo*- a portable hand-held extensometer'. British Journal of Dermatology. Vol.100, pp.161-163.

Hagins M., Pappas E., Kremenic I., Orishimo K., Rundle A., 2007, 'The effect of an inclined landing surface on biomechanical variables during a jumping task'. Clinical Biomechanics. Vol.22, No.9, pp.1030-1036.

Hamill J., Emmerik R., Heiderscheit B., Li L., 1999, 'A dynamical systems approach to lower extremity running injuries'. Clinical Biomechanics. Vol.14, No.5, pp.297-308.

Harrigan T.P., Harris W.H., 1991, 'A finite element study of the effect of diametral interface gaps on the contact areas and pressures in uncemented cylindrical femoral total hip components'. Journal of Biomechanics. Vol.24, pp.87-91.

Harrigan T.P., Karah J.A., O'Connor D.O., Burke D.W., Harris W.H., 1992, 'A finite element study of the initiation of failure of fixation in cemented femoral total hip components'. International Orthopaedics Research. Vol.10, pp.134-144.

Hayes W.C., Gran J.D., Nagurka M.L., Feldman J.M., Oatis C., 1983, 'Leg motion analysis during gait by multiaxial accelerometry: theoretical foundations and preliminary validation'. Journal of Biomechanical Engineering. Vol.105, pp.283–289.

Hennessy K., Burns J., Penkala S., 2007, 'Reducing plantar pressure in rheumatoid arthritis: a comparison of running versus off-the-shelf orthopaedic footwear'. Clinical Biomechanics. Vol.22, pp.917–923.

Hennig E.M., Milani T.L., 1995, 'In-shoe pressure distribution for running in various types of footwear'. Journal of Applied Biomechanics. Vol.11, pp.299-310.

Higbie E.J., Contractor B.S., Tis L.L., Johnson B.F., 1999, 'Foot structure and in shoe plantar pressure differences between males and females', Medicine & Science in Sports & Exercise. Vol.31, pp.129.

Hollister S.J., Brennan J.M., Kikuchi N., 1994, 'A homogenisation sampling procedure for calculating trabecular bone effective stiffness and tissue level stress'. Journal of Biomechanics. Vol.27, pp.433-444.

Hollister S.J., Fyhrie D.P., Jepsen K.J., Goldstein S.A., 1991, 'Application of homogenisation theory to the study of trabecular bone mechanics'. Journal of Biomechanics. Vol.24, pp.825-839.

Hoyt R.W., Knapik J.J., Lanza J.F., Jones B.H., Stab J.S., 1994, 'Ambulatory foot contact monitor to estimate metabolic cost of human locomotion'. Journal of Applied Physiology. Vol.76, pp.1818-1822.

Huiskes R., 1982, 'On the Modelling of Long Bones in Structural Analyses'. Journal of Biomechanics. Vol.15, pp.65–69.

Jacob S., Patil M.K., 1999, 'Three-dimensional foot modelling and analysis of stresses in normal and early stage Hansen's disease with muscle paralysis'. Journal of Rehabilitation Research and Development. Vol.36, pp.252-263.

Jozsa L., Kannus P., 1997, 'Overuse injuries of tendons. In: Jozsa L, Kannus P, editors. Human tendons. Anatomy, physiology, and pathology'. Human Kinetics. Vol.1997, No.67, pp.277-279.

Kauer M., 2001, *Inverse finite element characterization of soft tissue with aspiration experiments*. Degree of Doctor of Technical Sciences, Swiss Federal Institute of Technology.

Ker R.F., 1996, 'The time dependent mechanical properties of the human heel pad in the context of locomotion'. The Journal of Experimental Biology. Vol.199, No.7, pp.1501–1508.

Ker R.F., Alexander R.M., Bennett M.B., 1998, 'Why are mammalian tendons so thick'. Journal of Zoology. Vol.216, pp.309-324.

Kernozek T.W., Zimmer K.A., 2000, 'Reliability and running speed effects of in-shoe loading measurements during slow treadmill running'. Foot Ankle International. Vol.21, pp.749-752.

Klaue K., Hansen S.T., Masquelet A.C., 1994, 'Clinical, Quantitative Assessment of the Tarso-Metatarsal Mobility in the Sagittal Plane and Its Relation to Hallux Valgus Deformity'. Foot & Ankle. Vol.15, pp.9-13.

Khan K.M., Cook J.L., Kannus P., Maffuli N., Bonar S.F., 2002, 'Time to abandon the "tendonitis" myth'. British Medical Journal. Vol.324, No.738, pp.626–627.

Kimura M., Mochimaru M., Kanade T., *Measurements of 3d foot shape deformation in motion*. Digital Human Symposium Tokyo 2009.

Kitagawa Y., Ichikawa H., King A.I., Begeman P.C., 2000, 'Development of a human ankle/foot model'. In: Human Biomechanics and Injury Prevention. Springer: Tokyo.

Kitaoka H.B., Luo Z.P., An K.N., 1997, 'Effect of plantar fasciotomy on stability of arch of foot'.

Clinical Orthopaedics. Vol.344, pp.307–312.

Klaesner J.W., Commean P.K., Hastings M.K., Zou D., Mueller M. J., 2001, 'Accuracy and reliability testing of a portable soft tissue indenter'. IEEE Transactions on neural systems and rehabilitation engineering. Vol.9, No.2, pp.232-240.

Komi P.V., Fukashiro S., Jarvinen M., 1992, 'Biomechanical loading of Achilles tendon during normal locomotion'. Clinical Sports in Medicine. Vol.11, pp.521-531.

Kong X., Yang Q., Li B., Rothwell G., English R., Ren X.J., 2008, 'Numerical study of strengths of spot-welded joints of steel'. Materials and Design. Vol.29, pp.1554-1561.

Kongsgaard M., Aagaard P., Kjaer M., Magnusson S.P., 2005, 'Structural achilles tendon properties in athletes subjected to different exercise modes and in achilles tendon rupture'. Journal of Applied Physiology. Vol.8, pp.90-98.

Kura H., Kitaoka H.B., Luo Z.P., An K.N., 1998, 'Measurement of surface contact area of the ankle joint'. Clinical Biomechanics. Vol.13, pp.365-370.

LaBella C.R., 2007, 'Common acute sports-related lower extremity injuries in children and adolescents'. Clinical Pediatric Emergency Medicine. Vol.1, pp.31 – 42.

Ledoux W.R., Blevins J.J. 2007, 'The compressive material properties of the plantar soft tissue'. Journal of Biomechanics. Vol.40, pp.2975-2981.

Lake M.J., 2000, 'Determining the protective function of sports footwear'. Ergonomics. Vol.43, pp.1610-1621.

Lemmon D., Shiang T.Y., Hashmi A., Ulbrecht J.S., Cavanagh P.R., 1997, 'The effect of insoles in therapeutic footwear: a finite element approach'. Journal of Biomechanics. Vol.30, pp.615–620.

Leonard W.R., Katzmarzyk P.T., Stephen M.A., Ross A.G.P., 1995, 'Comparison of the heart rate-monitoring and factorial method: assessment of energy expenditure in highland and costal Ecuadoreans'. American Journal of Clinical Nutrition. Vol.61, No.5, pp.1146–1152.

Levy J.M., 1978, 'Stress fractures of the first metatarsal'. American Journal of Roentgenology. Vol.130, pp.679-681.

Lewis G., 2003, 'Finite element analysis of a model of a therapeutic shoe: effect of material selection for the outsole'. Biomedical Material Engineering. Vol.13, pp.75-81.

Li B., Gu Y.D., Rothwell G., English R., Ren X.J., 2009, 'Characterisation of Nonlinear Material Parameters of Foams Based on Indentation Tests'. Materials & Design, Vol.30, pp.2708-2714.

Li C.Y., Imaishi K., Shiba N., Tagawa Y., Maeda T., Matsuo S., Goto T., Yamanaka K., 2000, 'Biomechanical evaluation of foot pressure and loading force during gait in rheumatoid arthritis patients with and without foot orthosis'. Kurume Medical Journal. Vol.47, pp.211–217.

Li Z.P., Kim J.E., Davidson J.S., Etheridge B.S., Alonso J.E., Eberhardt A.W., 2007, 'Biomechanical response of the pubic symphysis in lateral pelvis impacts: a finite element study'. Journal of Biomechanics. Vol.40, pp.2758-2766.

Lichtwark G.A, Wilson A.M., 2005, 'In vivo mechanical properties of the human Achilles tendon during one-legged hopping'. Journal of Experimental Biology. Vol.208, pp.4715-4725.

Logan A.J., Dabke H., Finlay D., Makwana N., 2007, 'Fifth metatarsal base fractures: A simple classification'. The Journal of Foot and Ankle Surgery. Vol.13, pp.30-34.

Lotz J.C., Cheal E.J., Hayes W.C., 1991, 'Fracture prediction for the proximal femur using finite element models. Parr I - linear analysis. Part II – nonlinear analysis'. Journal of Biomechanical Engineers. Vol.113, pp.353-365.

Madarevic M., Kolundzic R., Trkulja V., Mirkovic M., Pecina M., 2009, 'Biomechanical analysis of functional adaptation of metatarsal bones in statically deformed feet'. International Orthopaedics. Vol.33, No.1, pp.157 – 163.

Madsen M.T., Haller J., Commean P.K., Vannier, M.W., 2000, 'A device for applying static loads to prosthetic limbs of transtibial amputees during spiral CT examination'. Journal of Rehabilitation Research and Development Vol.37, No.4, pp.383-387.

Maffulli N., Wong J., 2003, 'Rupture of the Achilles and patellar tendons', Clinical Journal Sport Medicine. Vol.22, pp.761-776.

Malanga G.A., Ramirez J.A., 2008, 'Common injuries of the foot and ankle in the child and adolescent athlete'. Physical Medicine and Rehabilitation Clinics of North America. Vol.19, pp. 347-371.

Matheson G.O., Clement D.B., McKenzie D.C., Taunton J.E., Lloyd-Smith D.R., MacIntyre J.G., 1987, 'Stress fractures in athletes: a study of 320 cases'. The American Journal of Sports Medicine. Vol.15, pp.46 –58.

Mattei C.P., Zahouani H., 2004, 'Study of adhesion forces and mechanical properties of human skin *in vivo*'. Journal of Adhesion Science and Technology. Vol 18, No.15, pp.1739-1758.

McBryde A.M., 1985, 'Stress fractures in runners,' Clinical Journal of Sport Medicine. Vol.4, pp.737-752.

Meijer G.A., Wsterterp K.R., Verhoeven F.M., Koper H.B., ten Hoor F., 1991, 'Methods to assess physical activity with special reference to motion sensors and accelerrometers'. IEEE Transactions on Biomedical Engineering. Vol.38, No.3, pp.221–229.

Milgrom C., Giladi M., Stein M., Kashtan H., Margulies J.Y., Chisin R., 1985, 'Stress fractures in military recruits: A prospective study showing an unusually high incidence'. Journal of Bone and Joint Surgery. Vol.67, pp.732-735.

Mills N.J., Fitzgerald C., Gilchrist A., Verdejo R., 2003, 'Polymer foams for personal protection: cushions, shoes and helmets'. Composites Science and Technology. Vol.63, pp.2389–2400.

Miyoshi S., 2002, 'Analysis of the shape of the tibial tray in total knee arthroplasty using a three dimension finite element model'. Clinical Biomechanics. Vol.17, pp.521–525.

Mizel M.S., 1993, 'The role of the plantar first metatarsal first cuneiform ligament in weight bearing on the first metatarsal'. Foot and Ankle International. Vol.14, pp.82–84.

Moseley L., Smith R., Hunt A., Gant R., 2000, 'Three-dimensional kinematics of the rearfoot during the stance phase of walking in normal young adult males'. Clinical Biomechanics. Vol.11, pp.39–45.

Mow V.C., Flatow E.L., Ateshian G.A., 2000, Biomechanics. In Orthopaedic Basic Science: Biology and Biomechanics of the Musculoskeletal System, second ed. American Academy of Orthopaedic Surgeons, Rosemont, IL.

Mueller M.J., Sinacore D.R., Hoogstrate S., Daly L., 1994, 'Hip and ankle walking strategies: effect on peak plantar pressures and implications for neuropathic ulceration'. Archives of Physical Medicine and Rehabilitation. Vol.75, pp.1196–1200.

Mueller M.J., Strube M.J., 1996, 'Generalizability of in-shoe peak pressure measurement using the F-scan system'. Clinical Biomechanics. Vol.11, pp.159-164.

Muller R., Rtiegsegger P., 1996, 'Analysis of mechanical properties of cancellous bone under conditions of simulated bone atrophy'. Journal of Biomechanics. Vol.29, pp.1053-1060.

Muller R., Ruegsegger P., 1995, 'Three-dimensional finite element modelling of non-invasively assessed trabccular bone structures'. Medical Engineering and Physics, Vol.17, pp.126-133.

Murley G.S., Landorf K.B., Menz H.B., Bird A.R., 2009, 'Effect of foot posture, foot orthoses and footwear on lower limb muscle activity during walking and running: A systematic review', Gait & Posture, Vol.29, pp.172-187.

Narvaez J.A., Narvaez J., Ortega R., Aquilera C., Sanchez A., Andia E., 2000, 'Painful heel: MR imaging findings'. Radiographics. Vol.20, No.2, pp.333–352.

Nester C.J., Liu A.M., Ward E., Howard D., Cocheba J., Derrick T., Patterson P., 2007, '*In vitro* study of foot kinematic using a dynamic walking cadaver model'. Journal of Biomechanics. Vol.40. pp.1927-1937.

Nigg B.M., Bahlsen H.A., Luethi S.M., Stokes S., 1987, 'The influence of running velocity and midsole hardness on external impact forces in heel-toe running'. Journal of Biomechanics. Vol.20, pp.951-959.

Noe D.A., Voto S.J., Hoffmann M.S., Askew M.J., Gradisar I.A., 1993, 'Role of the calcaneal heel pad and polymeric shock absorbers in attenuation of heel strike impact'. Journal Biomedical Engineering. Vol.15, No.1, pp.23–26.

Oatis C.A., 2004, *Kinesiology: The mechanics and pathomechanics of human movement.* Philadelphia, Lipincott Williams & Wilkins.

Ouzounian T.J., Shereff M.J., 1989, '*In vitro* determination of midfoot motion'. Foot and Ankle Vol.10, pp.140-146.

Pailler-Mattei C., Zahouani H., 2006, 'Analysis of adhesive behaviour of human skin *in vivo* by an indentation test'. Tribology International. Vol.39, pp.12–21.

Papaioannou G., Demetropoulos C., Kong Y., 2010, 'Predicting the effects of knee focal articular surface injury with a patient-specific finite element model'. The Knee. Vol.17, pp.61-68.

Parreno E.M., 2007, Advanced tools for the design and sale of customized footwear: case studies. In The 2007 world conference on mass customization&personalization, Massachusetts Institute of Technology, Cambridge, MA.

Platzer W., Kahle W., 2004, *Color atlas and textbook of human anatomy: locomotor system.* Thieme Stutttgart New York USA.

Pontaga I., 2004, 'Ankle joint evertor–invertor muscle torque ratio decrease due to recurrent lateral ligament sprains'. Clinical Biomechanics. Vol.19, pp.760 – 762.

Popovic N., Jalali A., Georis P., Gillet P., 2005, 'Proximal fifth metatarsal diaphyseal stress fracture in football players'. Journal of Foot and Ankle Surgery. Vol.11, pp.135–141.

Putti A.B., Arnold G.P., Cochrane L., Abboud R.J., 2007, 'The pedar in-shoe system: repeatability and normal pressure values'. Gait & Posture. Vol.25, pp.401-405.

Raikin S.M., Slenker N., Ratigan B., 2008, 'The association of a varus hindfoot and fracture of the fifth metatarsal metaphyseal-diaphyseal junction: the Jones fracture'. The American Journal of Sports Medicine. Vol.36, No.7, pp.1367-1372.

Raspovic A., Newcombe L., Lloyd J., Dalton E., 2000, 'Effect of customized insoles on vertical plantar pressures in sites of previous neuropathic ulceration in the diabetic foot'. The Foot. Vol.10, pp.133–138.

Reger S.I., McGovern T.F., Chung K.C., 1990, Biomechanics of Tissue Distortion and Stiffness by Magnetic Resonance Imaging. In Pressure Sores - Clinical Practice and Scientific Approach. Macmillan Press, London.

Reiber G.E., Pecoraro R.E., Koepsell T.D., 1992, 'Risk factors for amputation in patients with diabetes mellitus. A case–control study'. Annals of Internal Medicine. Vol.117, pp.97–105.

Ren X.J., Silberschmidt V.V., 2008, 'Numerical modelling of low-density cellular materials'. Computational Materials Science, Vol.43, pp. 65-74.

Ren X.J., Smith C.W., Evans K.E., Dooling P., Burgess A., Wiechers J., Zahlan N., 2006, 'Experimental and numerical investigations of the deformation of soft materials under tangential loading'. International Journal of Solids and Structure.Vol.43, pp.2364-2377.

Ren X.J., Smith, C.W., Evans, K.E., Dooling, P.J., Burgess, A. Wiechers, J.W., 2005, 'Experimental testing and numerical modelling of mechanical properties of the human skin'. International Foundation of Society of Cosmetic Chemists. Vol.1, pp.95-98.

Rho J.Y., Tsui T.Y., Pharr G.M., 1997, 'Elastic properties of human cortical and trabecular lamellar bone measured by nanoindentation'. Biomaterials. Vol.18, No.20, pp.1325–1330.

Ribu L., Hanestad B.R., Moum T., Birkeland K., Rustoen T., 2007, 'Health-related quality of life among patients with diabetes and foot ulcers: association with demographic and clinical characteristics'. Journal of Diabetes and Its Complications. Vol.21, pp.227-236.

Robbins S., Waked E., Rappel R., 1995, 'Ankle taping improves proprioception before and after exercise in young men'. British Journal of Sports Medicine. Vol.29, pp.242-247.

Rome K., 1998, 'Mechanical properties of the heel pad: current theory and review of the literature'. The Foot. Vol.8, pp.179-185.

Rome K., Webb P., Unsworth A., Haslock I., 2001, 'Heel pad stiffness in runners with plantar heel pain'. Clinical Biomechanics. Vol.16, pp.901-905.

Rohen J., Yokochi C., 1988, Color Atlas of Anatomy—A Photographic Study of the Human Body, Second ed. Igaku-Shoin, New York, NY.

Rosenbaum D., Lübke B., Bauer G., Claes L., 1995, 'Long-term effects of hindfoot fractures evaluated by means of plantar pressure analyses'. Clinical Biomechanics, Vol.10, pp.345-351.

Sarrafian S.K., 1993, Functional anatomy of the foot and ankle. In Anatomy of the foot and ankle. Philadelphia: Lippincott.

Saunders M.M., Schwentker E.P., Kay D.B., Bennett G., Jacobs C.R., Verstraete M.C., Njus G.O., 2003, 'Finite element analysis as a tool for parametric prosthetic foot design and evaluation. Technique development in the solid ankle cushioned heel (sach) foot'. Computer Methods in Biomechanics and Biomedical Engineering. Vol.6, pp.75-87.

Schon L.C., Glennon T.P., Baxter D.E., 1993, 'Heel pain syndrome: electrodiagnostic support for nerve entrapment'. Foot and Ankle. Vol.14, pp.129-135.

Schuenke M., Schulte E., Schumacher U., Rude J., 2006, Thieme atalas of anatomy: general anatomy and musculoskeletal system. Thieme Stutttgart New York USA.

Schwellnus M.P., Jordaan G., Noakes T.D., 1990, 'Prevention of common overuse injuries by the use of shock absorbing insoles: a prospective study'. The American Journal of Sports Medicine. Vol.18, No.6, pp.636–641.

Scott G., Menz H., Newcombe L., 2007, 'Age-related differences in foot structure and function'. Gait & Posture. Vol.26, pp.68–75.

Scott S.H., Winter D.A., 1991, 'Talocrural and talocalcaneal joint kinematics and kinetics during the stance phase of walking'. Journal of Biomechanics. Vol.24, pp.743–752.

Serup J., Jemec G., 1999, Hand book of non-invasive methods and the skin, CRC Press, London.

Shanthikumar s., Low Z., Falvey E., McCrory P., Franklyn-Miller A., 2010, 'The effect of

gait velocity on calcaneal balance at heel strike; Implications for orthotic prescription in injury prevention'. Gait&Posture, Vol.31, No.1, pp.9-12.

Shiang T.Y., 1997, 'The nonlinear finite element analysis and plantar pressure measurement for various shoe soles in heel region'. Proceedings of National Science Council. Republic of China B. 168-174.

Shorten M.R., 2000, Running shoe design: protection and performance. In Marathon Medicine. Royal Society of Medicine, London, pp.159–169.

Simkin A., 1982 Structural Analysis of the Human Foot in Standing Posture; PhD Thesis, Tel Aviv University.

Smith K.E., Commean P.K., Mueller M.J., Robertson D.D., Pilgram T., Johnson J., 2000, 'Assessment of the diabetic foot using spiral computed tomography imaging and plantar pressure measurements: a technical report'. Journal of Rehabilitation Research and Development. Vol.37, No.1, pp.31-40.

Siegler S., Block J., Schneck C.D., 1988, 'The mechanical characteristics of the collateral ligaments of the human ankle joint'. Foot & Ankle. Vol.8, pp.234–242.

Sijbrandij E.S., van Gils A.P.G., Lange E., 2002, 'Overuse and sports-related injuries of the ankle and hind foot: MR imaging findings'. European Journal of radiology. Vol.43, pp.45-56.

Simon J., Doederlein L., McIntosh A.S., Metaxiotis D., Bock H.G., Wolf S.I., 2006, 'The Heidelberg foot measurement method: development, description and assessment'. Gait & Posture Vol.23, No.4, pp.411–24.

Stebbins J., Harrington M., Thompson N., Zavatsky A., Theologis T., 2006, 'Repeatability of a model for measuring multi-segment foot kinematics in children'. Gait & Posture. Vol.23, No.4, pp.401–405.

Sugihara T., Ohura T., Homman K., Igawa H.H., 1991, 'The extensibility in human skin: variation according to age and site'. British Journal of Plastic Surgery. Vol.44, pp.418-422.

Syngellakis S., Arnold M.A., Rassoulian H., 2000, 'Assessment of the non-linear behaviour of plastic ankle foot orthoses by the finite element method'. Proceedings of the Institution Mechanical Engineers. pp.527-539.

Tao K., Wang D., Wang C., Wang X., Liu A., Nester C., Howard D., 2009, 'An *in vivo* experimental validation of a computational model of human foot'. Journal of Bionic Engineering. Vol.6, pp.387-397.

Tong J., Lim C.S., Goh O.L., 2003, 'Technique to study the biomechanical properties of the human calcaneal heel pad'. The Foot. Vol.13, pp.83–91.

Tryfonidis M., Jackson W., Mansour R., Cooke P.H., The J., Ostlere S., Sharp R.J., 2008, 'Acquired adult flat foot due to isolated plantar calcaneonavicular (spring) ligament insufficiency with a normal tibialis posterior tendon'. Foot and Ankle Surgery. Vol.14, No.2, pp.89-95.

Tsung B.Y., Zhang M., Mak A.F., Wong M.W., 2004, 'Effectiveness of insoles on plantar pressure redistribution'. Journal of Rehabilitation Research and Development.Vol.41, pp.767–774.

Vandamme M., Ulm F.J., 2006, 'Viscoelastic solutions for conical indentation'. International Journal of Solids and Structures. Vol.43, pp.3142-3165.

Vannah W.M., Childress D.S., 1996, 'Indenter tests and finite element modelling of bulk muscular tissue *in vivo*'. Journal of Rehabilitation Research and Development.Vol.33 No.3, pp.239-252.

Van Rietbergen B., Weinans H., Huiskes R. Odgaard A., 1995, 'A new method to determine

trabecular bone elastic properties and loading using micromechanical finite-element models'. Journal of Biomechanics. Vol.28, pp.69-81.

Van Rietbergen B., Odgaard A., Kabel J., Huiskes R., 1996, 'Direct mechanics assessment of elastic symmetries and properties of trabecular bone architecture'. Journal of Biomechanics. Vol.29, pp.1653-1657.

Verdejo R., Mills N.J., 2004, 'Simulating the effects of long distance running on shoe midsole foam'. Polymer Test. Vol.23, No.4, pp.567-574.

Vescovo P., Varchon D., Humbert P., 2002, '*In vivo* tensile tests on human skin: the extensometers'. In Bioengineering of the Skin: Skin Biomechanics. London, CRS Press LLC.

Viswanathan V., Madhavan S., Gnanasundaram S., Gopalakrishna G., Das B.N., Rajasekar S., 2004, 'Effectiveness of different types of footwear insoles for the diabetic neuropathic foot: a follow-up study'. Diabetics Care. Vol.27, pp.474–477.

Vitasalo J.T., Kvist M., 1983, 'Some biomechanical aspects of the foot and ankle in athletes with and without shin splints'. American Journal of Sport Medicine. Vol.11, pp.125-130.

Vonhof J., 2006, *Fixing your feet: prevention and treatments for athletes.* Wilderness Press. Berkeley, CA.

Washburn, R., Chin, M.K., Montoye, H.J., 1980, 'Accuracy of pedometer in walking and running'. Research Quarterly for Exercise & Sport. Vol.51, pp.695–702.

Weaver J. B., Doyley M., Cheung Y., Kennedy F., Madsen E. L., Van Houten E. E., Paulsen K., 2005, 'Imaging the shear modulus of the heel fat pads'. Clinical Biomechanics. Vol.20, No.3, pp.312-319.

Watson A.W.S., 1999, 'Ankle sprains in players of the field-games Gaelic football and hurling'. Journal of Sports Medicine and Physical Fitness. Vol.36, pp.66–70.

Weinfeld S.B., Haddad S.L., Myerson M.S., 1997, 'Metatarsal stress fractures'. Clinical Sports Medicine.Vol.16, pp.319–338.

Weiss J.A., Gardiner J.C., 2001, 'Computational modeling of ligament mechanics'. Critical Reviews in Biomedical Engineering. Vol.29, pp.1-70.

Werner F.W., Ayers D.C., Maletsky L.P., Rullkoetter P.J., 2005, 'The effect of valgus/varus malalignment on load distribution in total knee replacements'. Journal of Biomechanics. Vol.38, pp.349-355.

Willems T., Witvrouw E., Delbaere K., De Cock A., De Clercq D., 2005, 'Relationship between gait biomechanics and inversion sprains: a prospective study of risk factors'. Gait and Posture. Vol.21, pp.379-387.

Williams D.S., McClay I.S., Hamill J., Buchanan T.S., 2001, 'Lower extremity kinematic and kinetic differences in runners with high and low arches'. Journal of Applied Biomechanics. Vol.17, pp.153–163.

Winter D.A., 1979, *Biomechanics of Human Movement.* New York: Wiley.

Wren T.A., Yerby S.A., Beaupre G.S., Carter D.R., 2001, 'Mechanical properties of the human achilles tendon'. Clinical Biomechanics. Vol.16, pp.245-251.

Wright I.C., Neptunea R.R., van den Bogertb A.J., Nigg B.M., 2000, 'The influence of foot positioning on ankle sprains'. Journal of Biomechanics. Vol.33, pp.513-519.

Yosibash Z., Trabelsi N., Milgrom C., 2007, 'Reliable simulations of the human proximal femur by high-order finite element analysis validated by experimental observations'. Journal of Biomechanics. Vol.40, pp.3688-3699.

Zheng Y.P., Mak A.F., Lue B., 1999, 'Objective assessment of limb tissue elasticity: Development of a manual indentation procedure'. Journal of Rehabilitation Research and Development. Vol.36, No. 2, pp.71–85.

Zheng Y.P., Choi Y.K., Wong K., Chan S., Mak A.F., 2000, 'Biomechanical assessment of plantar foot tissue in diabetic patients using an ultrasound indentation system'. Ultrasound in Medicine and Biology. Vol.26, pp.451–456.

.

Glossary

Abduction — movement of a limb away from the midline in the frontal plane.

Adduction — movement of a limb towards the midline in the frontal plane.

Anatomical position — used for anatomical descriptions: standing upright with the feet together and the arms by the sides and the palms forward.

Biofeedback — allowing a person to see how well they are performing a task, so that they can make immediate improvements.

Center of gravity — used in mechanical calculations. The point within an object at which it can be assumed that the mass of the object is concentrated.

Center of pressure — the point beneath the foot through which it can be assumed that the ground reaction force is passing.

Dorsiflexion — movement of the foot towards the knee.

Electromyogram (EMG) — recording of the electrical activity of a muscle.

Eversion — internal rotation about the long axis of the foot.

Extension — sagittal plane movement at a joint, in which the distal segment usually moving posteriorly.

Flexion — sagittal plane movement at a joint, in which the distal segment usually moving anteriorly.

Force platform — common piece of gait analysis equipment for measuring the ground reaction force.

Forefoot — the five metatarsal bones and the toes.

Frontal plane — the plane divides a body part into front and back portions.

Gait — the manner or style of walking.

Ground reaction force — the upward force applied by the ground to the foot in response to the downward force applied by the foot to the ground.

Hallux — the big toe or great toe.

Heel strike — a distinct impact between the heel and the ground at initial contact.

Hindfoot — two bones in the foot: talus and calcaneus.

Initial contact — event in the gait cycle when first contact is made between the foot

and ground; this is made by the heel in normal gait, marking the transition from swing phase to stance phase.

Inversion — external rotation about the longitudinal axis of the foot.

Kinetics — the study of the relationships between forces and their effects on bodies at statics and bodies in dynamics.

Lateral — away from the midline of the body.

Marker — an object fixed to a point on the skin, so that it is visible to an optical measurement system. Typically a small sphere covered in reflective tape.

Medial — towards the midline of the body.

Midfoot — five tarsal bones: navicular, cuboid and the medial, intermediate and lateral cuneiforms.

Mid-stance — period in the stance phase of the gait cycle between opposite toe off and heel rise.

Moment — a turning effect; typically a force being applied in such a way that it causes a rotation.

Orthosis — an external support for some part of the body; also known as brace.

Plantarflexion — movement of the foot away from the knee.

Pronation — a combination of eversion, dorsiflextin and forefoot abduction.

Proprioception — unconscious feedback on joint position, force in ligaments and tendons, etc.

Proximal — towards the rest of the body.

Push off — period in the stance phase of the gait cycle between opposite initial contact and toe off.

Sagittal plane — divides part of the body into right and left portions.

Stance phase — that part of the gait cycle for one side in which the foot is on the ground.

Statics — a branch of kinetics dealing with bodies at rest.

Supination — inversion, plantarflexion and forefoot adduction.

Toe off — event in the gait cycle when the foot leaves the ground, which marks the transition from the stance phase to the swing phase.

Torsion — twisting. It is often applied to a long bone in which a 'twist' is present between the proximal and distal ends.

Transverse plane — divides a body part into upper and lower portions.

Ulcer — loss of covering skin or epithelium.

Valgus — joint angulation with the distal segment sloping away from the midline.

Varus — joint angulation, with the distal segment sloping towards the midline.

Publication list

Journal papers:

1. **Gu Y.D.**, Ren X.J., Li J.S., "Image based midsole insert design and the material effects on heel plantar pressure distribution during simulated walking loads," *Computer Methods in Biomechanics and Biomedical Engineering*. (accepted).

2. **Gu Y.D.**, Li J.S., Lake M., Ren X.J, "Foot contact surface effect to metatarsals loading character during inversion landing", *International Journal for Numerical Methods in Biomedical Engineering*. (accepted).

3. **Gu Y.D.**, Li J.S., Lake M., Ren X.J., and Zeng Y.J., "Biomechanical effects of foam inserts on forefoot load during high heeled gait: A pilot study", *Journal of Mechanics in Medicine and Biology*. (accepted)

4. **Gu Y.D.**, Ren X.J., Li J.S., Lake M., and Zeng Y.J., "Heel skin stiffness effect on the hind foot biomechanics during heel-strike", *Skin Research and Technology*. doi: 10.1111/j.1600-0846.2010.00425.x

5. **Gu Y.D.**, Ren X.J., Li J.S., Lake M., and Zeng Y.J., "Computer simulation of stress distribution in the metatarsals at different inversion angles using the finite element method", *International Orthopaedics*. 2010; 34: 669-676.

6. Li B., **Gu Y.D.**, Rothwell G., English R. and Ren X.J., "Characterisation of nonlinear material parameters of foams based on indentation tests", *Materials & Design*. 2009; 30: 2708-2714.

Contribution to conferences:

7. **Gu Y.D.**, Li J.S., Ruan G.Q., Lake M., Ren X.J., "Lower limb muscles semg activity during high-heeled Latin dancing", *6th World Congress on Biomechanics*. Singapore, 2010.

8. **Gu Y.D.**, Li J.S., Lake M., Ren X.J. (abstract), "Midsole design effects on heel plantar pressure distribution during simulated walking loads", *International Society of Biomechanics*. Cape Town, South Africa, 2009.

9. **Gu Y.D.**, Li J.S., Lake M., Ren X.J. (abstract), "Plantar force characterization during rowing for top athletes", *International Convention on Science Education and Medicine in Sport*. Guangzhou, China, 2008.